

STUDIES ON COMPOSITE POLYMER ELECTROLYTES BASED ON CO-POLYMER FOR SECONDARY LITHIUM BATTERIES

(File.No.41.839/2012(SR) dtd.18.07.2012)

**Final Progress Report
for the period 01.07.2012 to 31.12.2015**

Submitted to



**UNIVERSITY GRANTS COMMISSION
BAHADUR SHAH ZAFAR MARG
NEW DELHI – 110 002**



By

Dr. M.SIVAKUMAR

Associate Professor

Principal Investigator- UGC-MRP

#120, Energy Materials Lab, Department of Physics

Science Block, Alagappa University

Karaikudi-630 003, Tamil Nadu

**UNIVERSITY GRANTS COMMISSION
BAHADUR SHAH ZAFAR MARG
NEW DELHI – 110 002**

**PROFORMA FOR SUBMISSION OF INFORMATION AT THE TIME OF SENDING THE
FINAL REPORT OF THE WORK DONE ON THE PROJECT**

1. Title of the Project: **‘Studies on composite polymer electrolytes based on co-polymer for secondary lithium batteries’**
2. NAME AND ADDRESS OF THE: **Dr. M. SIVAKUMAR,**
PRINCIPAL INVESTIGATOR Assistant Professor,
Department of Physics,
Alagappa University,
Karaikudi – 630 003.
3. NAME AND ADDRESS OF THE INSTITUTION: **Alagappa University,**
Karaikudi – 630 003.
4. UGC APPROVAL LETTER NO. AND DATE: F.No.41.839/2012(SR), dated 18.07.2012
5. DATE OF IMPLEMENTATION: 01.07.2012
6. TENURE OF THE PROJECT: 01.07.2012 to 31.12.2015
7. TOTAL GRANT ALLOCATED: **Rs.11,20,800/-**
8. TOTAL GRANT RECEIVED: **Rs.8,29,926/-**
9. FINAL EXPENDITURE: Rs7,94,107/- + Unspent Amount remitted Rs.35,819/- with an interest of Rs.6,044/- at Total of **Rs.41,863/- (Total Rs.835,970/-)**
10. TITLE OF THE PROJECT: **‘Studies on composite polymer electrolytes based on co-polymer for secondary lithium batteries’**
11. OBJECTIVES OF THE PROJECT
 - To prepare the composite polymer electrolyte using copolymers like (PVdF-co-HFP), (PVdF-co-PAN), (PVdF-co-PVC) with high ionic conductivity and favorable properties by Solution Casting Technique.
 - To study the nanocomposite polymer electrolyte, nanocomposite materials are to be prepared using any one method such as sol-gel, solid state reaction, arrested precipitation, microwave method, etc., also the prepared nanocomposite material have been studied for its properties.

- To characterize the electrochemical performances of the prepared electrolyte sample EIS, LSV, CV, Lithium ion transference number studies are carried out.
- The structural, surface morphology, etc., of the samples are to be determined using XRD, SEM, FTIR also the thermal properties of the electrolytes can be studied using TG/DTA, DSC, etc., Charge/Discharge studies of the samples are also to be carried out.

12. WHETHER OBJECTIVES WERE ACHIEVED

(GIVE DETAILS)

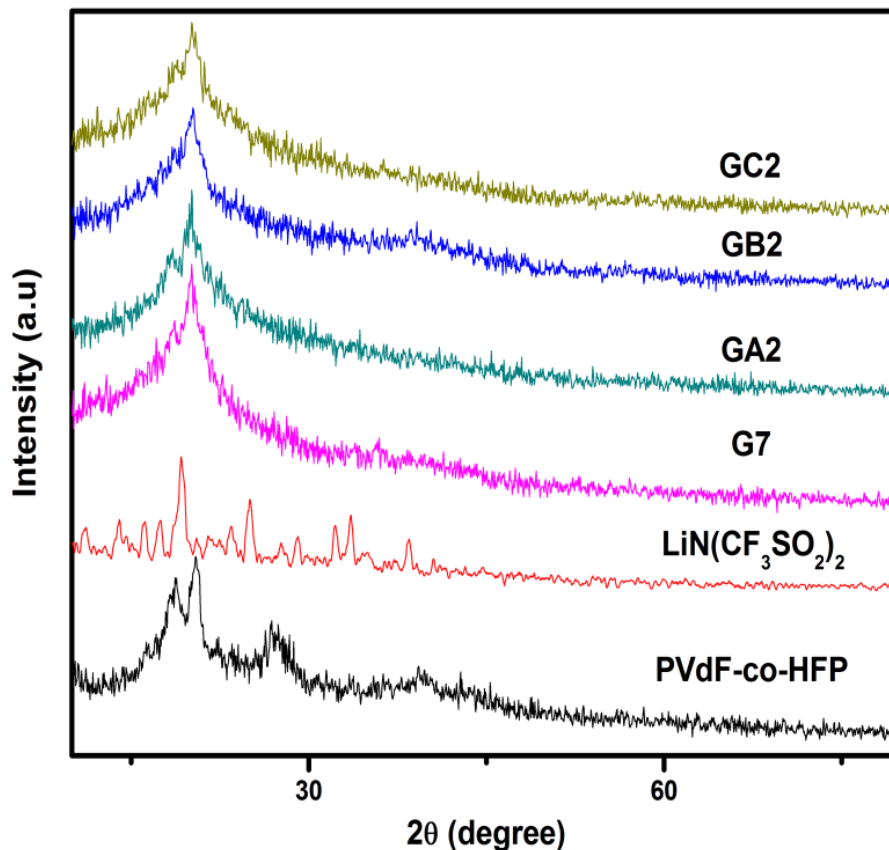
- PVdF-co-HFP polymer electrolytes were enthusiastically studied with various compositions and various ionic liquids via solution casting technique in view of feasible ionic conductivity. Also, PS-MMA copolymer electrolytes were also synthesized and studied.
- CeO₂, ZrO₂ nano particles have been prepared using different methods by varying several parameters namely pH, temperature, surfactant, etc., and they were adapted to make composite lithium solid and gel polymer electrolytes.
- To ascertain the structure, complexation, surface morphology, XRD, FT-IR, FE-SEM, HR-TEM have been performed and all the analysis were carried out for the prepared composite materials and for the as-prepared polymer electrolytes too.
- The thermal history of the materials was analyzed using TG/DTA, DTA etc, and reported.
- The electrochemical properties of the prepared electrolytes were analyzed using Electrochemical Impedance Spectroscopy, Linear Sweep Voltammetry, Cyclic Voltammetry, etc. Also, the optimized Ionic liquid based electrolytes, and optimized composite polymer electrolytes were subjected for the Charge/ Discharge analysis towards estimating the discharge capacity.

13. ACHIEVEMENTS FROM THE PROJECT

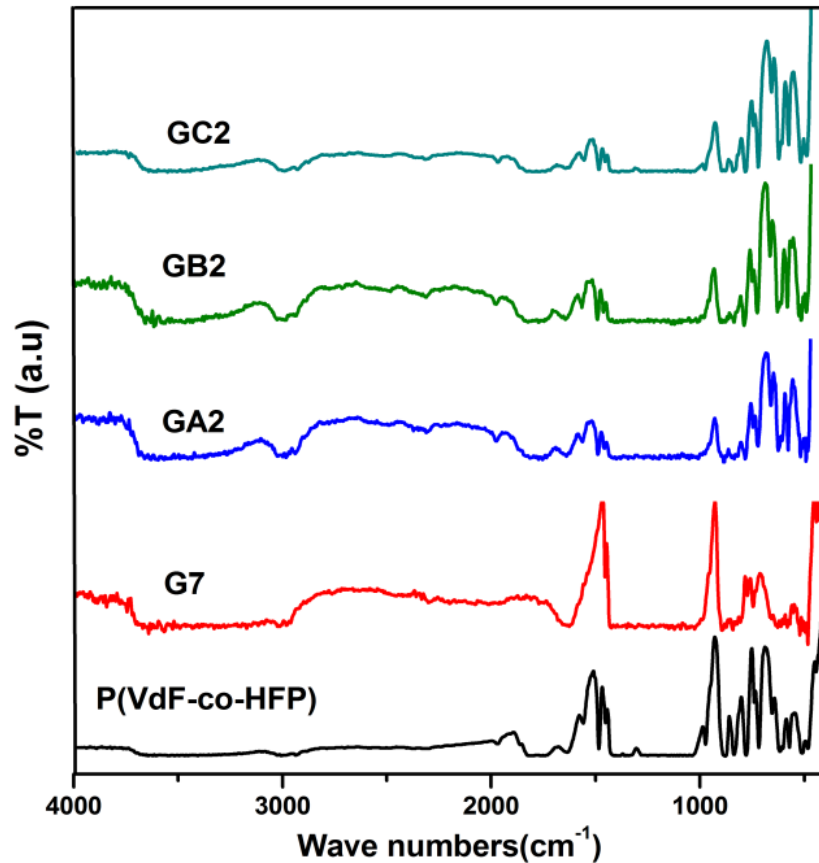
A systematic study has been performed based on PVdF-co-HFP polymer. The objective of the present work has focused on the preparation and characterization of ionic conducting polymer electrolyte using alkali metal salt and ionic liquid for the application in the lithium battery. The polymer electrolyte samples have been prepared using the conventional solution casting technique, which is the preferred for its simplicity. For comparison, alkali salt based polymer electrolyte, sulfonium and phosphonium ionic liquid based electrolytes have been prepared and characterized in the viewpoint of their physical and electrochemical properties.

In order to understand the role of lithium cation, an attempt has been made to prepare the solid, gel and composite polymer electrolytes using PVdF-co-HFP with LiN (CF₃SO₂)₂ via solution casting technique. Initially, the solid polymer electrolytes were optimized in view point of its ionic conductivity value at room temperature and 80 wt% of PVdF-co-HFP and 20wt% of LiN (CF₃SO₂)₂, has exhibited high ionic conductivity of 1.93×10^{-5} S/cm at 303K. A drop in conductivity value has been noticed at higher concentration above 25 wt% of LiN (CF₃SO₂)₂ salt. This is due to the effect of higher amount of lithium salt forms ionic aggregation such as ion doublets and triplets, which restricts the polymer segmental motion. From the above studies, three concentrations of high ionic conducting SPE have been chosen to prepare GPE. The gel polymer electrolytes have been optimized with ethylene carbonate (EC) and propylene carbonate (PC) plasticizers in 1: 1 ratio. The high dielectric constant of plasticizers dictates the complete dissolution of the charge carriers and leads to higher ionic conductivity. But, the higher content of plasticizers leads more dispersion of charge carriers in polymer matrix and result a drop in conductivity. From the AC impedance studies, it is observed that the conductivity has been increased by two orders of magnitude (1.72×10^{-3} S/cm at 303K) by the addition of plasticizers. It is strongly supported by the other

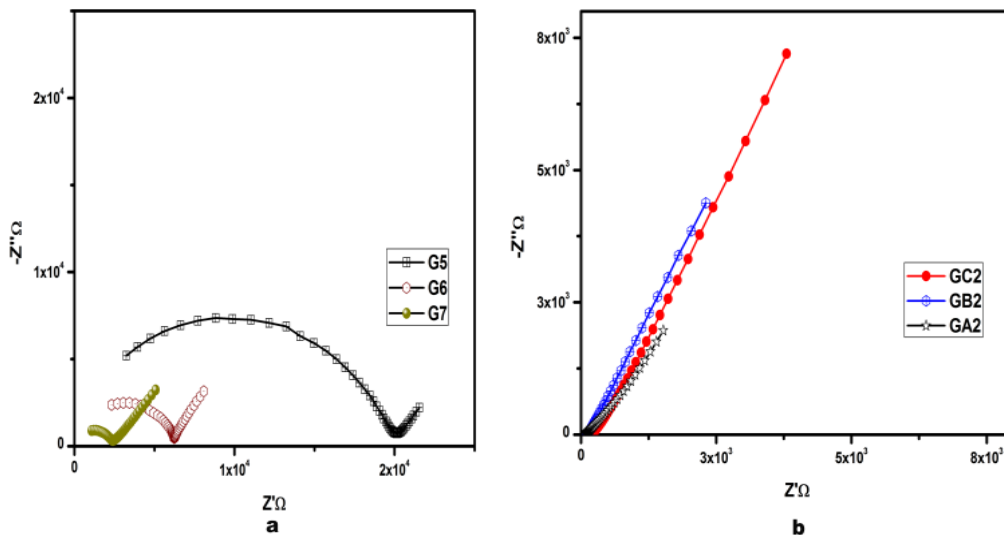
characterization techniques such as SEM, TG/DTA, etc. The optimized ratio (80:20) of PVdF-co-HFP:LiN(CF₃SO₂)₂40 wt% - EC+PC 60 wt% was subjected for electrochemical studies. The electrochemical stability of the electrolyte (4.2 V) has been confirmed using Linear Sweep Voltammetry (LSV). It also possesses a discharge capacity of 117 mAh/g for the cell couple Li/PE/LiFePO₄ at 0.1C. The Zirconium dioxide based fillers were optimized with the GPE (PVdF-co-HFP:LiN(CF₃SO₂)₂40 wt%- EC+PC 60 wt%). The inorganic filler particle present in the polymer matrix enhances the ionic conductivity and maximum ionic conductivity value of 4.46×10^{-3} S/cm has been obtained for the sample K2 with 6 wt% of ZrO₂. Discharge capacity of 126 mAh/g has been obtained for the coin cell containing Li / CGPE / LiFePO₄ at 0.1 C rate.



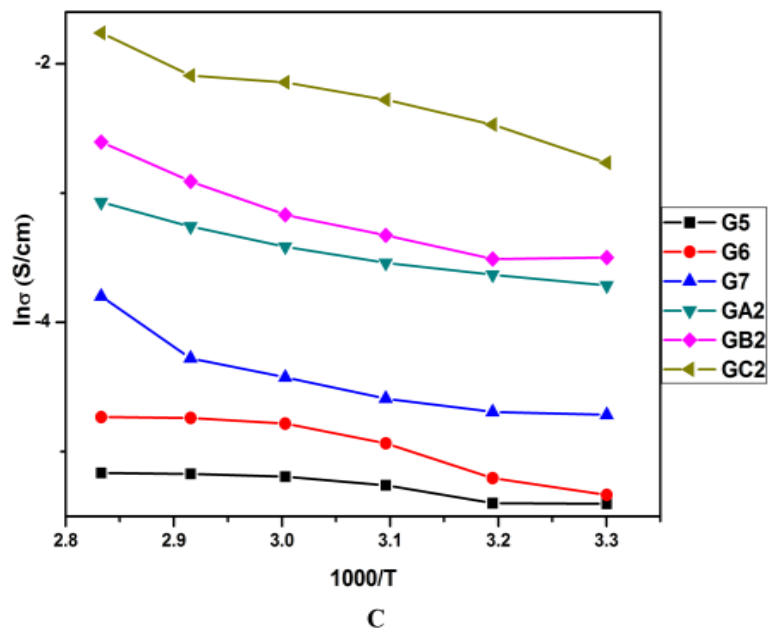
X-Ray diffraction pattern of PVdF-co-HFP, LiN(CF₃SO₂)₂, G7 - PVdF-co-HFP (80 wt%) + LiTFSI (20 wt%), GPE, GA2 – 85:20, GB2 – 82:18,GC2 – 80:20 ratio of PVdF-co-HFP : LiTFSI +EC+PC (60) wt%



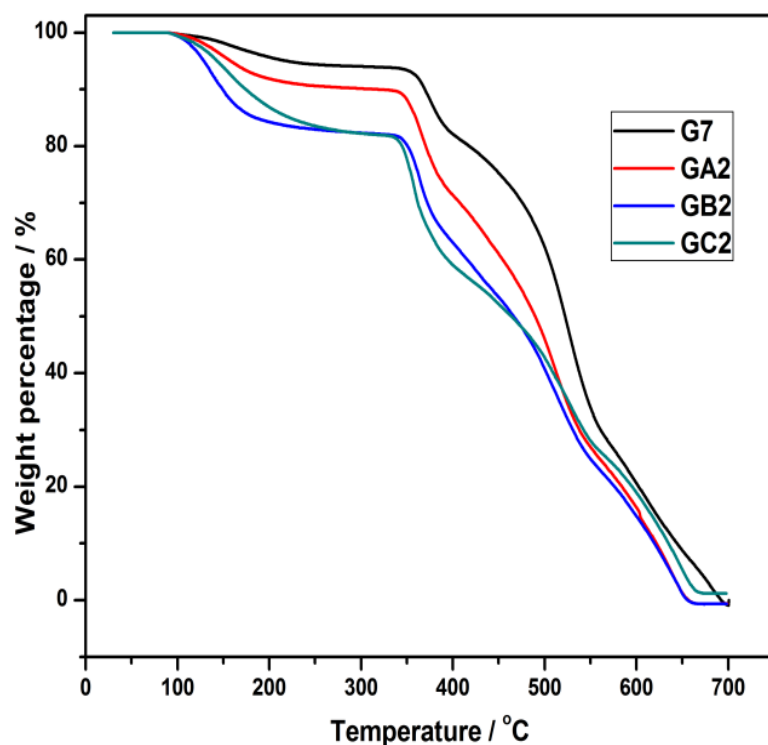
FTIR spectra of PVdF-co-HFP, G7 - PVdF-co-HFP (80 wt%) + LiTFSI (20 wt%), GPE, GA2 - 85:20, GB2 - 82:18, GC2 - 80:20 ratio of PVdF-co-HFP : LiTFSI +EC+PC (60 wt%)



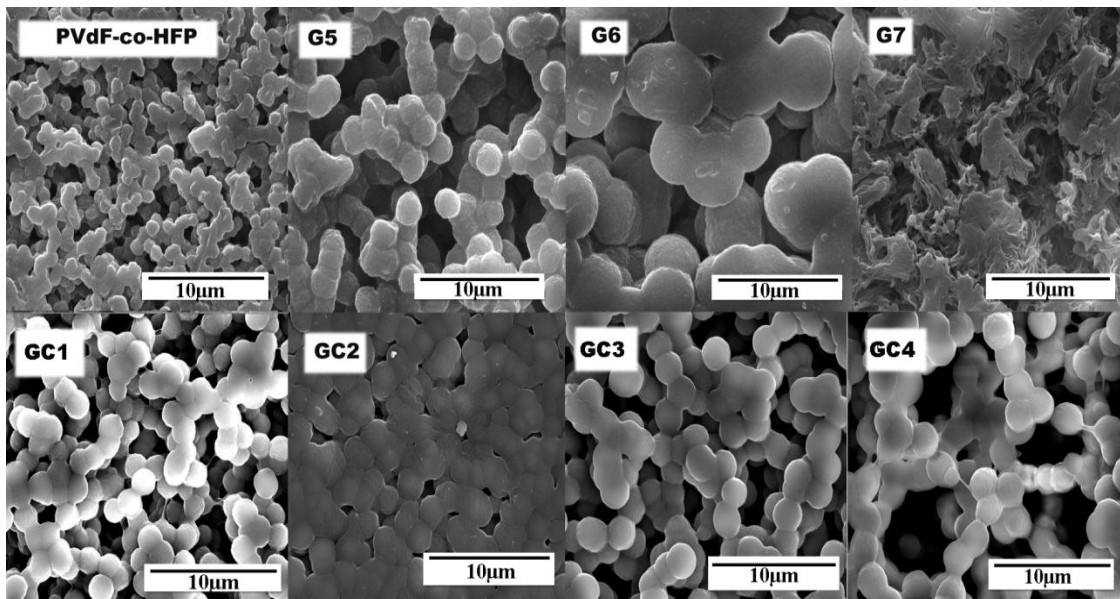
CI plot of SPEs G5-85:15, G6 - 82:18, G7 - 80:20 of PVdF-co-HFP + LiTFSI, 3A.3b CI plot of GPEs GA2 85:15, GB2 - 82:18, GC2 - 80:20 ratio of PVdF-co-HFP : LiTFSI (40 wt%) + EC /PC (60 wt%) at room temperature



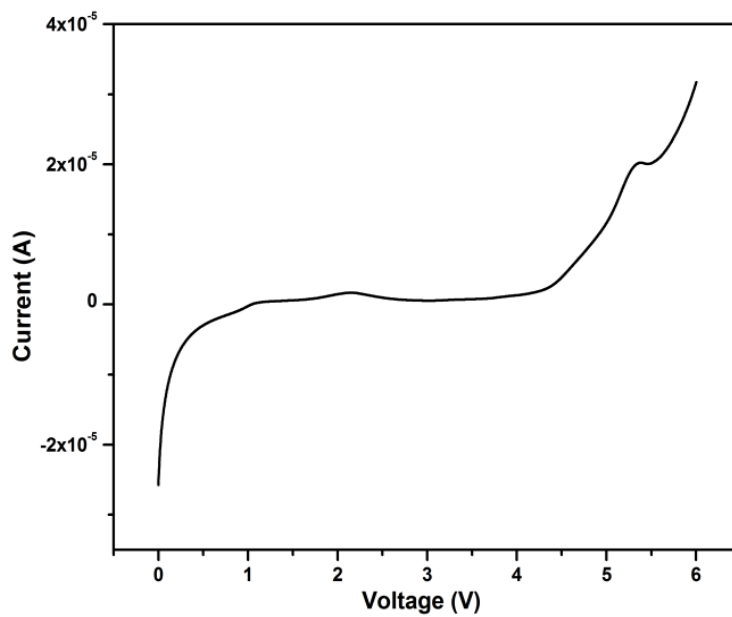
Arrhenius plots of SPEs G5-85:15, G6 - 82:18, G7 – 80:20 of PVdF-co-HFP + LiTFSI, GPEs GA2-85:15, GB2 - 82:18, GC2 – 80:20 ratio of PVdF-co-HFP : LiTFSI (40 wt%) + EC /PC (60 wt%)



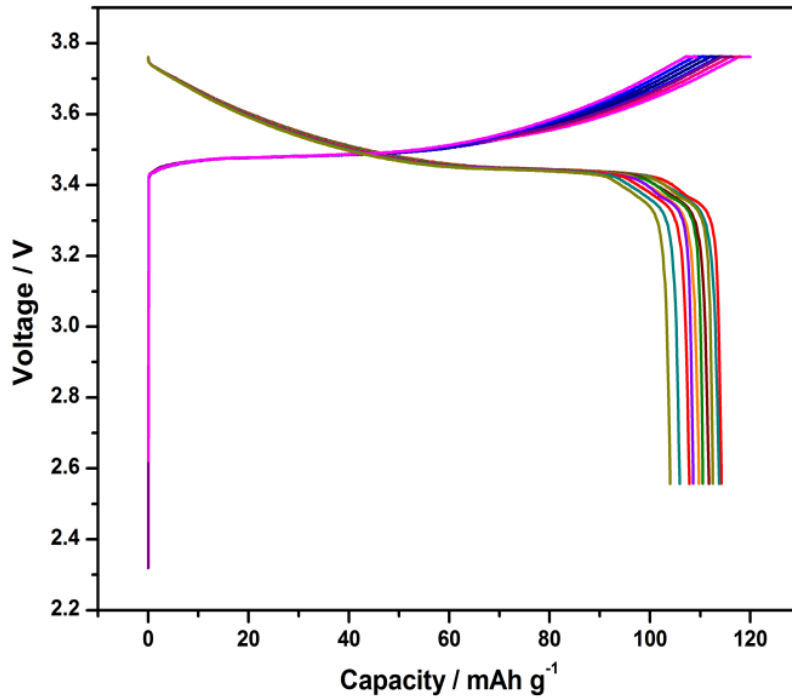
TG graph of G7 - PVdF-co-HFP (80 wt%) + LiTFSI (20 wt%), GPEs GA2 -85:15, GB2 - 82:18, GC2 – 80:20 ratio of PVdF-co-HFP : LiTFSI (40 wt%) + EC /PC (60 wt%)



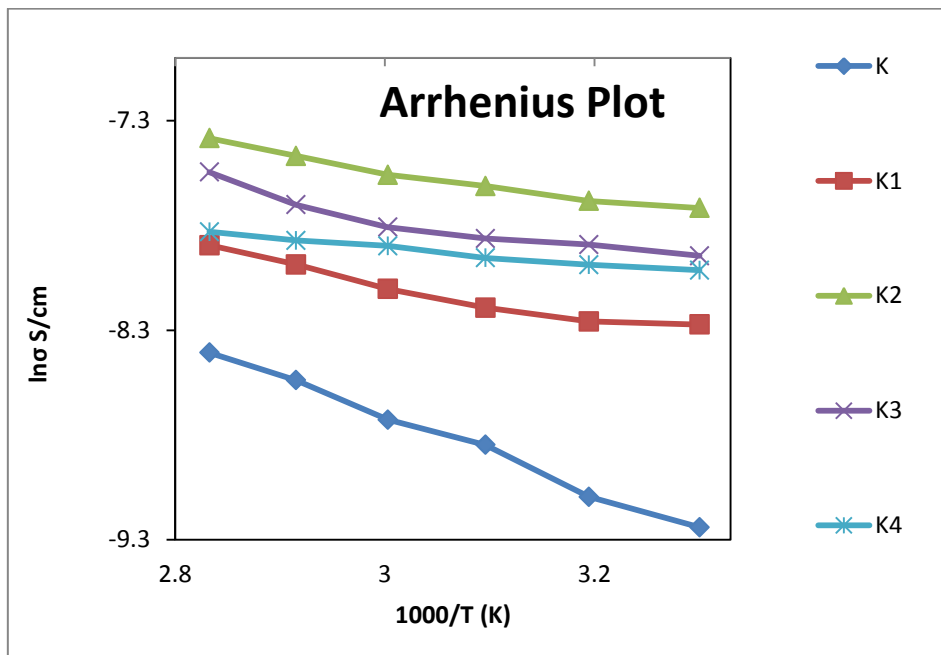
SEM image of SPEs G5-85:15, G6 - 82:18, G7 – 80:20 ratio of PVdF-co-HFP + LiTFSI, GPEs PVdF-co-HFP (30 wt%) + LiTFSI (10 wt%) + EC+PC (GC1-55, GC2-60, GC3=65, GC4=70 wt%)



Linear sweep voltammetry of GC2 - PVdF-co-HFP (30 wt%) + LiTFSI (10 wt%) + EC /PC (60 wt%)



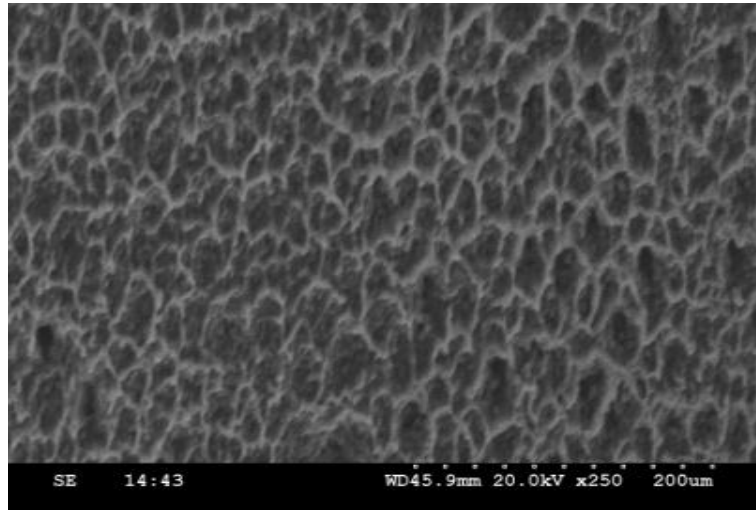
Charge discharge profile of GC2 - PVdF-co-HFP (30 wt%) + LiTFSI (10 wt%) + EC /PC (60 wt%)



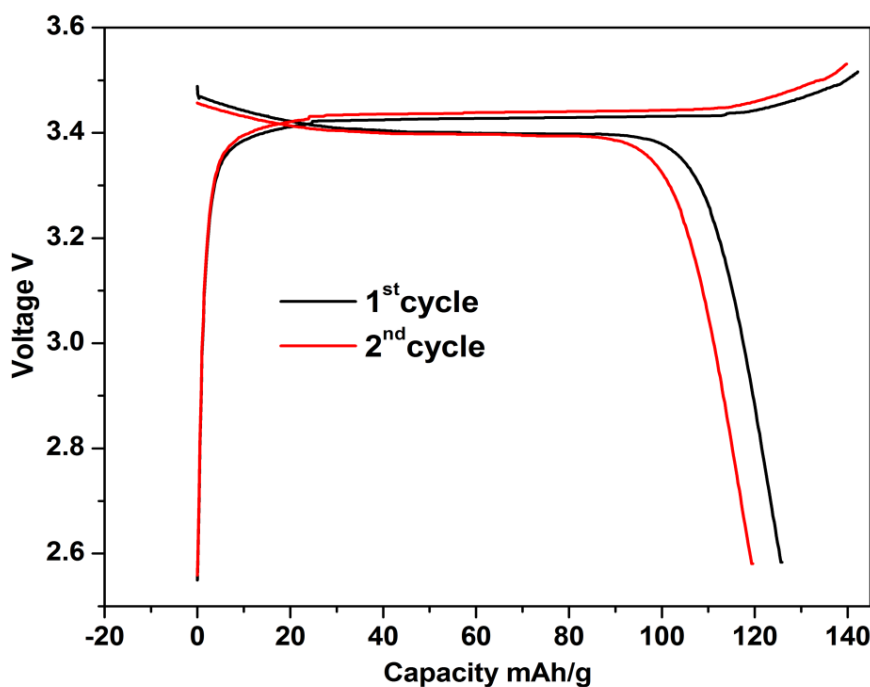
Temperature depended conductivity plot of PVdF-co-HFP (32%) + LiTFSI (8%) + EC+PC (60%) + ZrO₂(0%, 3%, 6%, 9%, 12%)

| Sample code | Ionic Conductivity value $\times 10^{-3}$ S/cm at | | | | | | E_a values eV |
|-------------|---|------|------|------|------|------|-----------------|
| | 303K | 313K | 323K | 333K | 343K | 353K | |
| K | 0.97 | 1.11 | 1.43 | 1.62 | 1.95 | 2.23 | 0.235 |
| K1 | 2.55 | 2.59 | 2.77 | 3.03 | 3.4 | 3.73 | 0.219 |
| K2 | 4.46 | 4.61 | 4.95 | 5.22 | 5.71 | 6.21 | 0.213 |
| K3 | 3.55 | 3.74 | 3.85 | 4.06 | 4.52 | 5.29 | 0.223 |
| K4 | 3.31 | 3.4 | 3.51 | 3.72 | 3.82 | 3.97 | 0.228 |

Conductivity values and activation energy of the prepared electrolyte samples PVdF-co-HFP(32%) + LiTFSI (8%) + EC+PC (60%) + ZrO₂(0%, 3%, 6%, 9%, 12%)



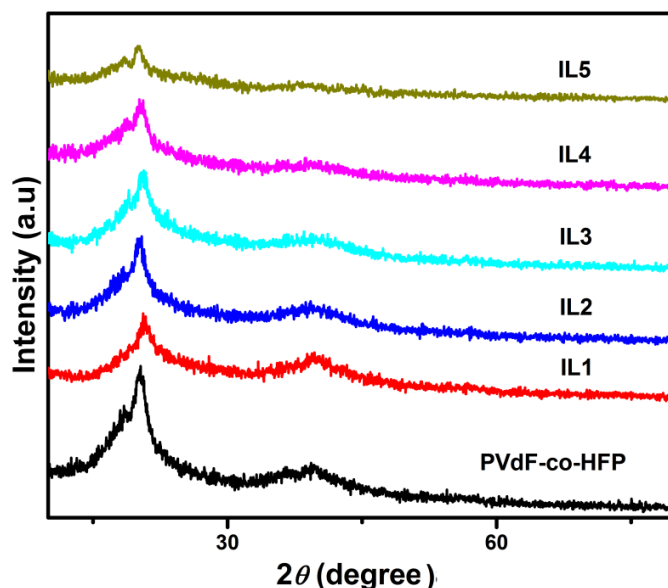
SEM image of K2 at $\times 250$



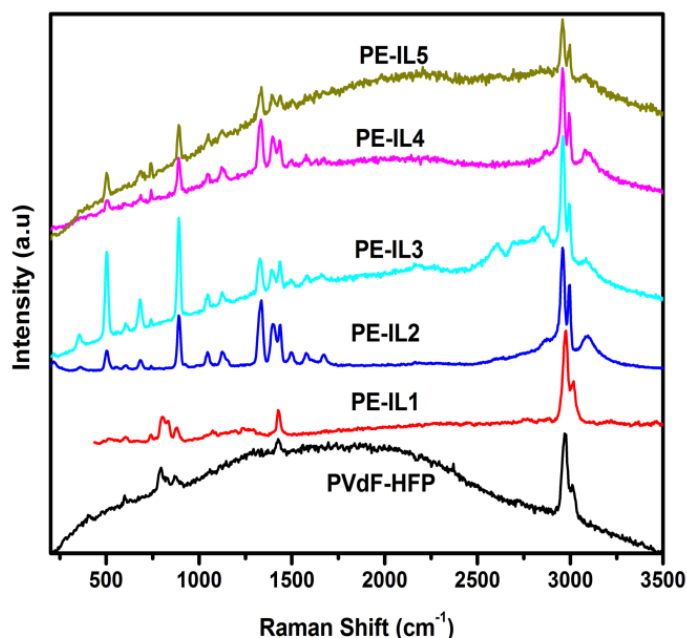
Charge discharge profile of PVdF-co-HFP(32%) + LiTFSI (8%) + EC+PC (60%) + ZrO₂ (6%)

The ionic liquid has unique property such as higher ionic conductivity, non-flammable, non-volatile and low vapour pressure. In general, ionic liquid has high ionic conductivity as well as high thermal stability and used as an electrolyte medium in many electrochemical devices. In the view of attaining higher conductivity with environmental friendly nature, the sulfonium ionic liquid SET₃TFSI has been chosen in place of alkali metal salt. Five different combinations of PVdF-co-HFP and SET₃TFSI have been prepared using solution casting technique. Among them, 75:25 wt% of PVdF-co-HFP and SET₃TFSI has higher ionic conductivity of 6.93×10^{-5} S/cm at room temperature. It is found that higher the IL content, higher the conductivity, which is due to more amount of charge carriers and produces flexible network. The maximum thermal stability of 240 °C supports the results obtained in the AC impedance studies. The optimized sample PE-IL5 has been subjected for electrochemical studies such as LSV, CV and charge/discharge. The electrolyte decomposition has been observed around 4.4V, which is evidenced from LSV and cyclic

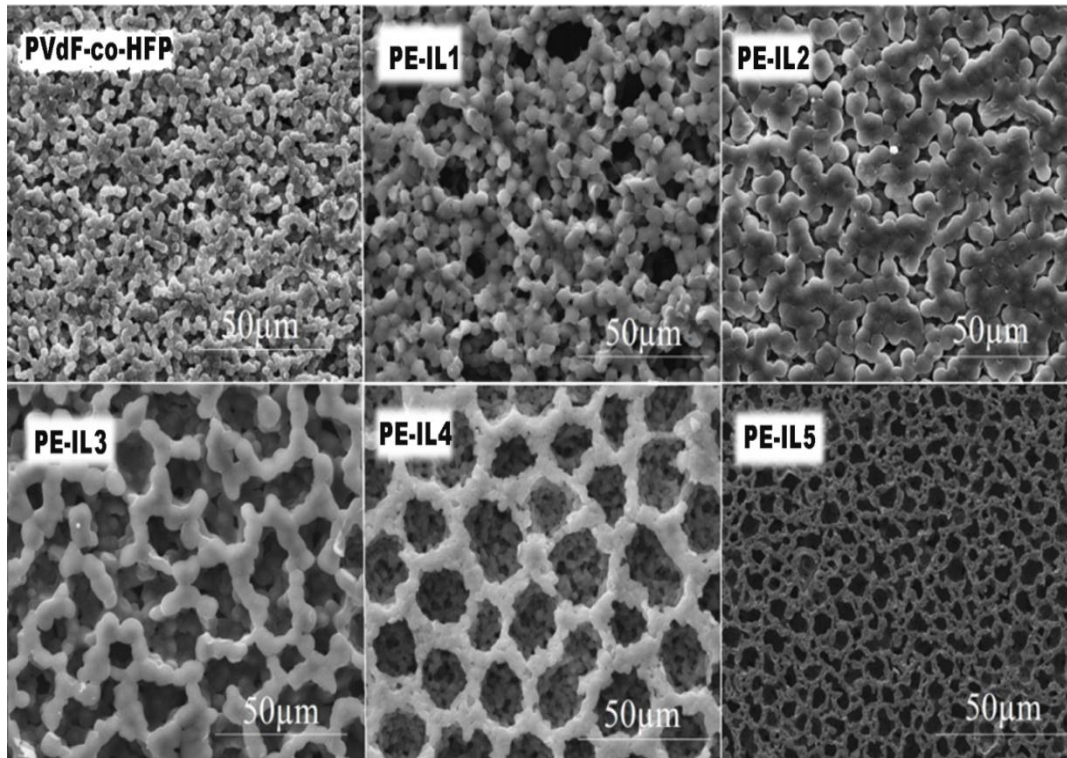
voltammetry provides the electrochemical window of the prepared electrolyte. An appreciable discharge capacity of 133 mAh/g has also been obtained for PE-IL5 electrolyte containing Li/LiFePO₄ cell couple up to ten cycles.



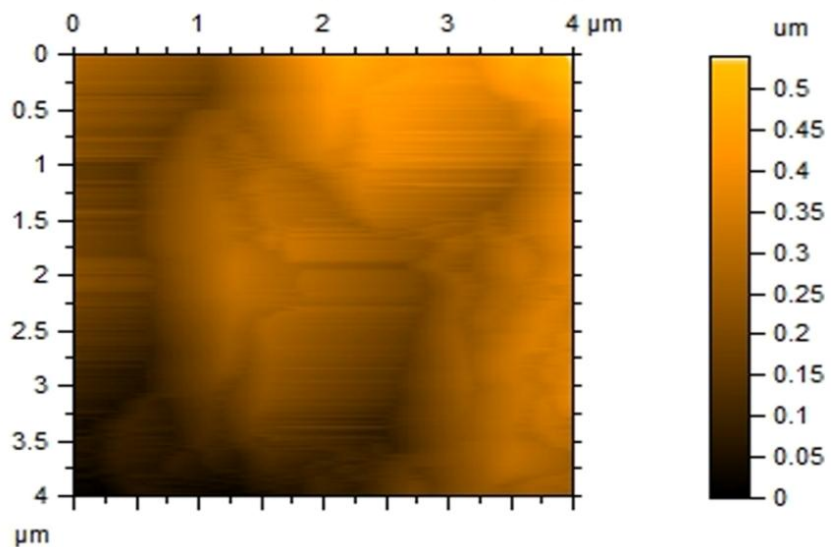
X-ray diffraction patterns of pure P(VdF-co-HFP), PE-IL1-95:5, PE-IL2-90:10, PE-IL3- 85:15, PE-IL4-80:20, PE-IL5-75:25 ratio of P(VdF-co-HFP) : SET₃TFSI



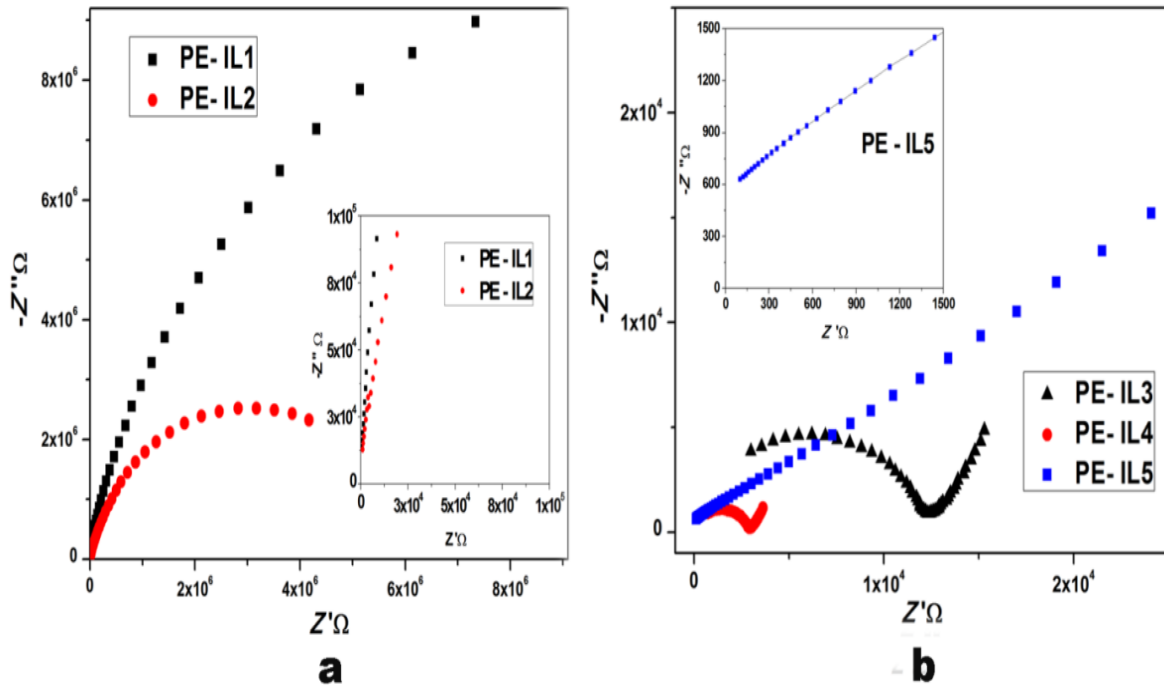
Raman spectra of pure PVdF-co-HFP, pure P(VdF-co-HFP), PE-IL1-95:5, PE-IL2-90:10, PE-IL3- 85:15, PE-IL4-80:20, PE-IL5-75:25 ratio of P(VdF-co-HFP) : SET₃TFSI



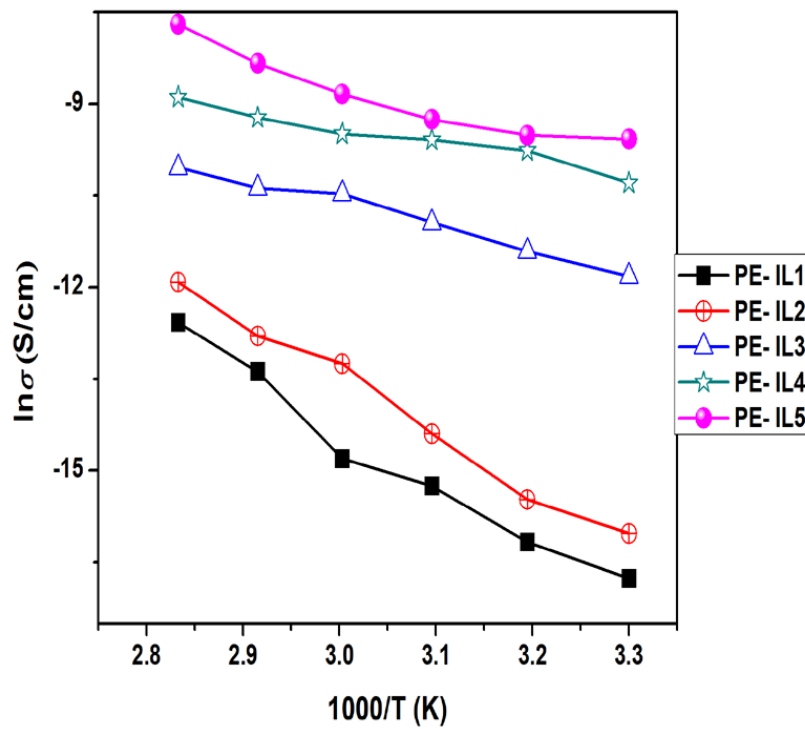
SEM images of pure P(VdF-co-HFP), PE-IL1-95:5, PE-IL2-90:10, PE-IL3- 85:15, PE-IL4-80:20, PE-IL5-75:25 ratio of P(VdF-co-HFP) : SEt₃TFSI with the magnification of 1 K.



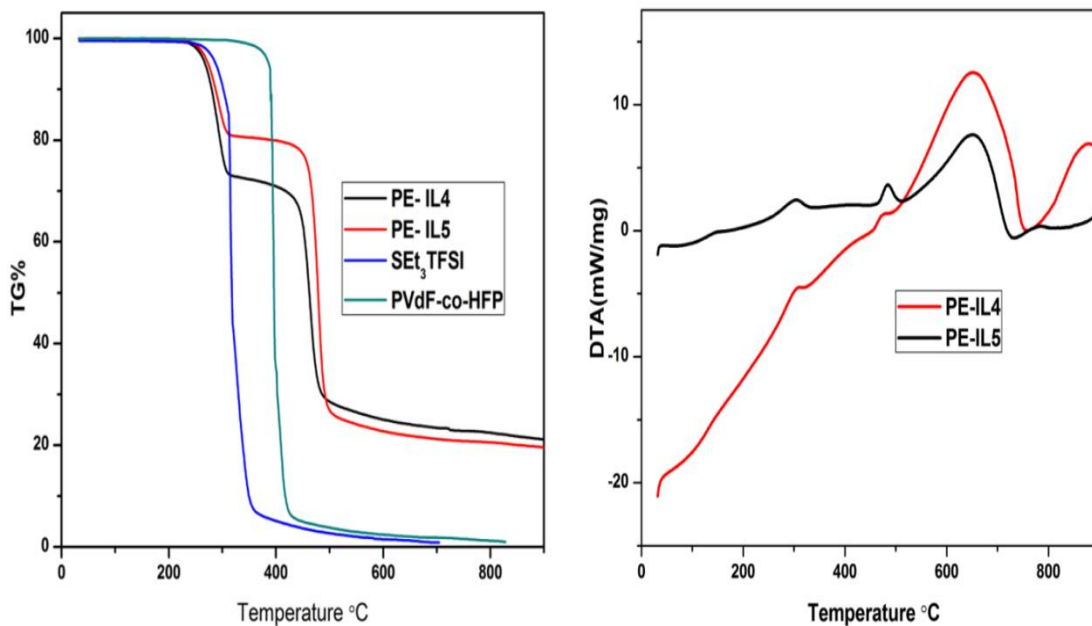
AFM image of PE-IL5-PVdF-co-HFP : SEt₃TFSI (75:25) wt%



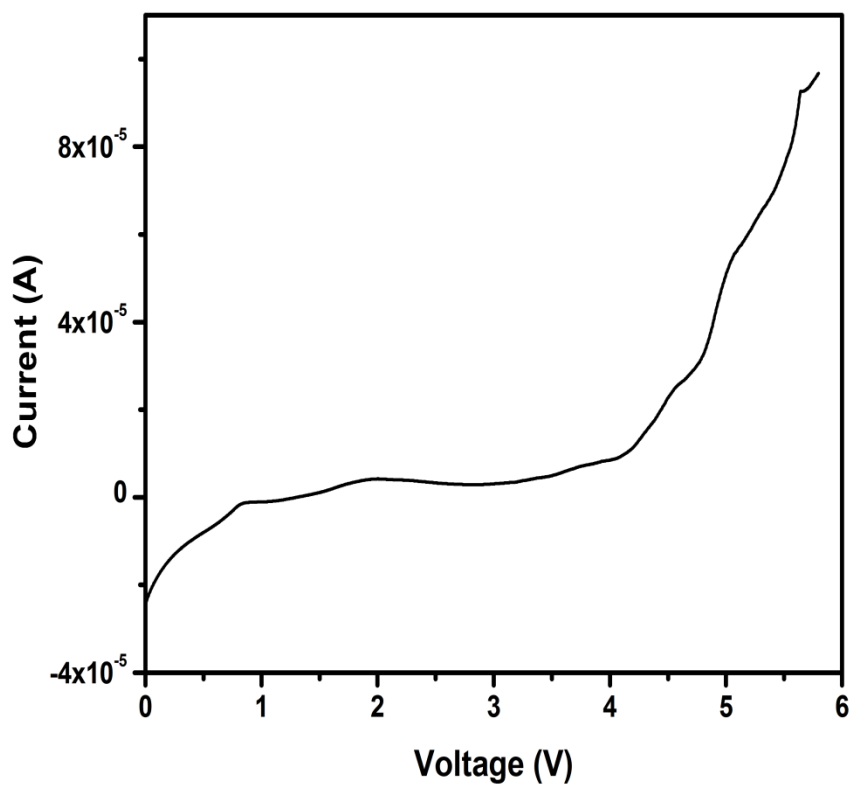
Room temperature complex impedance plot of PEs namely, PE-IL1-95:5, PE-IL2-90:10, PE-IL3-85:15, PE-IL4-80:20, PE-IL5-75:25 ratio of P(VdF-co-HFP) : SET₃TFSI



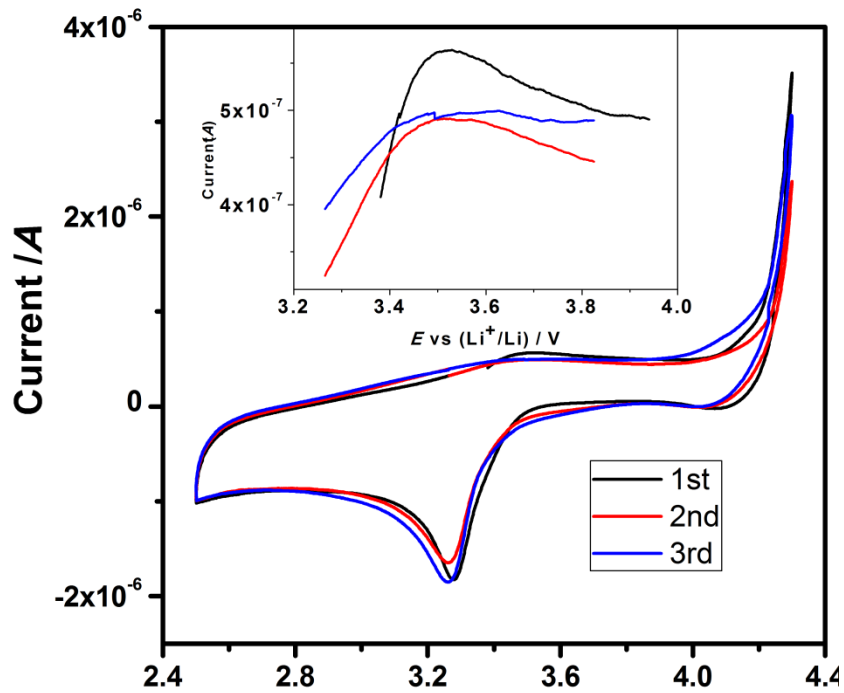
Temperature-dependent ionic conductivity plot



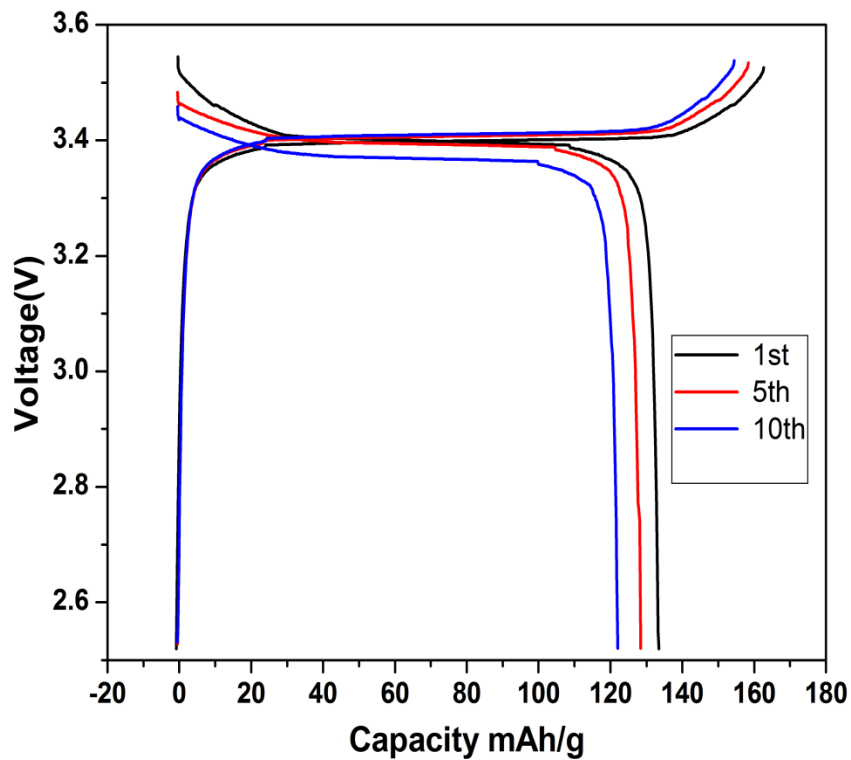
TG/DTA plot for the PEs namely PE-IL4- PVdF-co-HFP : SEt₃TFSI (80:20) and PE-IL5-PVdF-co-HFP : SEt₃TFSI (75:25) wt%



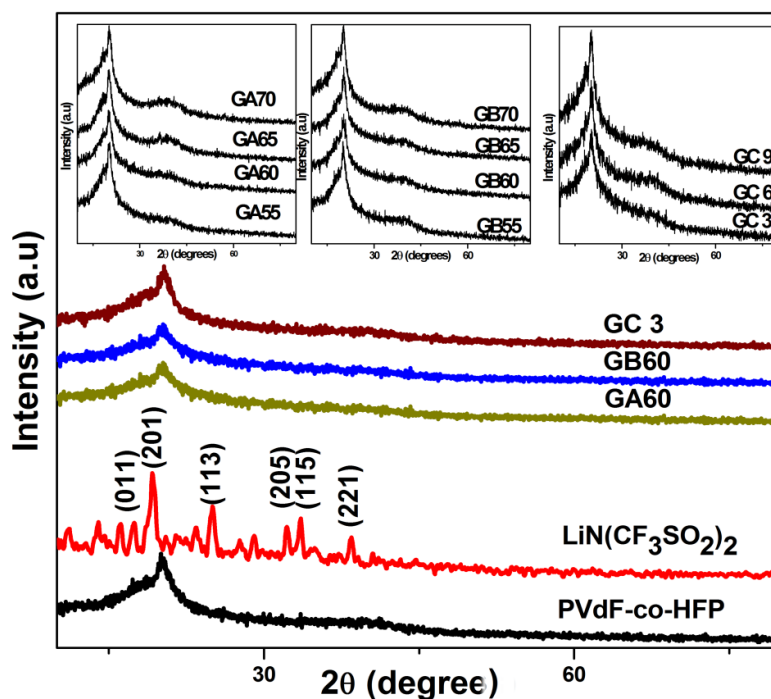
LSV of the coin cell containing PE-IL5 - PVdF-co-HFP : SEt₃TFSI (75:25) wt% and Li anode as well as Li cathode recorded at a scan rate of 5 mV/s



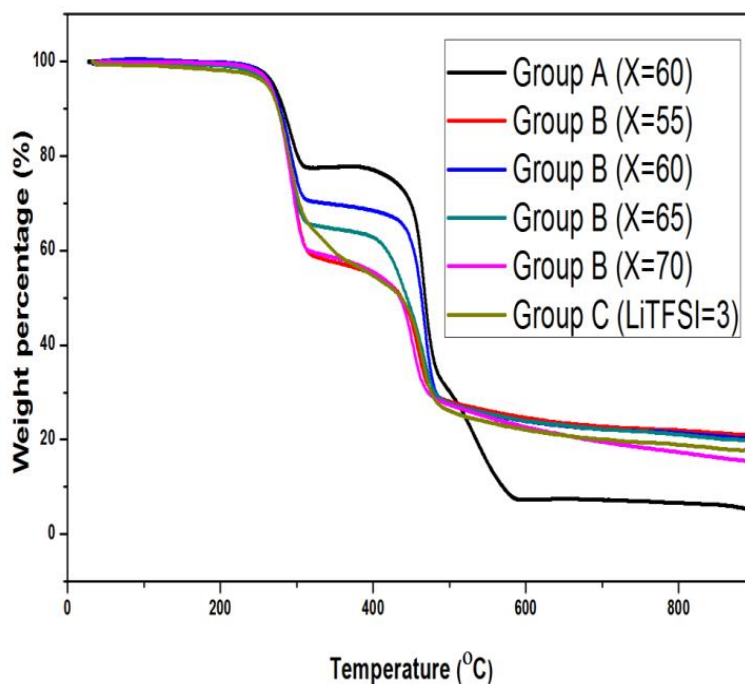
CV of the coin cell containing PE-IL5-PVdF-co-HFP : SEt3TFSI (75:25) wt% and Li anode as well as Li cathode recorded at a scan rate of 5 mV/s



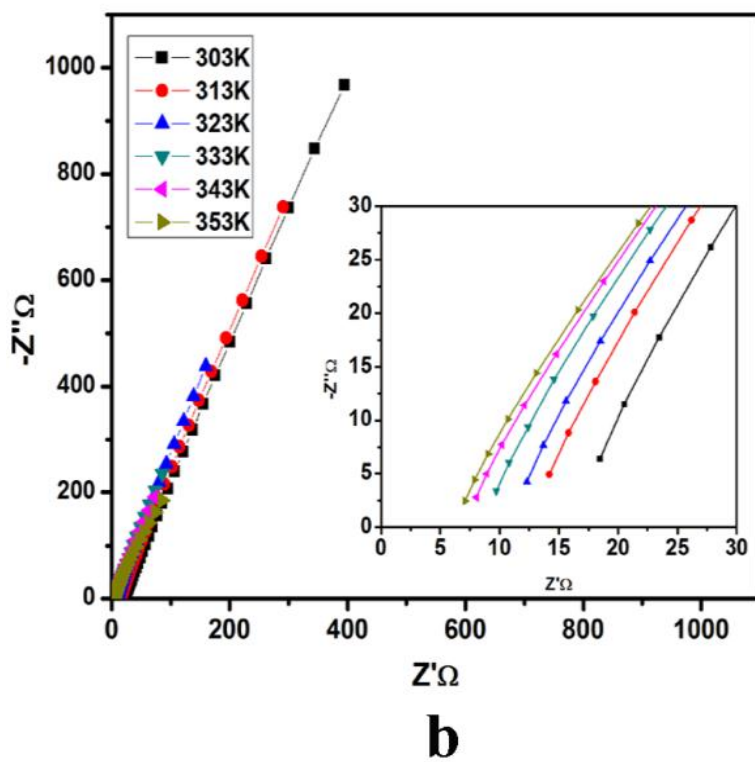
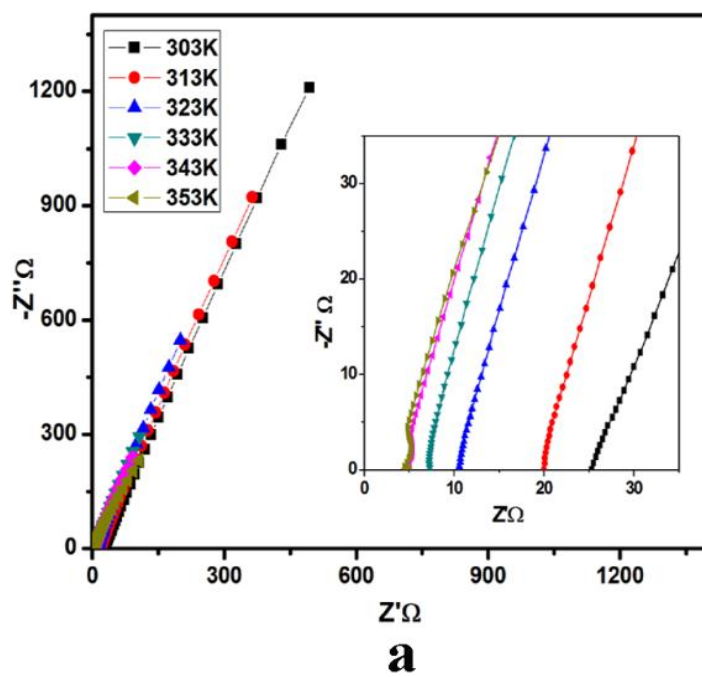
Charge-discharge characteristics of the coin cell containing PE-IL5-PVdF-co-HFP : SEt3TFSI (75:25) wt% and LiFePO_4 as the cathode and Li as the anode

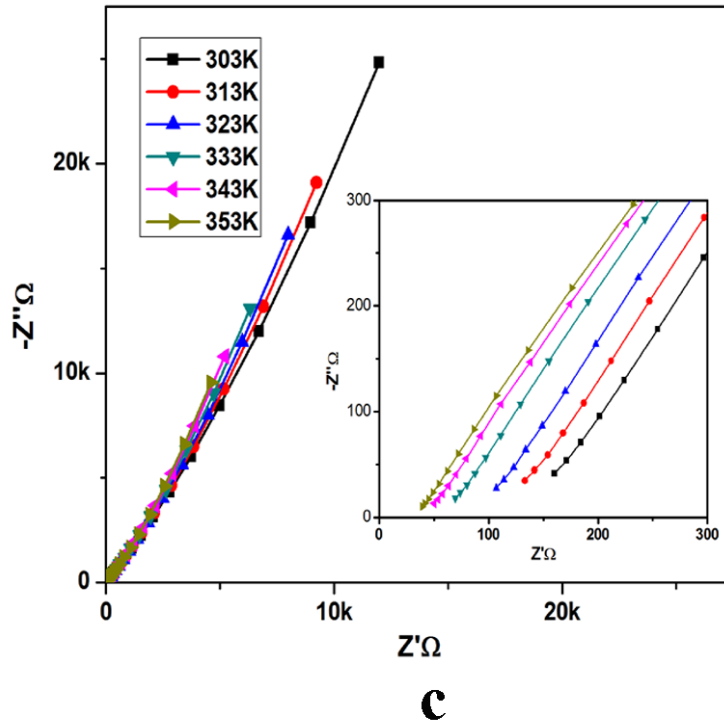


XRD diffraction pattern of pure PVdF-co-HFP, LiTFSI, Group A PVdF-co-HFP (80) + SEt₃TFSI (20) +EC/PC (X= 55, 60, 65, 70) wt%, Group B PVdF-co-HFP (75) + SEt₃TFSI (25) +EC/PC (X= 55, 60, 65, 70)wt%, Group C PVdF-co-HFP (75) + SEt₃TFSI (25) +EC/PC (60) + LiTFSI (X= 3, 6, 9)wt%

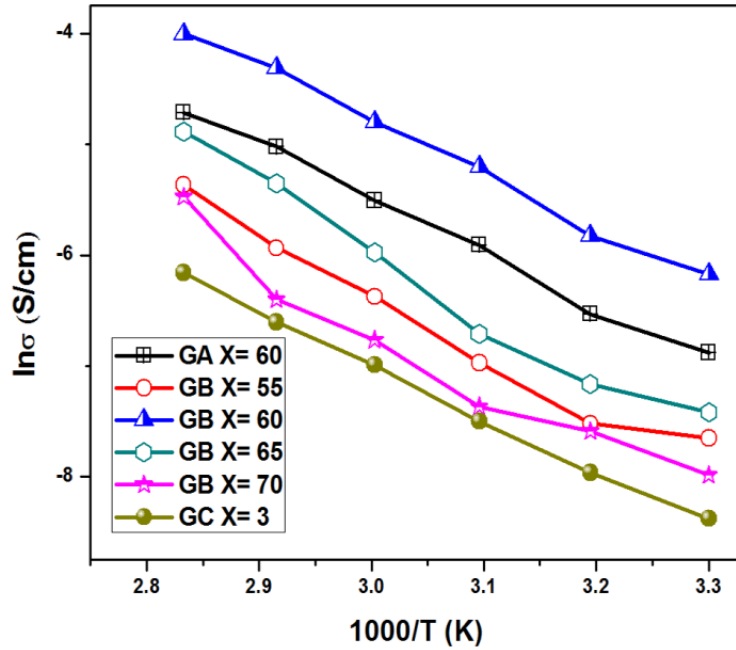


Thermo gravimetric plot for Group A PVdF-co-HFP (80) + SEt₃TFSI (20) +EC/PC (60) wt%, Group B PVdF-co-HFP (75) + SEt₃TFSI (25) +EC/PC (X= 55, 60, 65, 70)wt%, Group C PVdF-co-HFP (75) + SEt₃TFSI (25) +EC/PC (60) + LiTFSI(3)wt%

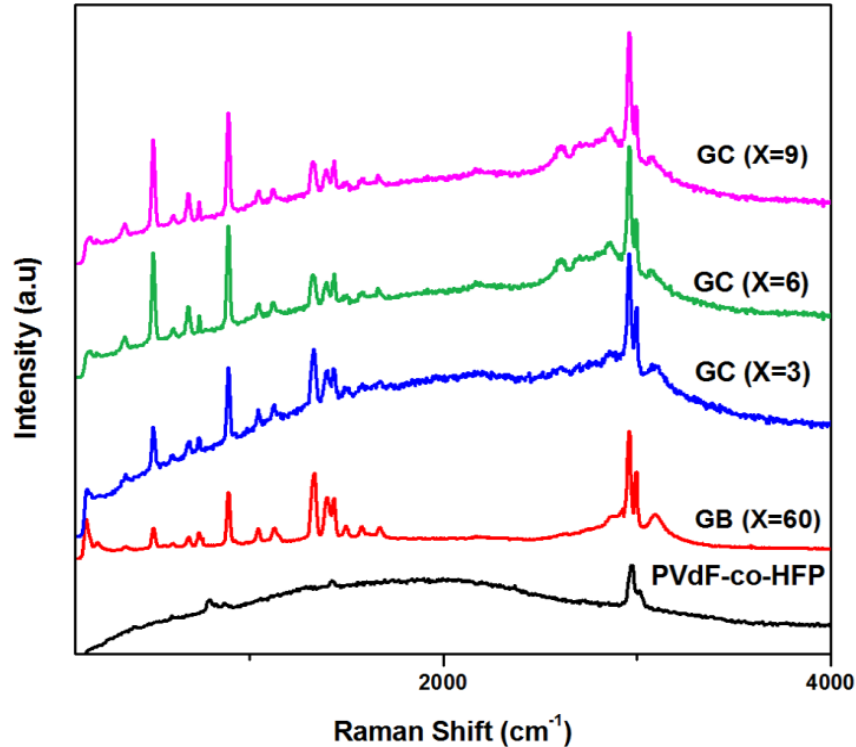




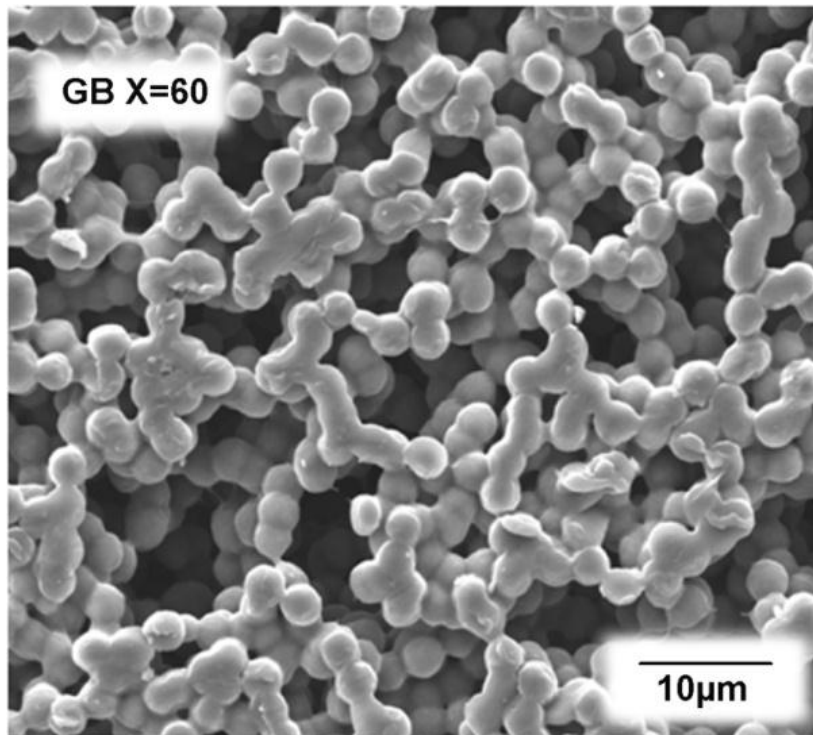
- (a) The complex impedance plot for Group A - PVdF-co-HFP (80) - SET₃TFSI (20) – EC+PC (60) wt%, 3.(b) Group B - PVdF-co-HFP (75) - SET₃TFSI (25) – EC+PC (60) wt%
- (b) The complex impedance plot for Group A - PVdF-co-HFP (80) - SET₃TFSI (20) – EC+PC (60) wt%, 3.(b) Group B - PVdF-co-HFP (75) - SET₃TFSI (25) – EC+PC (60) wt%
- (c) The complex impedance plot for Group C - PVdF-co-HFP (75) - SET₃TFSI (25) – EC+PC (60) + LiTFSI (3)wt%



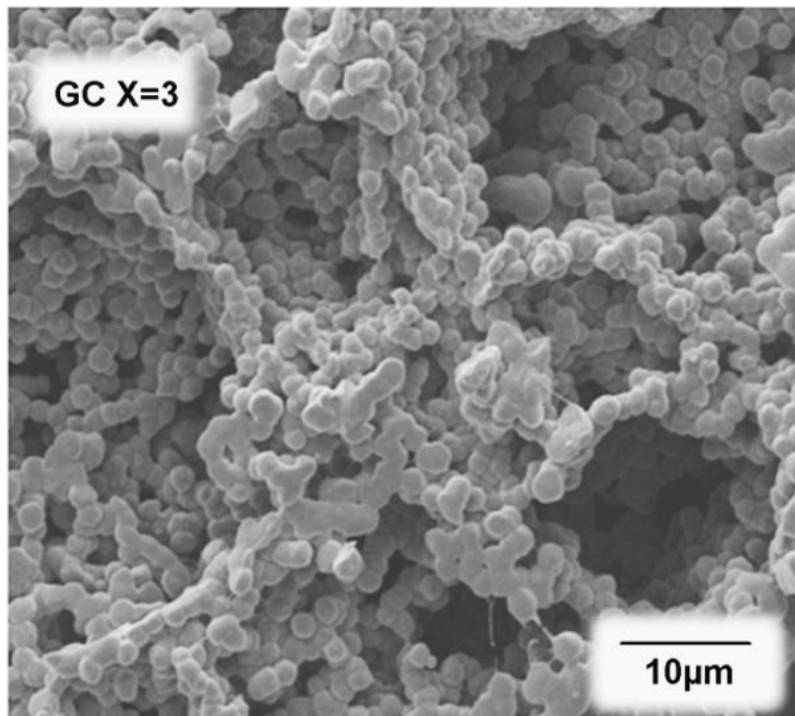
The temperature dependent ionic conductivity plot for Group A PVdF-co-HFP (80) + SEt₃TFSI (20) +EC/PC (60) wt%, Group B PVdF-co-HFP (75) + SEt₃TFSI (25) +EC/PC (X= 55, 60, 65, 70) wt%, Group C PVdF-co-HFP (75) + SEt₃TFSI (25) +EC/PC (60) + LiTFSI(3) wt%



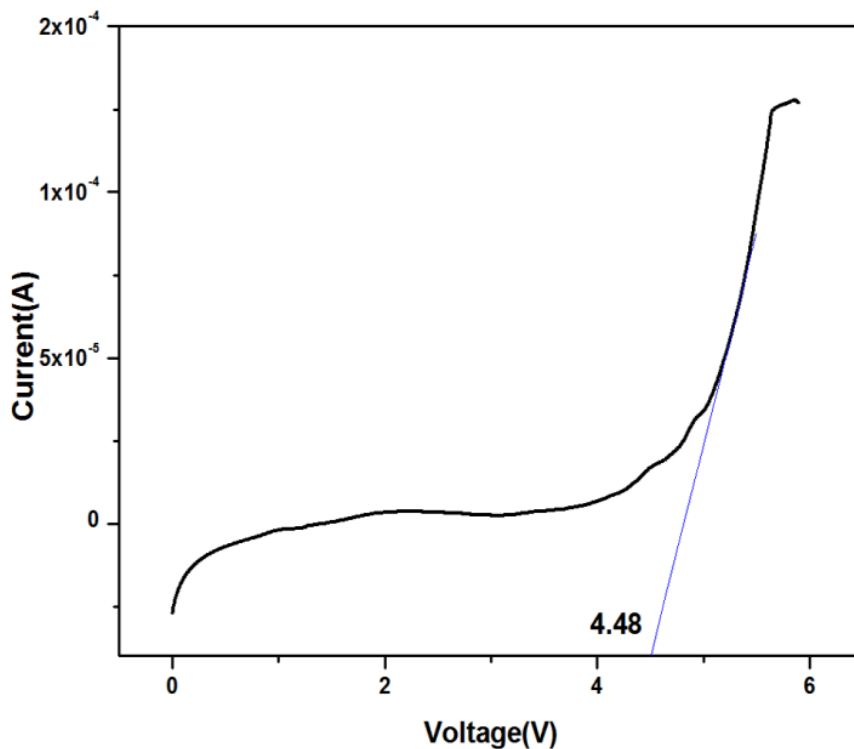
Raman spectra for pure PVdF-co-HFP, Group B P(VdF-co-HFP)/SEt₃TFSI (75:25) + EC/PC (60) wt%, Group C P(VdF-co-HFP)/SEt₃TFSI (75:25) + EC/PC (60) + LiTFSI (3, 6, 9)wt%



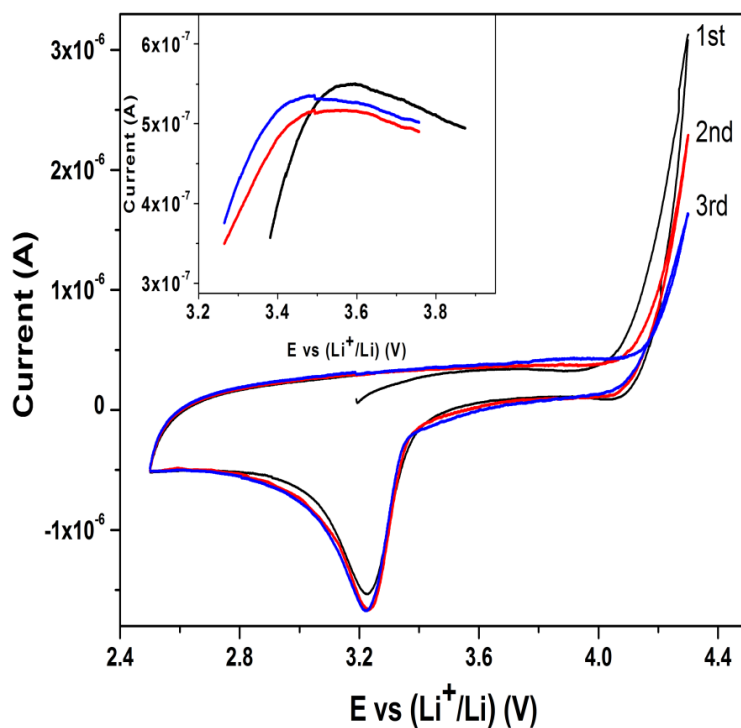
(a) Scanning electron microscopic images taken for GB X = PVdF-co-HFP (75) + SET₃TFSI (25) of (40 wt%) + EC/PC (60) wt%



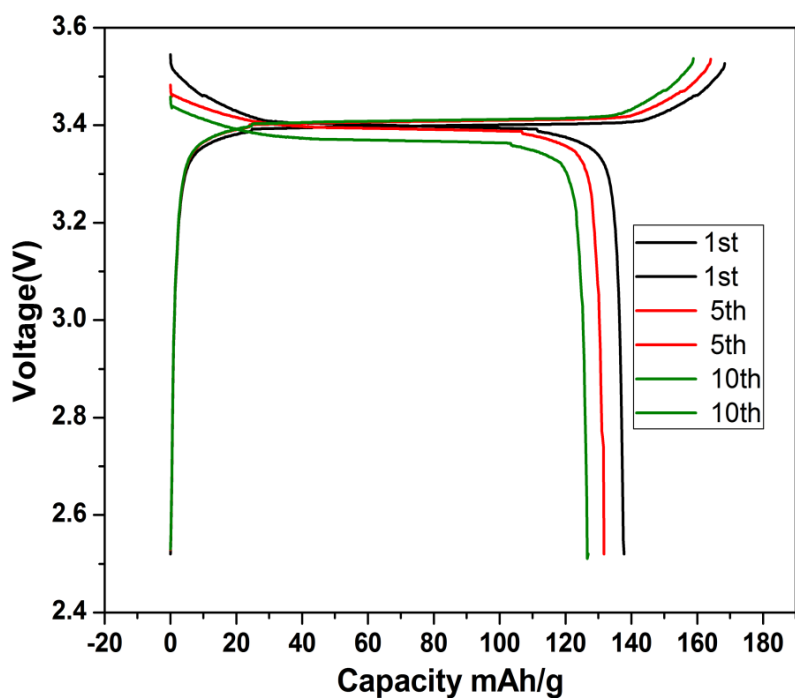
(b) GC X = PVdF-co-HFP (75) + SET₃TFSI (25) of (40 wt%) + EC/PC (60) + LiTFSI (3) wt%



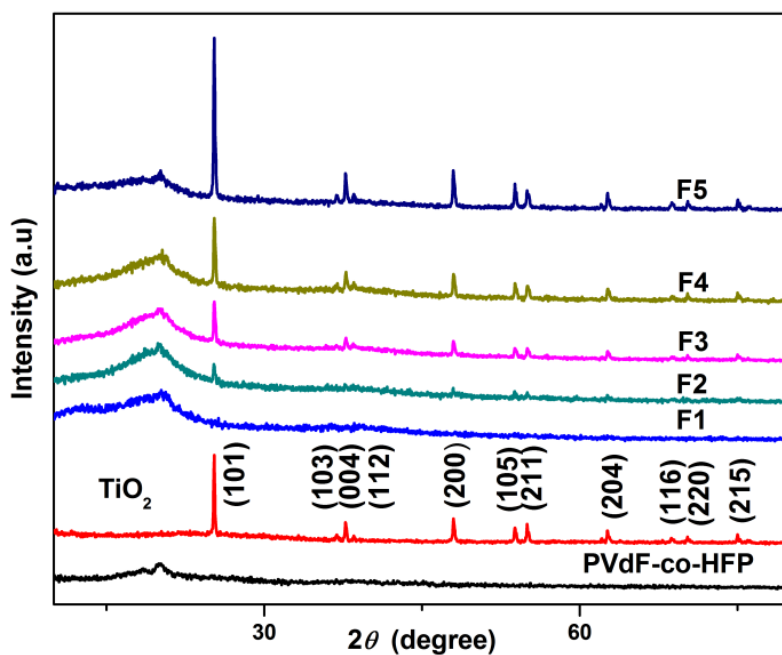
Linear sweep voltammograms (LSV) taken for PVdF-co-HFP (75) + SEt₃TFSI (25) of (40 wt%) +EC+PC (60) wt%



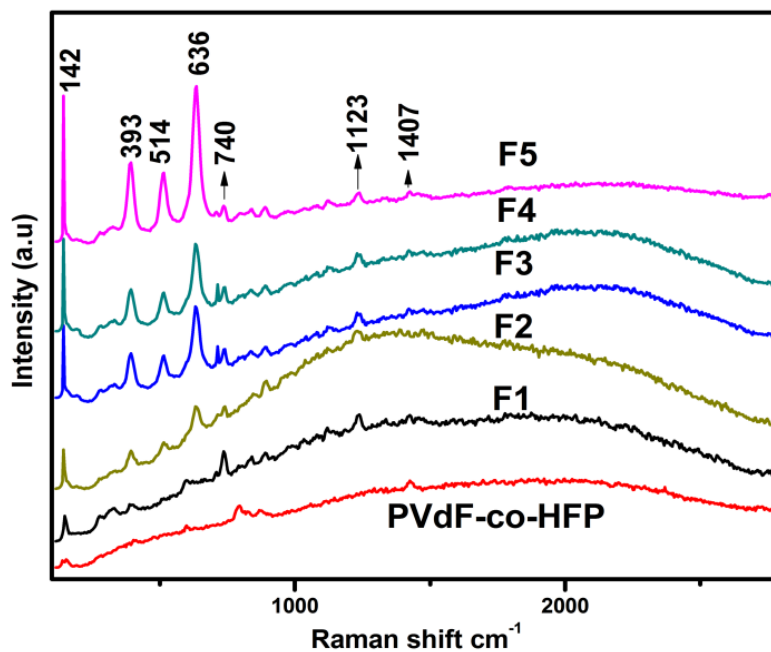
Cyclic voltammograms for PVdF-co-HFP + SEt₃TFSI 75:25 ratio of (40wt%) + EC/PC (60) wt%



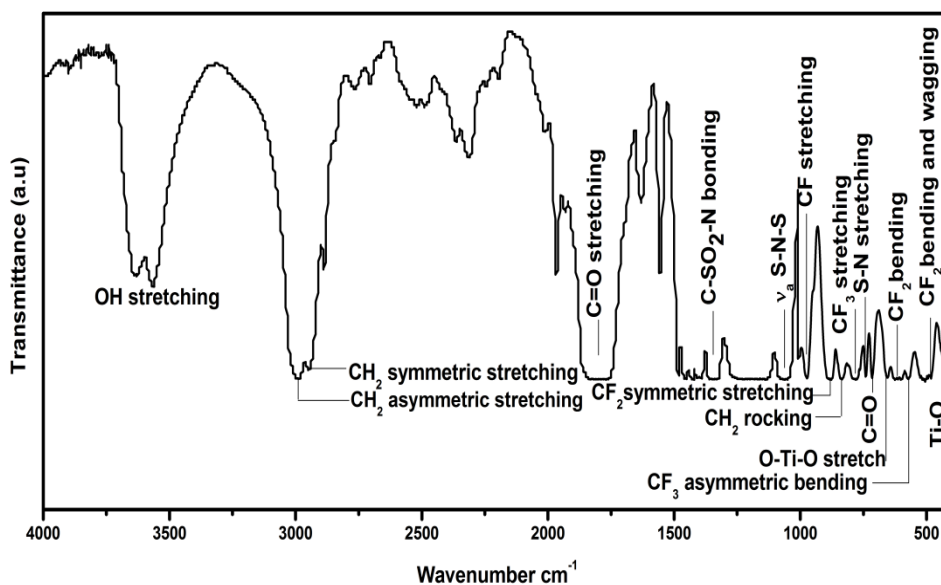
Charge discharge performance of PVdF-co-HFP (75) + SEt₃TFSI (25) of (40 wt%) + EC/PC (60) wt%



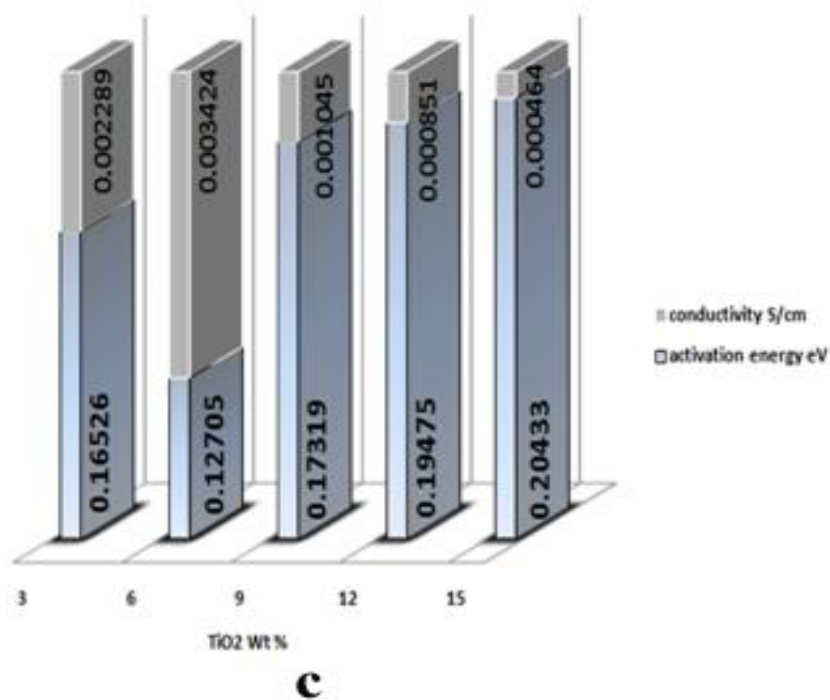
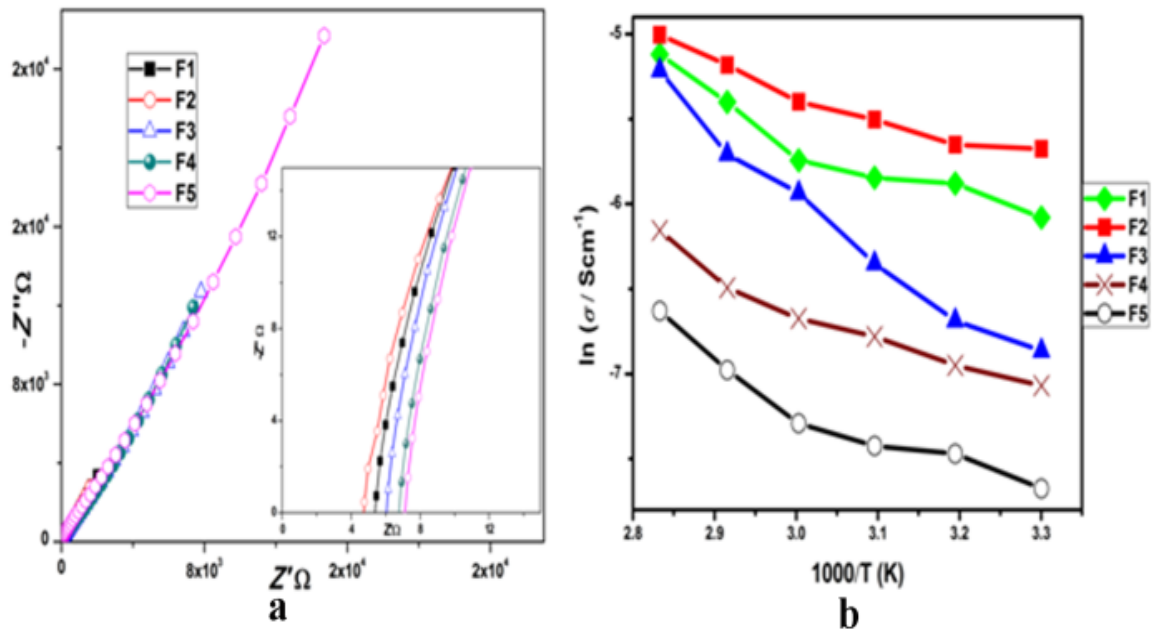
XRD diagram of pure P(VdF-co-HFP), TiO₂, ILCGPE 3(F1), 6(F2), 9(F3), 12(F4) and 15(F5) wt% of TiO₂ based P(VdF-co-HFP) (30) + SEt₃TFSI (10) + EC / PC (60) wt% system



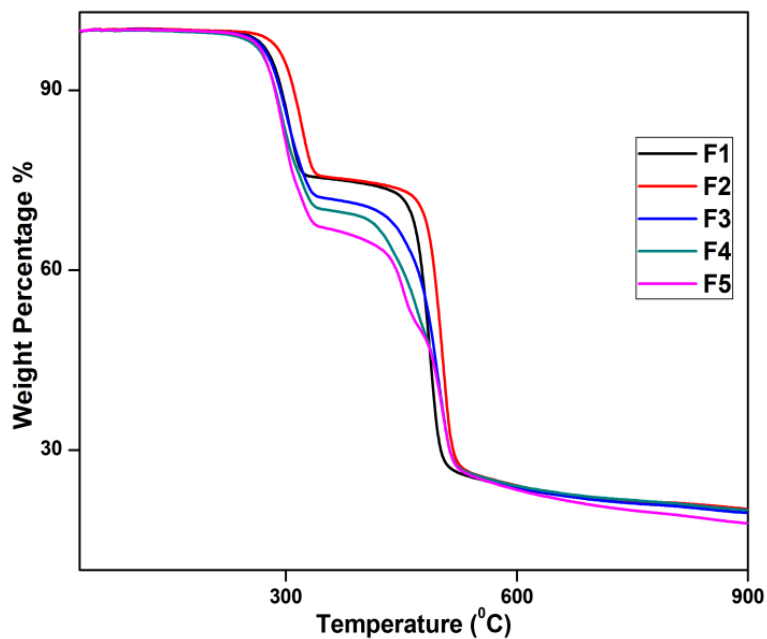
Raman spectra of pure P(VdF-co-HFP), TiO₂, ILCGPE 3(F1), 6(F2), 9(F3), 12(F4) and 15(F5) wt% of TiO₂ based P(VdF - co - HFP) (30) + SEt₃TFSI (10) + EC / PC (60) wt% system



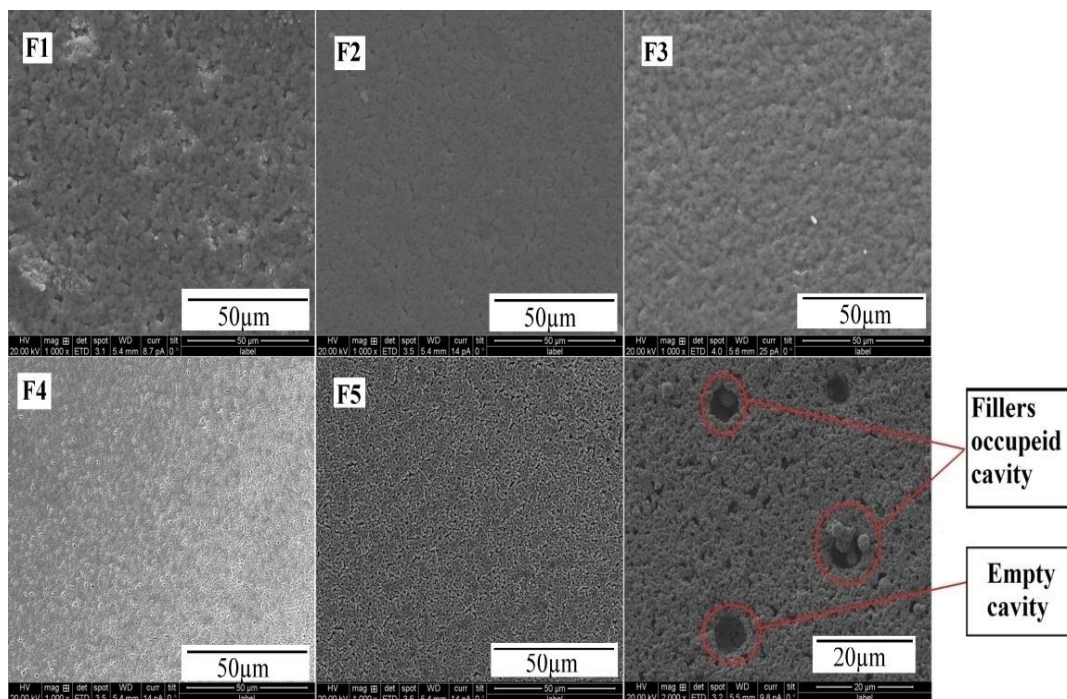
FTIR spectra of F2=P(VdF - co - HFP) (30) + SEt₃TFSI (10) + EC / PC (60) wt% + TiO₂ (6 wt%)



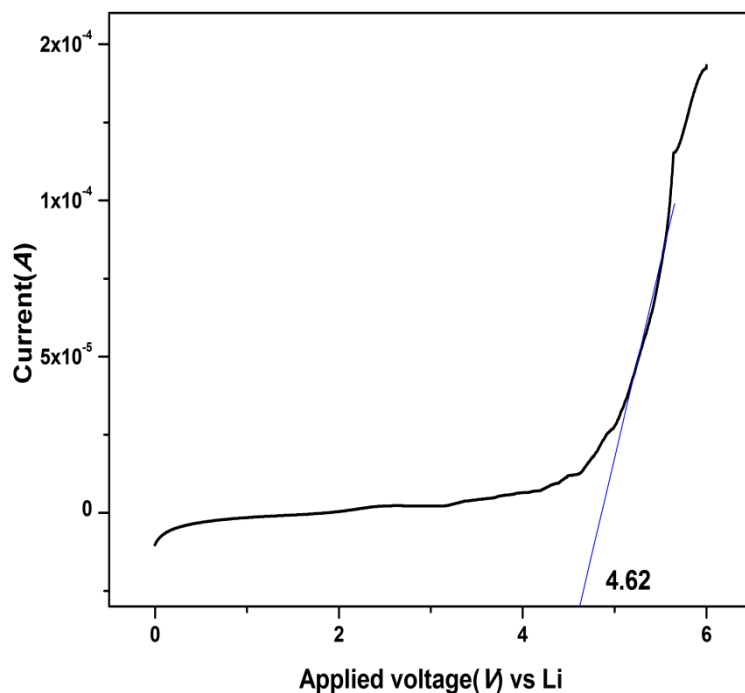
(a) The room temperature complex impedance plot, (b) Arrhenius plot, (c) activation energy (E_a) vs room temperature ionic conductivity of ILCGPE 3(F1), 6(F2), 9(F3), 12(F4) and 15(F5) wt% of TiO₂ based P(VdF - co - HFP) (30) + SEt₃TFSI (10) + EC / PC (60) wt% system



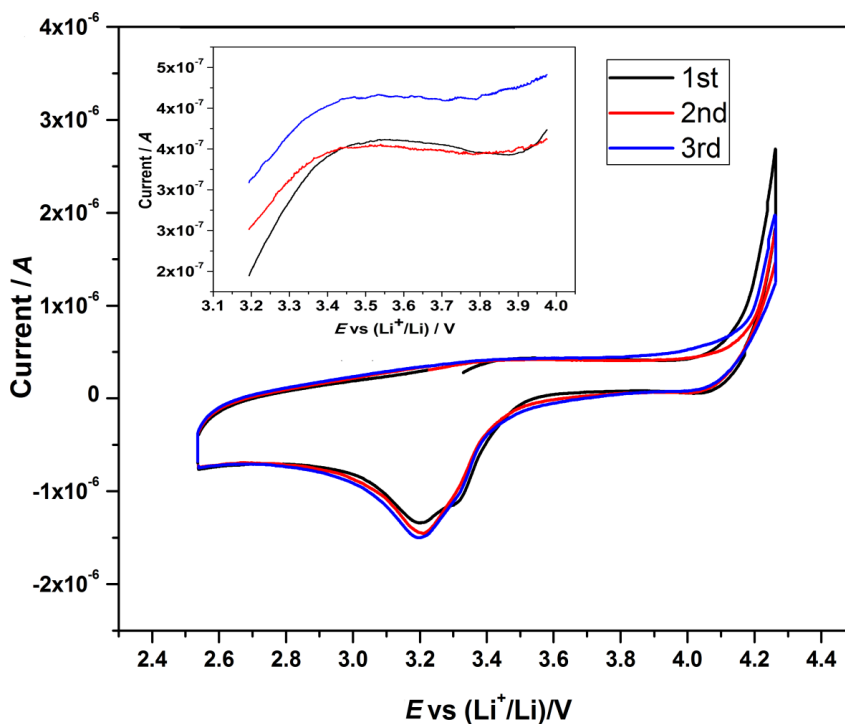
TG graphs of ILCGPE 3(F1), 6(F2), 9(F3), 12(F4) and 15(F5) wt% of TiO₂ based P(VdF - co - HFP) (30) + SET₃TFSI (10) + EC / PC (60) wt% system



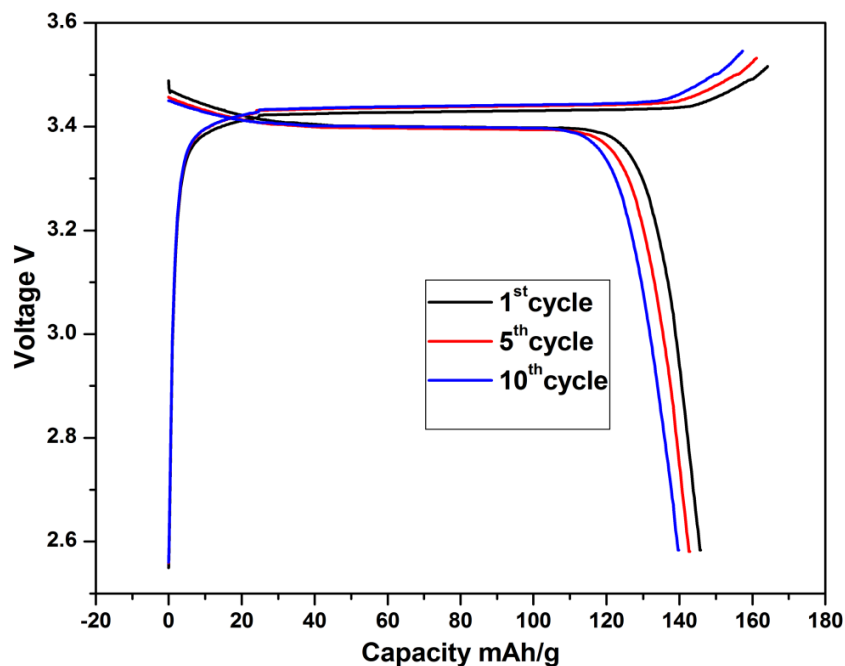
SEM images of ILCGPE 3(F1), 6(F2), 9(F3), 12(F4) and 15(F5) wt% of TiO₂ based P(VdF - co - HFP) (30) + SET₃TFSI (10) + EC / PC (60) wt% system, Last image Less than 1% of TiO₂ (trial sample image)



LSV of the coin cell containing F2-P(VdF - co - HFP) (30) + SEt_3TFSI (10) + EC / PC (60) + TiO_2 (6) wt% and Li anode as well as Li cathode recorded at a scan rate of 5 mV/s

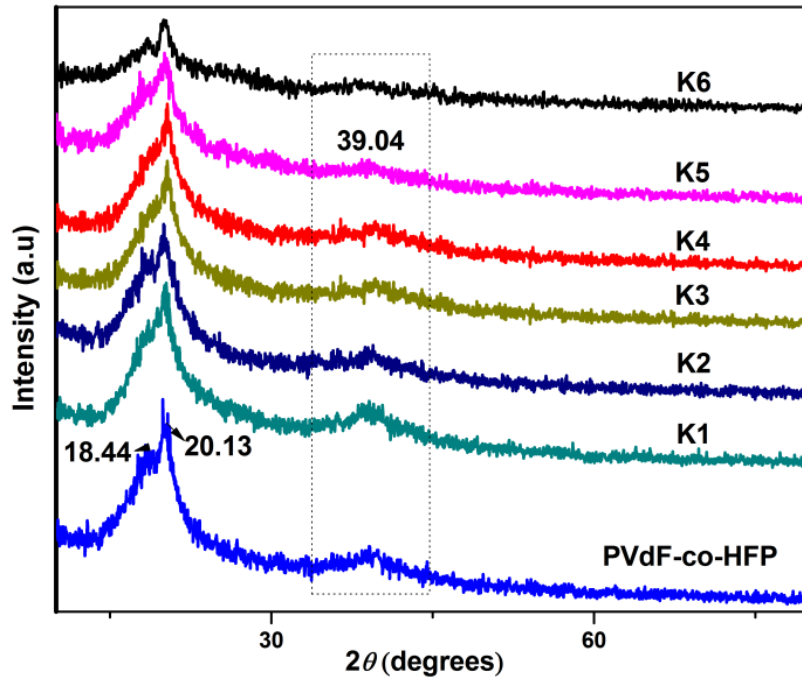


CV of the coin cell containing F2-P(VdF - co - HFP) (30) + SEt_3TFSI (10) + EC / PC (60) + TiO_2 (6) wt% and Li anode as well as Li cathode recorded at a scan rate of 5 mV/s

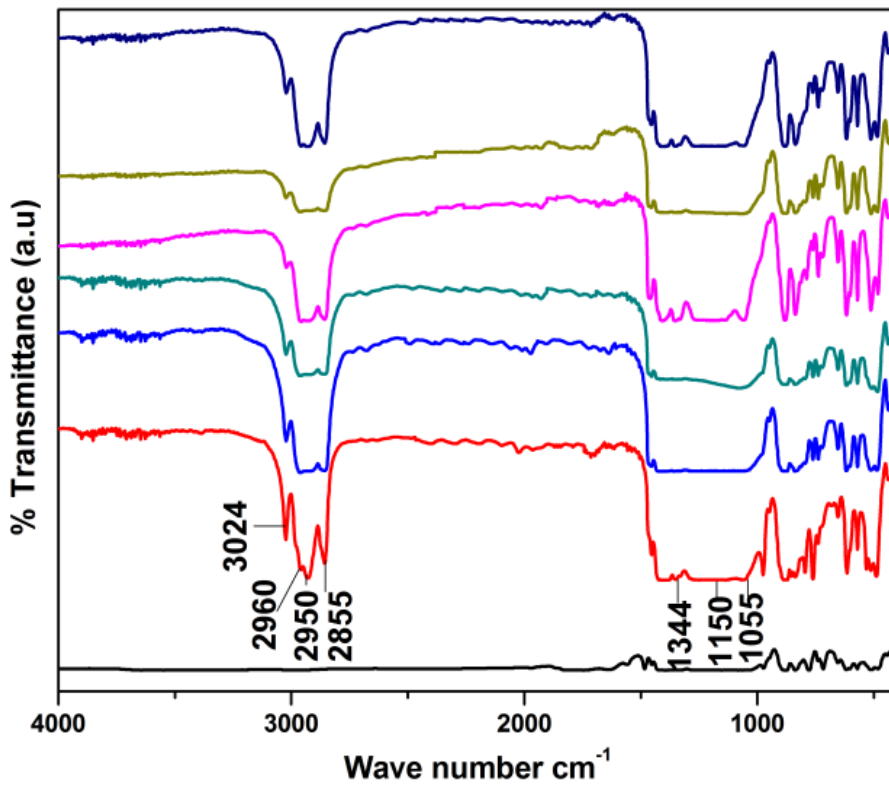


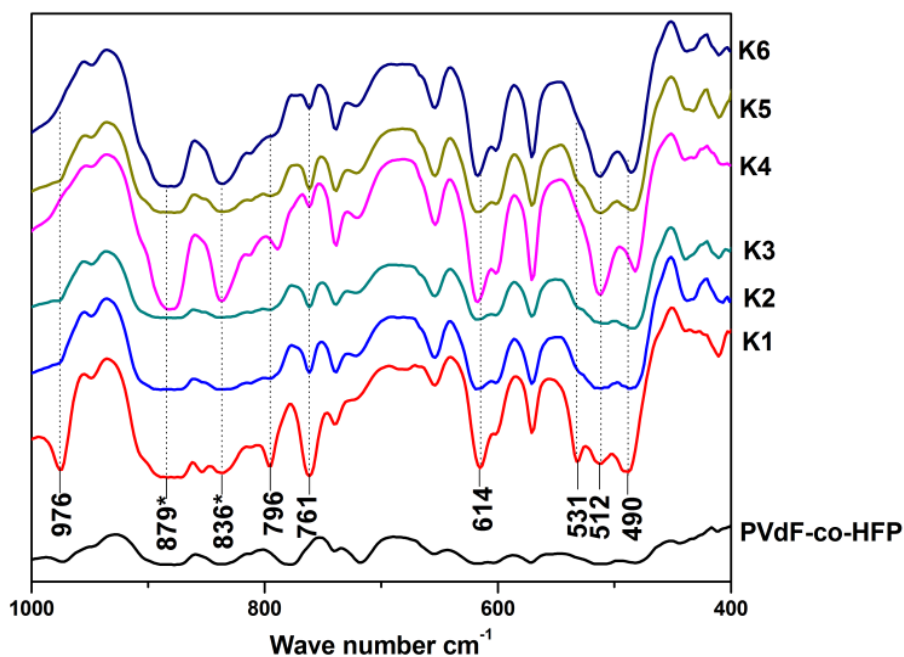
Charge-discharge characteristics of the coin cell containing F2-P(VdF - co - HFP) (30) + SEt₃TFSI (10) + EC / PC (60) + TiO₂ (6) wt% and LiFePO₄ as the cathode and Li as the anode

In view of enhancing the conductivity of the above SPE, an attempt has been made to prepare the polymer electrolyte with different plasticizer ratios with and without LiTFSI salt. The maximum ionic conductivity of 1.12×10^{-3} S/cm at 303K has been obtained for PVdF-co-HFP (75):SEt₃TFSI (25) + EC+PC (60) wt%. The inclusion of plasticizers induces the polymer chain flexibility and reduces the viscosity of ionic liquids. However, the lithium salts added into IL based gel polymer electrolytes shows a higher degree of crystallinity. Strong anodic stability of 4.67 V has been viewed from the LSV. There was a flat and stable voltage plateau and first discharge capacity of 138 mAh/g were noted with working voltage of 3.4 V.

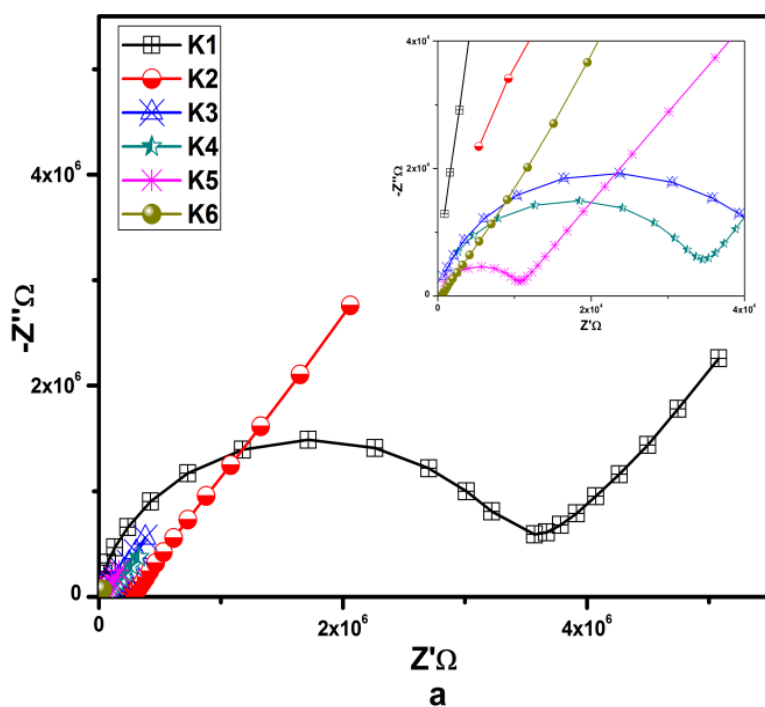


XRD diffraction pattern of pure PVdF-co-HFP, different SPE K1-(95:5), K2- (90:10), K3- (85:15), K4- (80:20), K5- (75:25) of PVdF-co-HFP + [P_{14,6,6,6}][Tf₂N] and GPE K6- PVdF-co-HFP + [P_{14,6,6,6}][Tf₂N] (75:25) + EC+PC (60) wt%

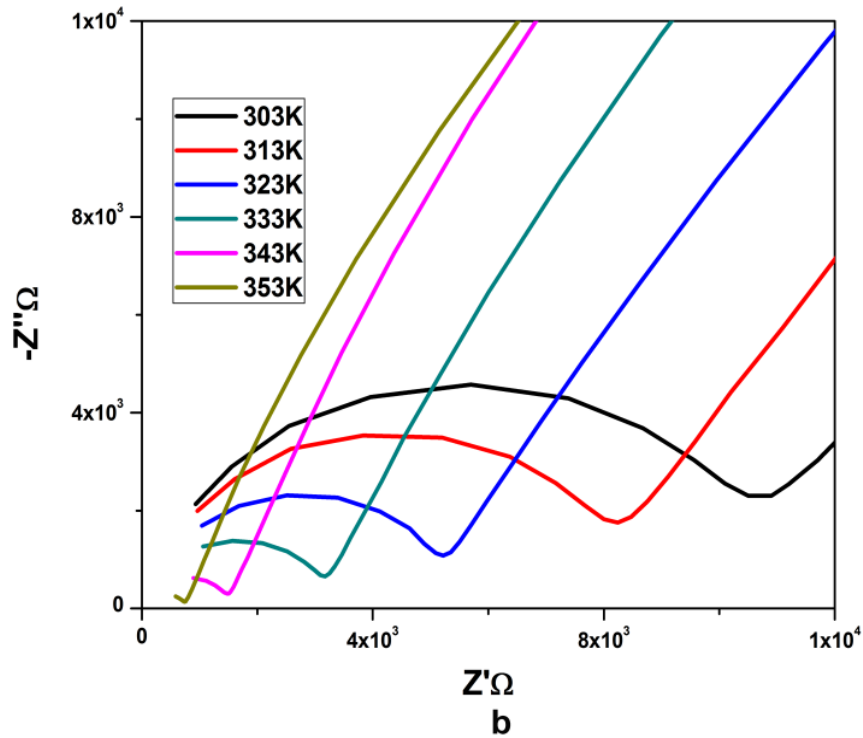




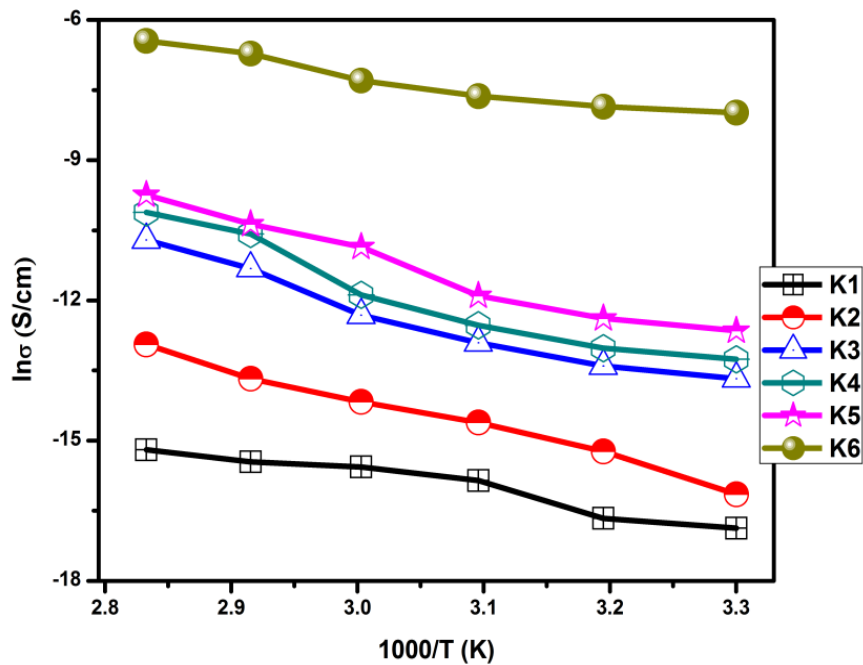
FTIR of pure PVdF-co-HFP, different SPE K1-(95:5), K2- (90:10), K3- (85:15), K4- (80:20), K5- (75:25) of PVdF-co-HFP + [P_{14,6,6,6}][Tf₂N] and GPE K6-PVdF-co-HFP + [P_{14,6,6,6}][Tf₂N] (75:25) + EC+PC (60) wt% system



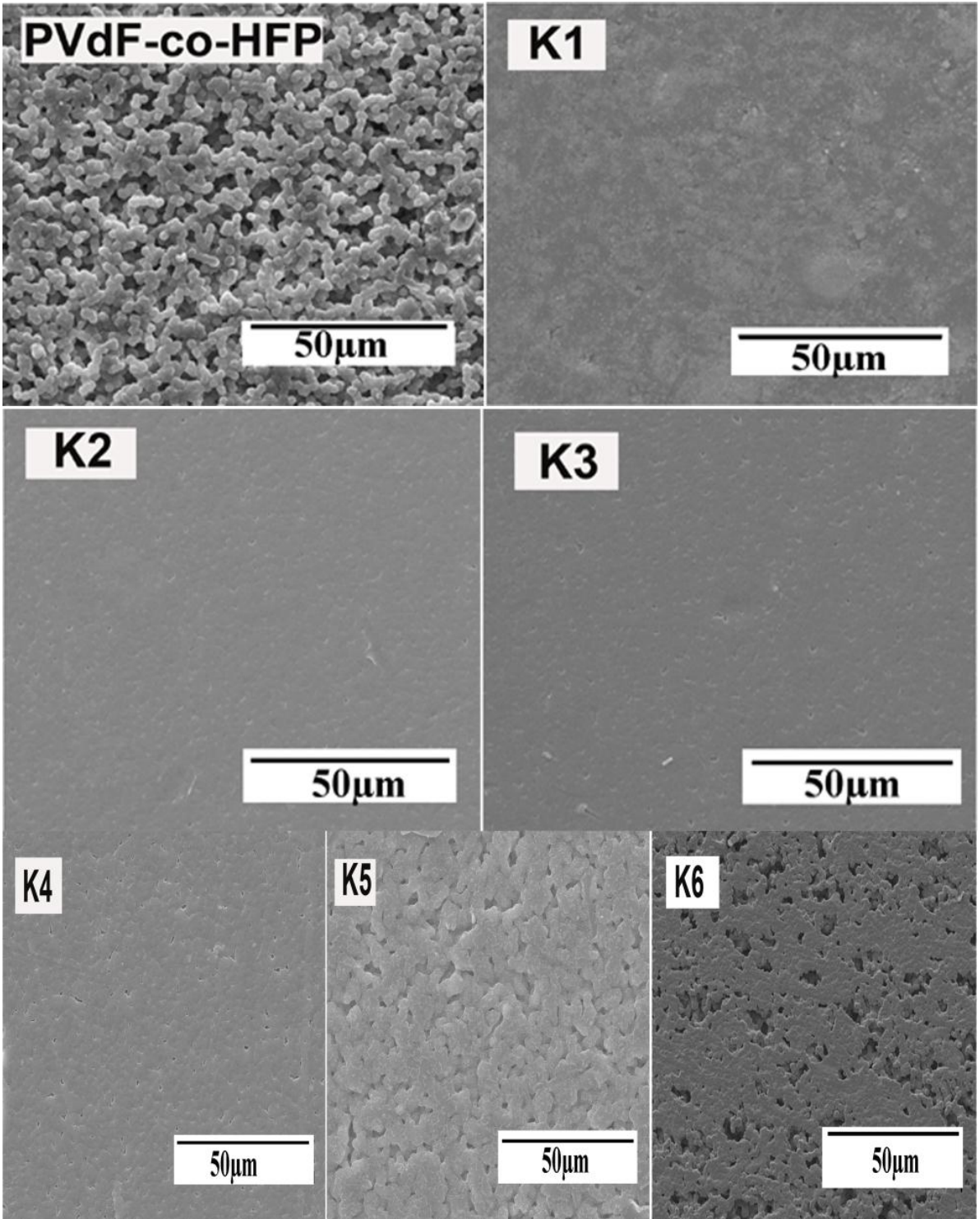
Complex impedance plot for SPE K1-(95:5), K2- (90:10), K3- (85:15), K4- (80:20), K5- (75:25) of PVdF-co-HFP + [P_{14,6,6,6}][Tf₂N] and GPE K6-PVdF-co-HFP + [P_{14,6,6,6}][Tf₂N] (75:25) + EC+PC (60) wt% in the SS/GPE/SS cell at room temperature



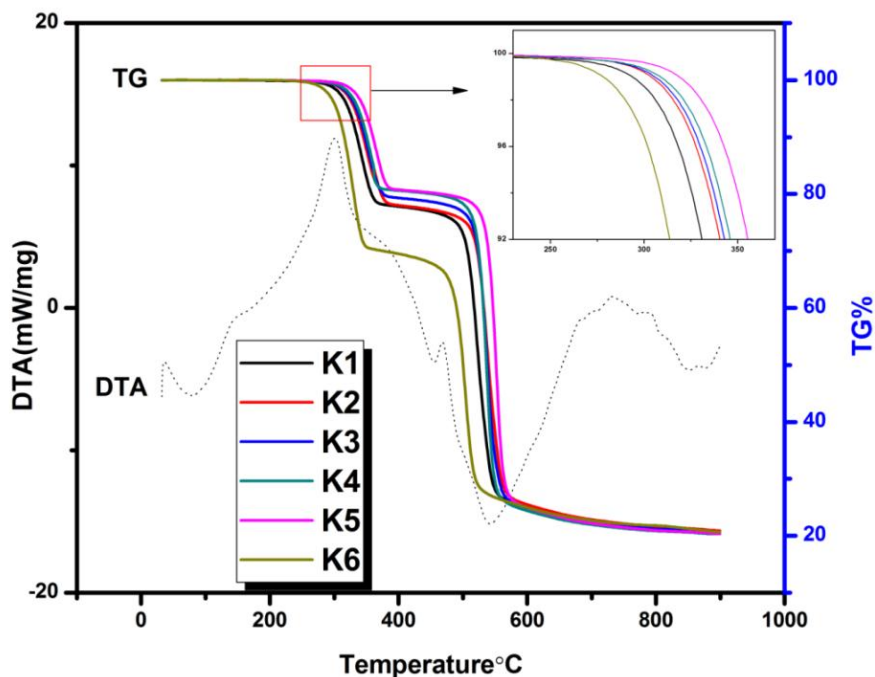
Complex impedance plot of K5 PVdF-co-HFP + [P_{14,6,6,6}][Tf₂N] (75:25) at different temperatures



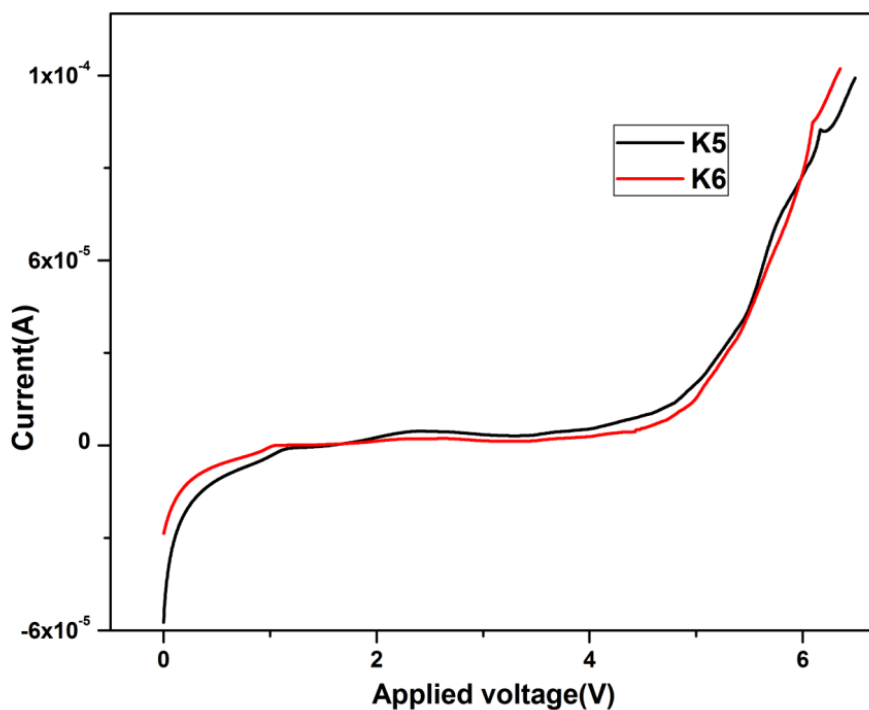
Arrhenius plot of samples SPE K1-(95:5), K2- (90:10), K3- (85:15), K4- (80:20), K5- (75:25) of PVdF-co-HFP + [P_{14,6,6,6}][Tf₂N] and GPE K6-PVdF-co-HFP + [P_{14,6,6,6}][Tf₂N] (75:25) + EC+PC (60) wt% between the temperature 303 to 353K



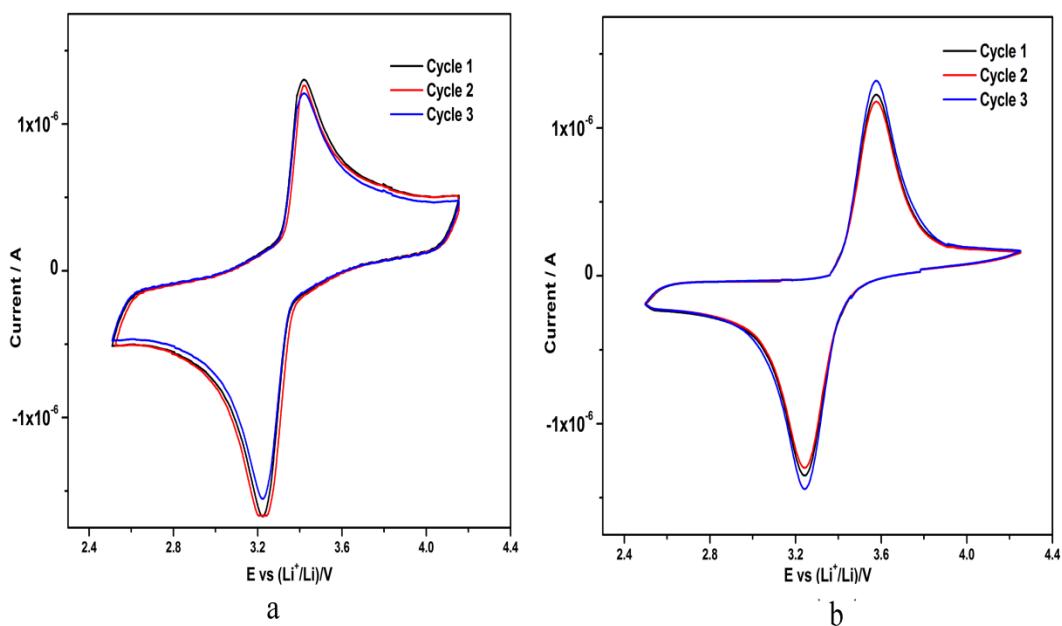
SEM image of pure PVdF-co-HFP, SPE K1-(95:5), K2- (90:10), K3- (85:15), K4- (80:20), K5- (75:25) of PVdF-co-HFP + [P_{14,6,6,6}][Tf₂N] and GPE K6-PVdF-co-HFP + [P_{14,6,6,6}][Tf₂N] (75:25) + EC+PC (60) wt% magnification of 1K



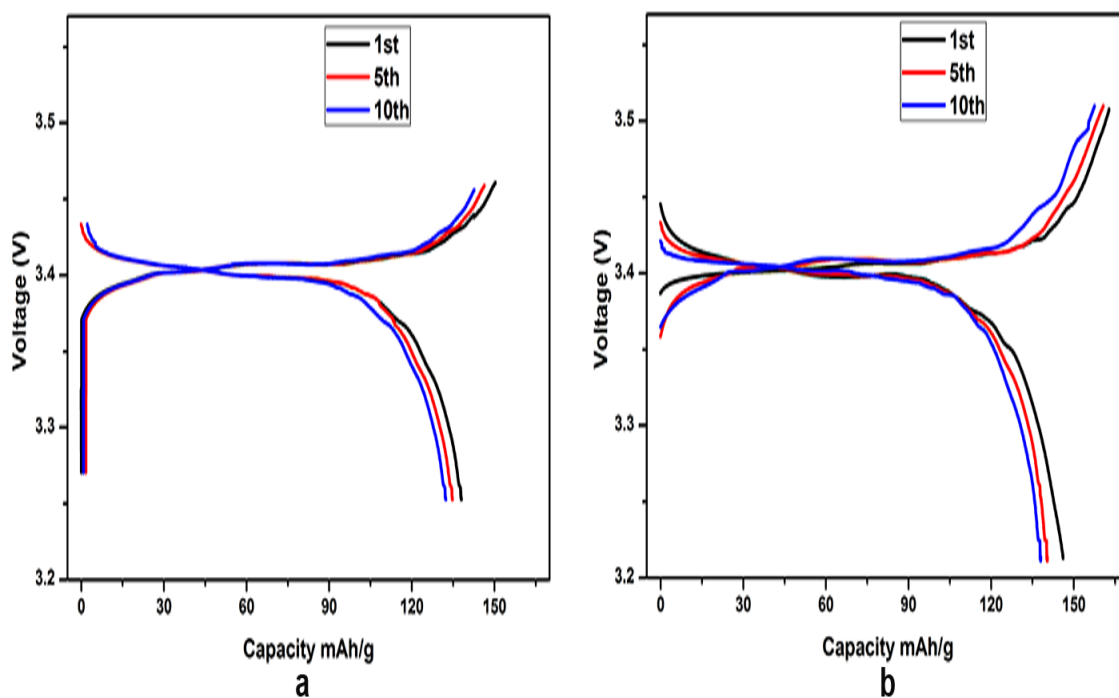
TGDTA graph of SPE K1-(95:5), K2- (90:10), K3- (85:15), K4- (80:20), K5- (75:25) of PVdF-co-HFP + [P_{14,6,6,6}][Tf₂N] and GPE K6-PVdF-co-HFP + [P_{14,6,6,6}][Tf₂N] (75:25) + EC+PC (60) wt% and typical DTA plot of SPE



LSV of SPE K5 PVdF-co-HFP + [P_{14,6,6,6}][Tf₂N] (75:25) and GPE K6-PVdF-co-HFP + [P_{14,6,6,6}][Tf₂N] (75:25) + EC+PC (60) wt% at a scan rate of 5mV/s



Cyclic voltammetry of (a) SPE K5 PVdF-co-HFP + [P_{14,6,6,6}][Tf₂N] (75:25) and (b) GPE K6-PVdF-co-HFP + [P_{14,6,6,6}][Tf₂N] (75:25) + EC+PC (60) wt% at a scan rate of 5mV/s



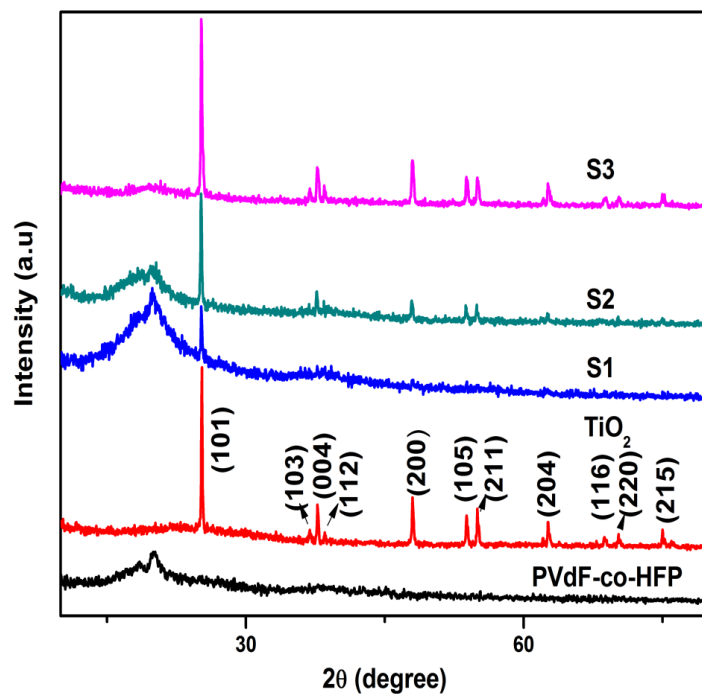
Charge discharge profile of (a) SPE K5 PVdF-co-HFP + [P_{14,6,6,6}][Tf₂N] (75:25), (b) GPE K6-PVdF-co-HFP + [P_{14,6,6,6}][Tf₂N] (75:25) + EC+PC (60) wt% for first ten cycles

The Titanium dioxide (TiO_2) has been added in the present IL based gel polymer electrolyte. In the meantime, the addition of inorganic fillers increases the ionic conductivity of the IL based GPEs. With the chosen ratio of (PVdF-co-HFP-SEt₃TFSI-EC/PC (30-10-60 wt%) different amounts of TiO_2 fillers were optimized. According to the results obtained from the complex impedance plot, 6 wt% of TiO_2 based sample has higher ionic conductivity of 3.42×10^{-3} S/cm at 303 K. Higher content of TiO_2 reduces the conductivity due to the formation of the aggregation. An electrochemical stability of 4.62 V and discharge capacity of 145 mAh/g have been observed for the coin cell containing Li / CGPE / LiFePO_4 at 0.1 C rate.

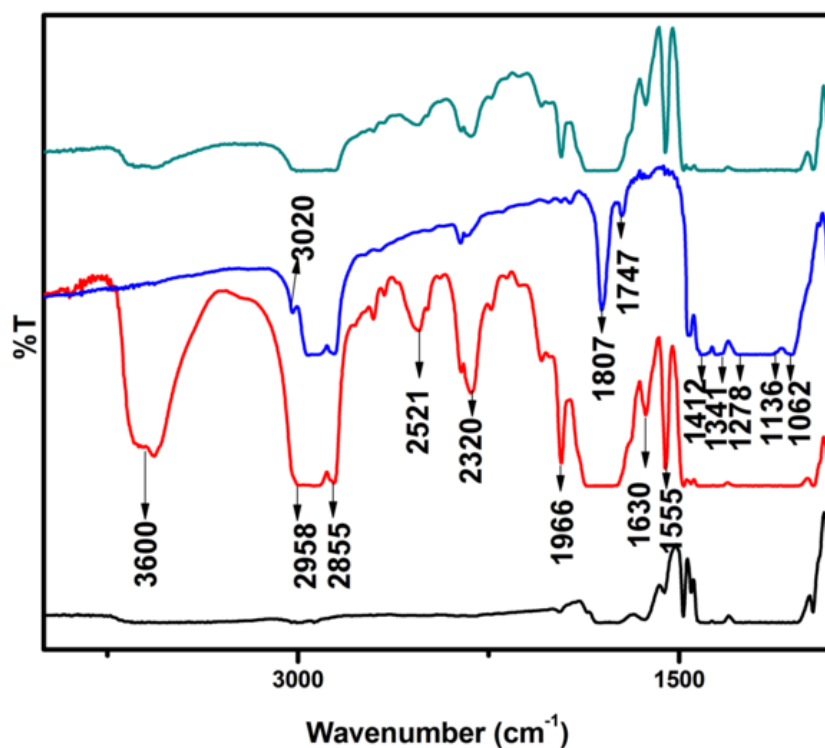
The sulfonium cation present in the IL reacts with the metal electrode and reduces its electrochemical performances. In order to reduce the hindrance present in the sulfonium based IL, an attempt has been made to prepare polymer electrolyte with phosphonium ionic liquid ($[\text{P}_{14,6,6,6}][\text{Tf}_2\text{N}]$). Here the solid, gel and composite polymer electrolytes were prepared and characterized. Initially, the solid polymer electrolyte, 75-25 wt% of PVdF-co-HFP - $[\text{P}_{14,6,6,6}][\text{Tf}_2\text{N}]$ exhibits better performances with 3.209×10^{-6} S/cm, while adding the plasticizer into the optimized system, PVdF-co-HFP (30 wt%) + $[\text{P}_{14,6,6,6}][\text{Tf}_2\text{N}]$ (10 wt%) + EC/PC (60 wt%) the conductivity has been enhanced to 3.40×10^{-4} S/cm at 303 K. The addition of plasticizer results wide working voltage with reduced thermal stability. Without plasticizer the electrolyte possesses discharge capacity of 139 mAh/g, and thermal stability of 500°C. The PVdF-co-HFP + $[\text{P}_{14,6,6,6}][\text{Tf}_2\text{N}]$ -EC/PC (60 wt%) exhibits thermal stability up to 265 °C, the wide electrochemical window of 5V and discharge capacity of 146 mAh/g at 0.1C rate.

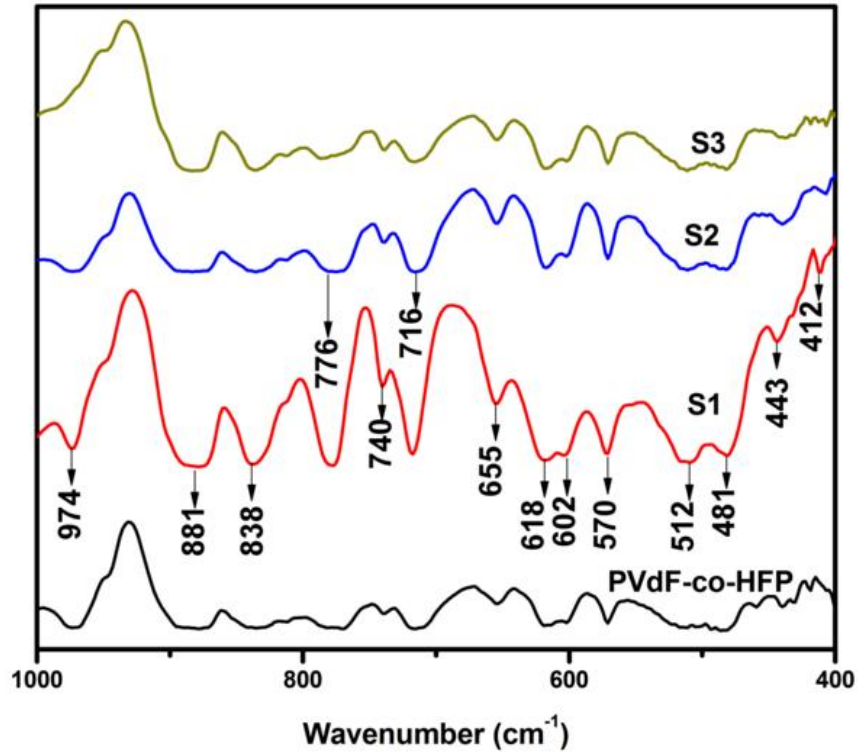
In the perspective to achieve high conductivity, different ratios of TiO_2 filler has also been incorporated with PVdF-co-HFP / $[\text{P}_{14,6,6,6}][\text{Tf}_2\text{N}]$ / EC+PC. The maximum ionic conductivity of 1.15×10^{-3} S/cm at 303K has been obtained for 6wt% of filler content based

sample. The electrochemical stability is up to 5.2V which is confirmed from LSV. The CGPE with 6wt% of TiO₂ produces excellent discharge capacity of 149 mAh/g at 0.1C rate.

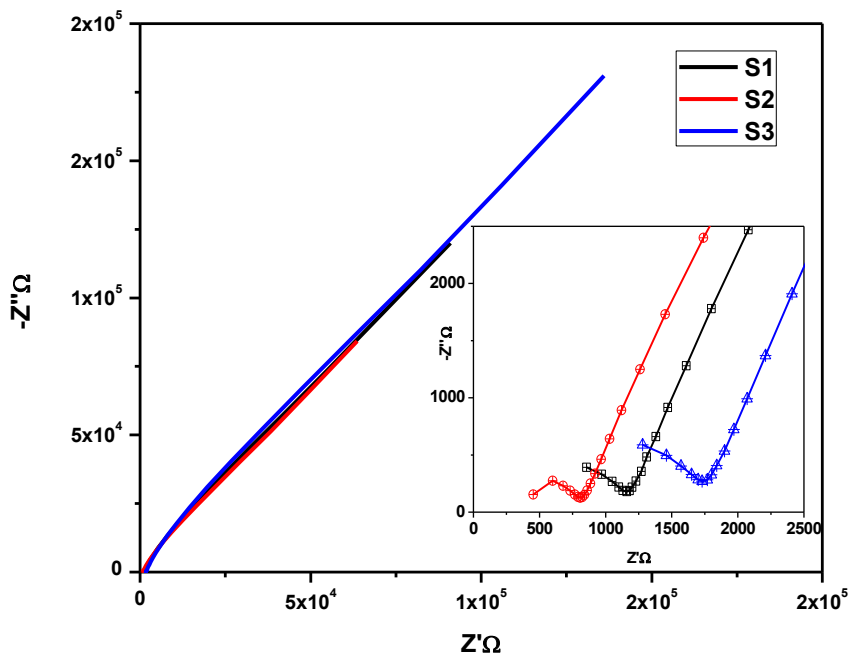


XRD patterns of pure PVdF-co-HFP, TiO₂, ILCGPE 3(S1), 6(S2) and 9(S3) wt% of TiO₂ based PVdF-co-HFP (30) + [P14,6,6,6][Tf₂N] (10) + EC+PC (60) wt% system





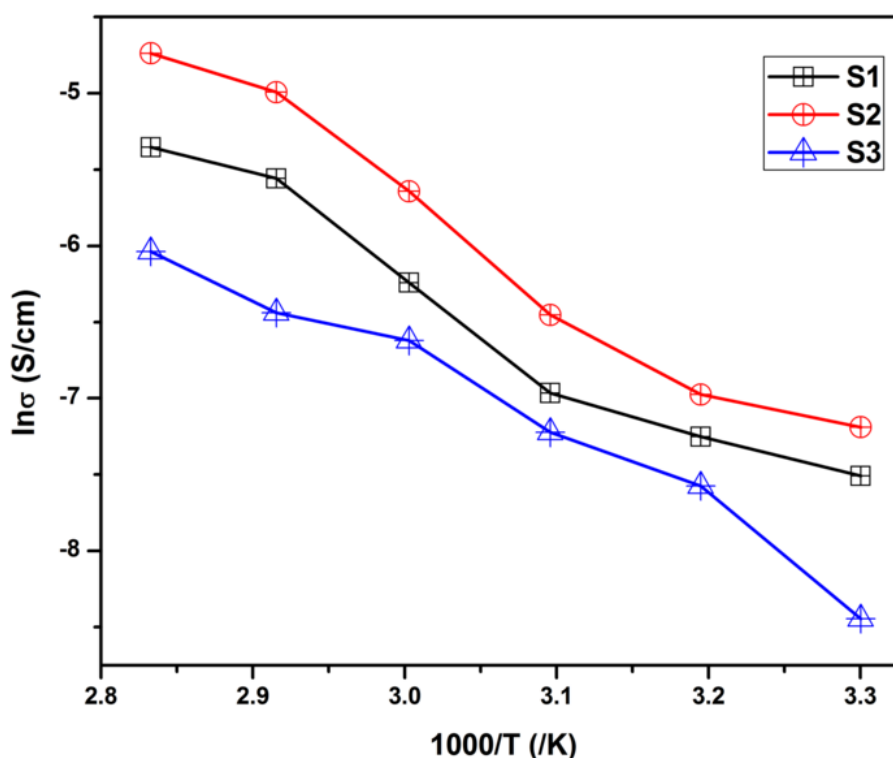
FTIR images of pure PVdF-co-HFP, ILCGPE 3(S1), 6(S2) and 9(S3) wt% of TiO_2 based PVdF-co-HFP (30) + [P14,6,6,6][Tf_2N] (10) + EC+PC (60) wt% system



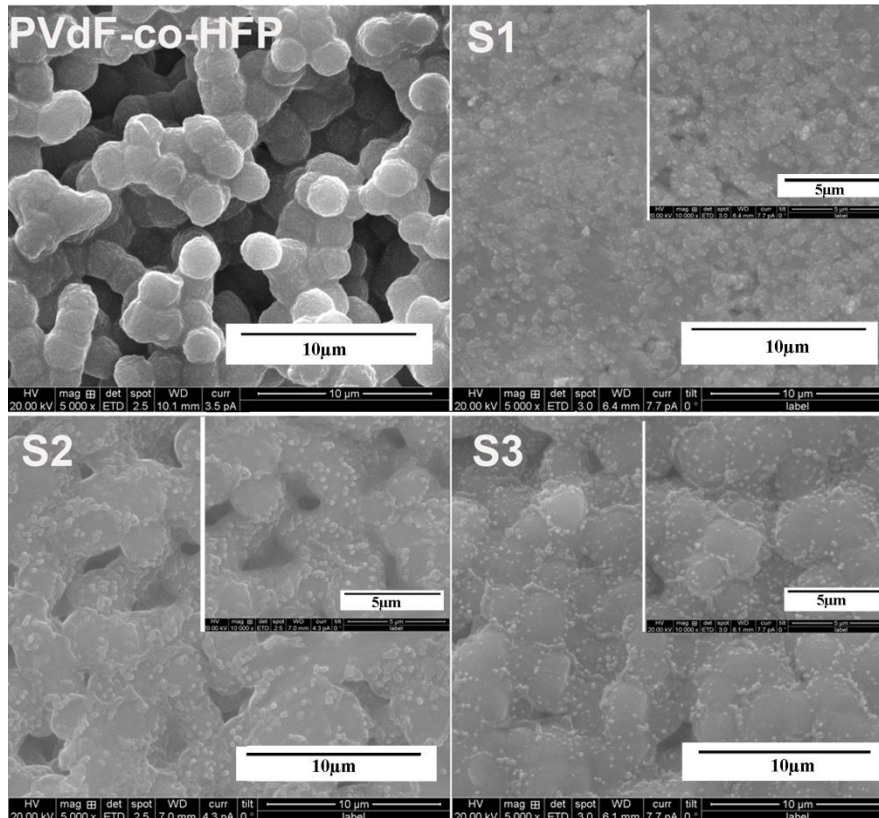
Complex impedance spectra of 3, 6, 9 wt% TiO_2 based PVDF – Co – HFP(30) IL(10) – EC+PC(60)wt% system at room temperature (Inset: High frequency region)

| Sample PVdF-co-HFP (30) + [P14,6,6,6][Tf2N] (10) +EC+PC (60) + TiO ₂ (X)wt% | Ionic conductivity $\times 10^{-4}$ S/cm at | | | | | | E _a (eV) |
|--|---|------|------|------|------|------|---------------------|
| | 303K | 313K | 323K | 333K | 343K | 353K | |
| S1=3 | 5.49 | 7.09 | 9.45 | 19.5 | 38.5 | 47.3 | 0.175 |
| S2=6 | 11.5 | 12.3 | 15.8 | 35.5 | 67.9 | 87.7 | 0.162 |
| S3=9 | 2.15 | 5.13 | 7.30 | 13.3 | 16.2 | 23.9 | 0.190 |

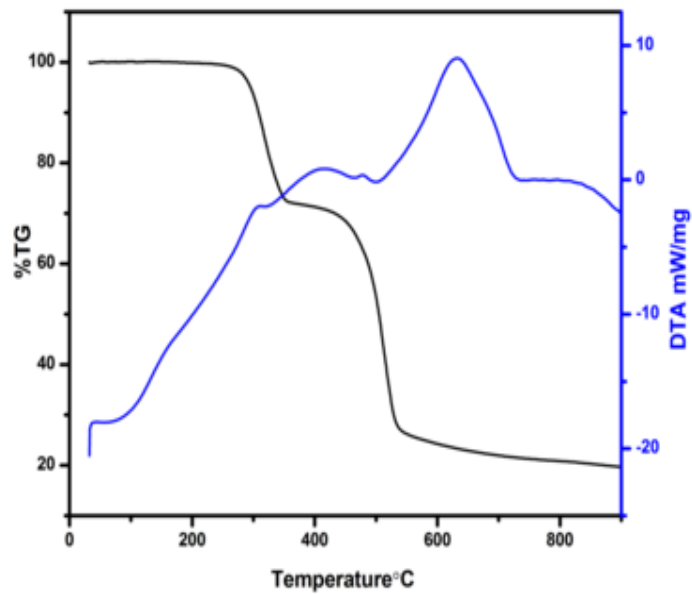
The calculated weight percentage, ionic conductivity and activation energy values



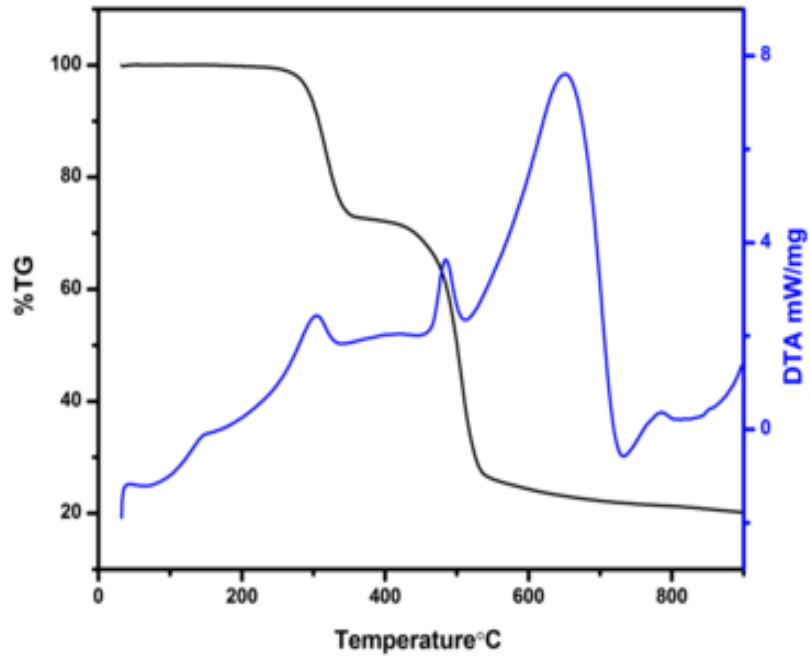
Arrhenius plot of 3, 6, 9 wt% TiO₂ based PVDF – co – HFP(30) IL(10) – EC+PC(60)wt% system



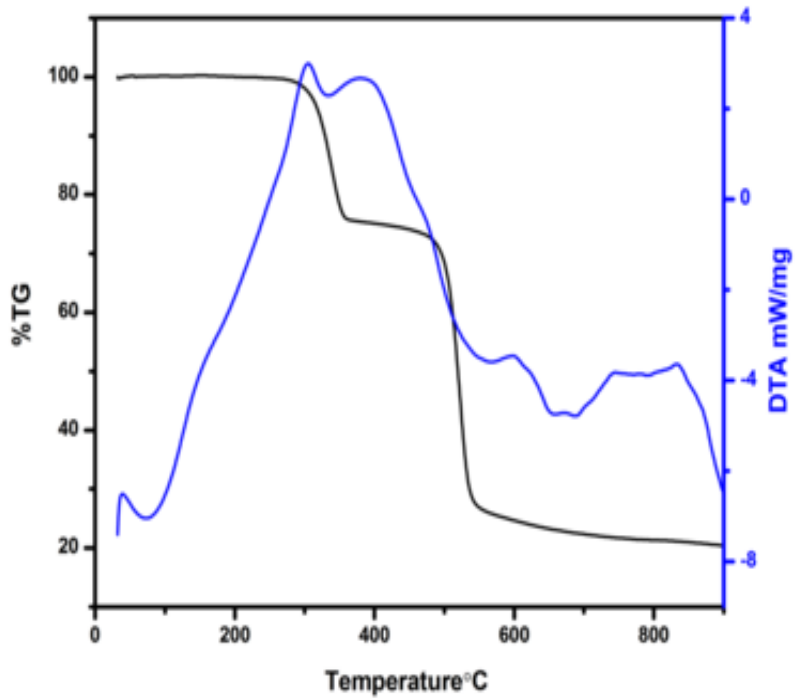
SEM image of pure PVdF-co-HFP, prepared ILCGPE 3, 6, 9 wt% TiO₂ based PVdF – co – HFP(30) IL(10) – EC+PC(60)wt% system



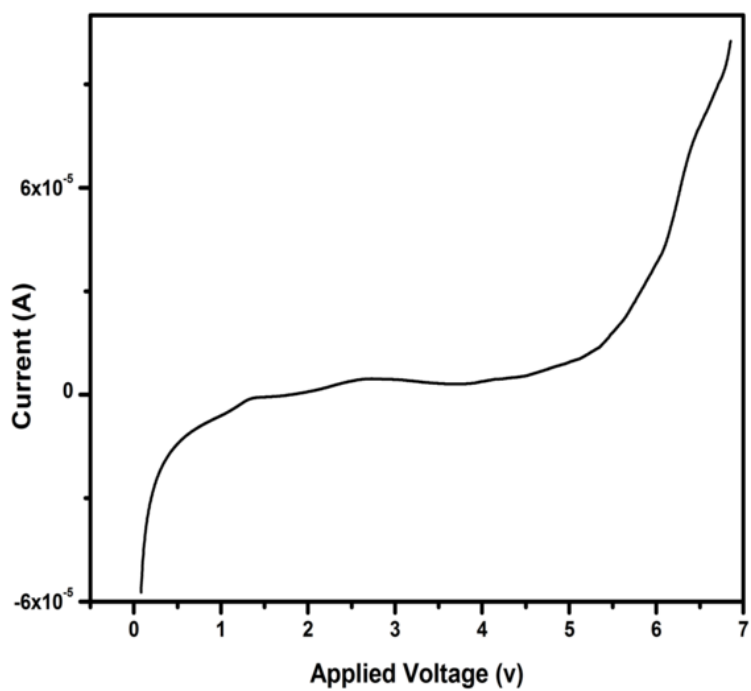
TGDTA graph of prepared ILCGPE S1 = S1= PVdF-co-HFP (30) + [P14,6,6,6][Tf₂N] (10) +EC+PC (60) + TiO₂ (3)wt%



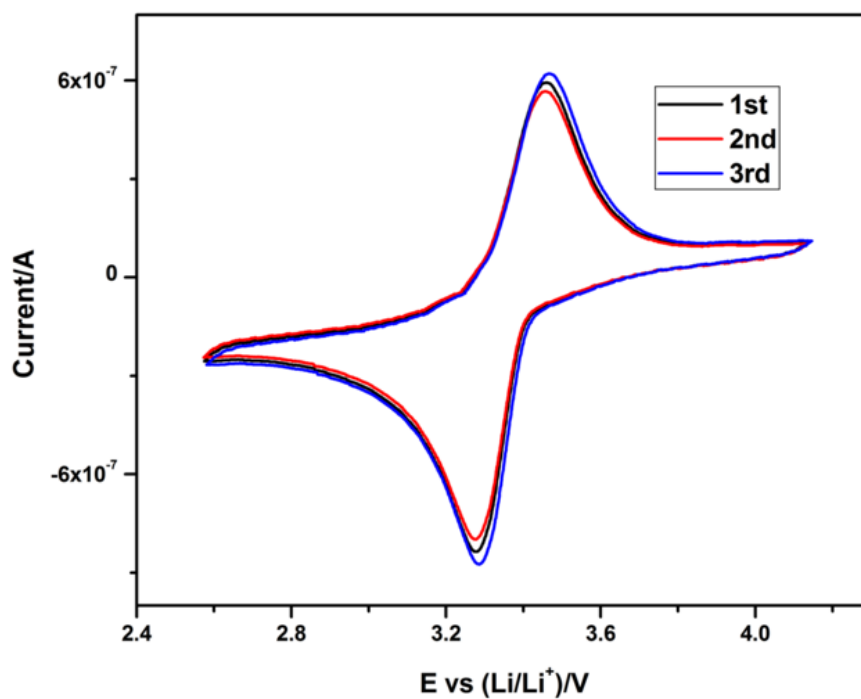
TGDTA graph of prepared ILCGPE S2= PVdF-co-HFP (30) + [P14,6,6,6][Tf₂N] (10) +EC+PC (60) + TiO₂ (6)wt%



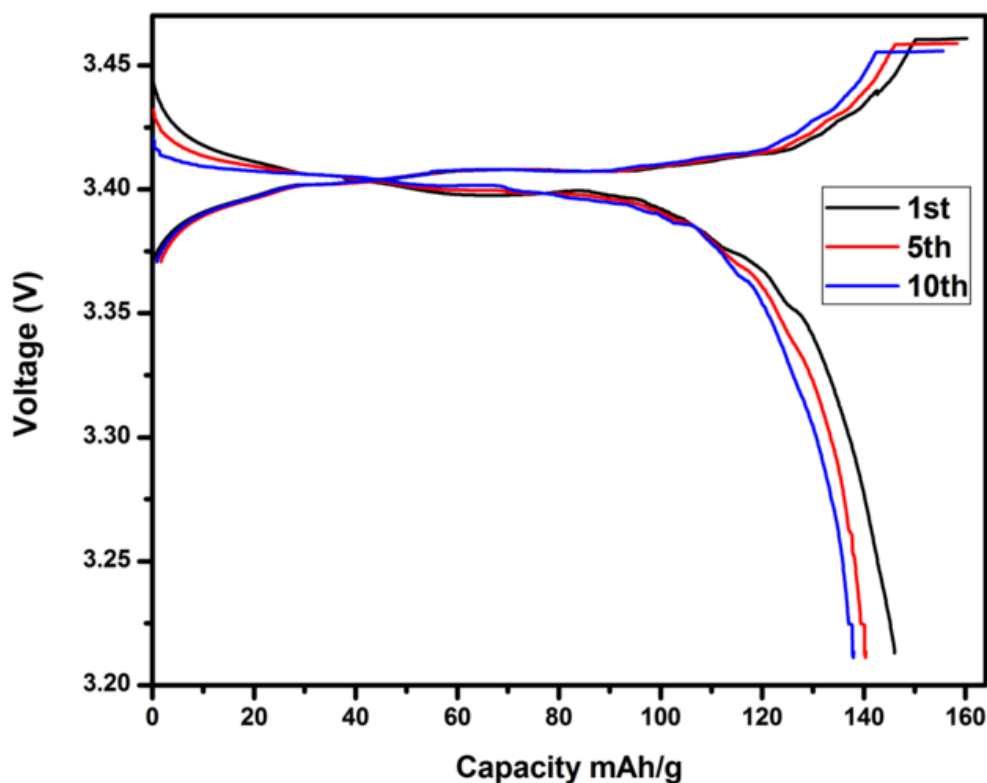
TGDTA graph of prepared composite polymer electrolyte represented as S1, S2 & S3



LSV of PVdF-co-HFP (30) + [P_{14,6,6,6}][Tf₂N] (10) +EC+PC (60) + TiO₂(6)wt% at a scan rate of 5mV/s



CV of PVdF-co-HFP (30) + [P_{14,6,6,6}][Tf₂N] (10) +EC+PC (60) + TiO₂ (6)wt% at a scan rate of 5mV/s



Charge discharge of PVdF-co-HFP (30) + [P_{14,6,6,6}][Tf₂N] (10) + EC+PC (60) + TiO₂ (6)wt% at a scan rate of 5mV/s

On summarizing the above results, the polymer electrolyte based on PVdF-co-HFP (as a host) has been prepared and characterized with Li/PE/LiFePO₄ cell couple. The Lithium cation (LiTFSI) based SPE exhibited ionic conductivity of 1.93×10^{-5} S/cm at 303 K, whereas in GPE (60 wt% of EC and PC), the ionic conductivity value has been increased to 1.72×10^{-3} S/cm at 303K and exhibits a discharge capacity of 117 mAh/g at 0.1C rate. When incorporating 6 wt% of dispersoid (ZrO₂) into the CGPE, ionic conductivity has been increased to 4.46×10^{-3} S/cm at 303K, which is higher than the solid and gel based polymer electrolytes. It exhibits a discharge capacity of 126 mAh/g. In order to improve the electrochemical properties of electrolytes, the incorporation of ionic liquid was tried in the polymer matrix in absence of alkali salts. The sulfonium cation based SPE possesses ionic conductivity of 6.93×10^{-5} S/cm at 303 K and offers discharge capacity of 133mA/g at 0.1C. The ionic conductivity value has been increased to 1.13×10^{-3} S/cm at 303 K in GPE and exhibited a discharge capacity of 138mAh/g. However, the addition of LiTFSI salt in ILPE

system, reduces the conductivity value to 4.26×10^{-4} S/cm at 303 K. The sulfonium cation based CGPE possessed ionic conductivity value of 3.42×10^{-3} S/cm at 303 K with an initial discharge capacity of 145 mAh/g. To rectify the corrosion effect of sulfonium cation, phosphonium cation based ILPE has been prepared. The SPE and GPE based on phosphonium cation shows an ionic conductivity value of 3.2×10^{-6} S/cm and 3.4×10^{-4} S/cm at 303K respectively. The optimized gelled sample revealed an excellent discharge capacity of 146 mAh/g. As from the CI plot the prepared CGPE film based on phosphonium cation has conductivity value of 1.15×10^{-3} S/cm at 303K and initial discharge capacity of 149 mAh/g at 0.1C rate. Hence, the phosphonium based CGPE electrolytes exhibits better performances among the systems studied and this could be used as a potential candidate for the lithium battery fabrication.

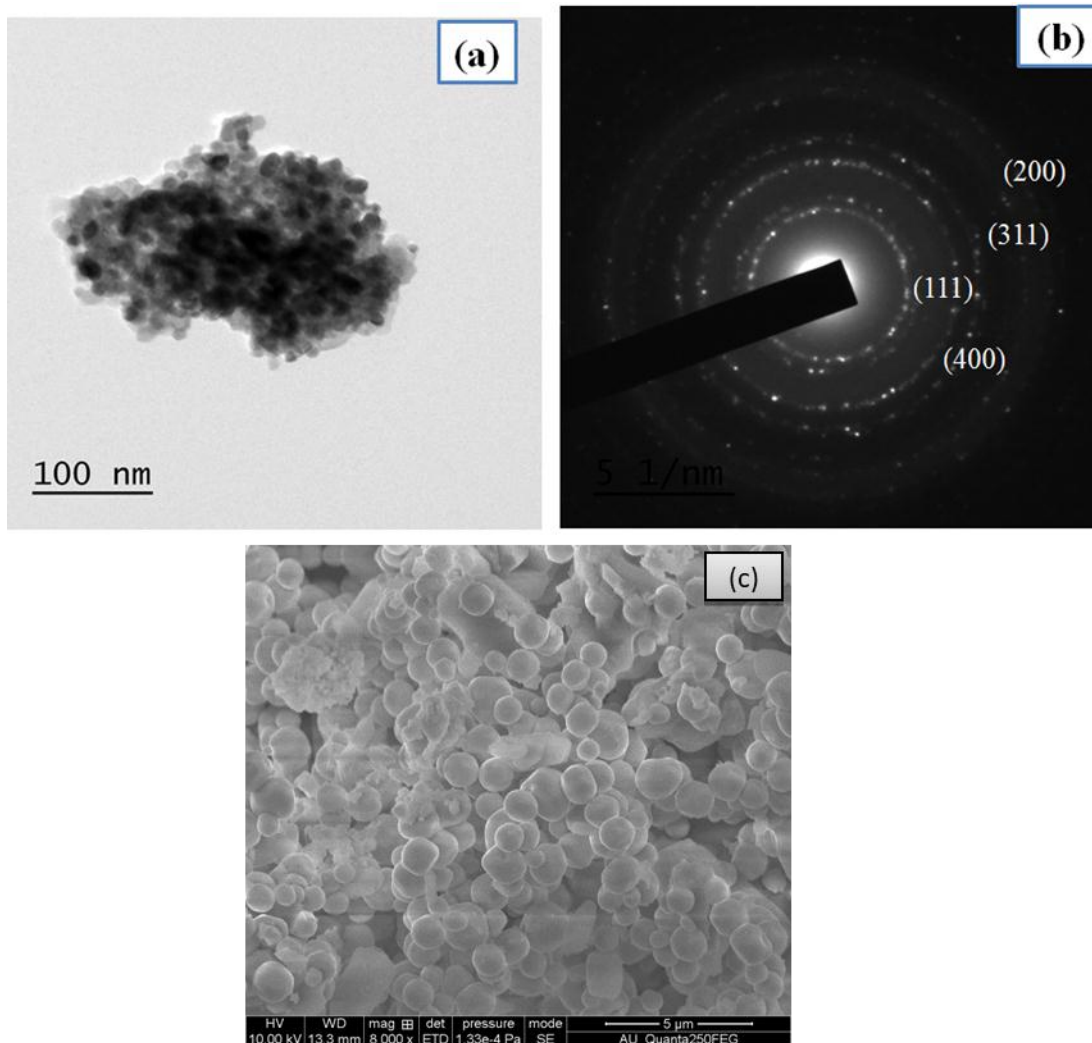
In the present project, zirconium oxide (dielectric constant $\epsilon=23$) and cerium oxide ($\epsilon=26$) have been synthesized using modified co-precipitation technique. Poly (styrene-methyl methacrylate), a co-polymer found to be a suitable promising material due to styrene unit, which enhances the mechanical strength of gel polymer electrolyte owing to its low attraction for liquid electrolyte and methyl methacrylate (MMA) acts as gelatinization agent in the electrolyte and high anodic stability. PVdF acts as host polymer which has high anodic stability due to the strong electron withdrawing functional group (-C-F-). It has a high dielectric constant ($\epsilon=8.4$), which can aid in greater ionization of Li-salts and thus afford a higher concentration of charge carriers. The higher dielectric constant of EC (89), and PC (64), are added in our synthesis process, which facilitates more charge carriers to the medium. Here, all electrolytes are prepared by conventional solution casting method.

The thermal history of precursor ZrO_2 and CeO_2 nano particles and thermal stability of the polymer matrices have been examined by TG/DTA analysis. XRD analysis dictates the structure of the prepared nano composites and ascertains the amorphous/crystalline nature of

the polymer electrolyte systems. The fundamental vibrational groups of the inorganic elements and existence of the complexation between the polymer matrix and its constituents have been analyzed through the FT-IR and RAMAN spectroscopic techniques. The presence of porous morphology network has been ascribed through scanning electron microscope and Transmission electron microscope analyses. The presence of the oxidation states and the existence of elements in the inorganic materials have been ascertained through XPS and EDX analyses. The ionic conductivity of the polymer matrix is a significant parameter and assures the specific application of the prepared electrolytes in Lithium secondary batteries. This has been measured with the help of AC impedance analysis. The anodic stability, cyclic reversibility and discharge capacity were analyzed by the techniques linear sweep voltammetry and cyclic voltammetry charge/ discharge studies for the Li/As-prepared composite polymer blend gel electrolyte (CB3)/LiFePO₄ cell couple.

The work reported in this thesis addresses a systematic investigation on the synthesis and optimization of ZrO₂ and CeO₂ nano particles using modified co-precipitation method. The following parameters are varying to optimize both the ceramic particles such as (i) precipitation agent (ii) pH (iii) concentration of raw material (iv) concentration of precipitation agent. The precipitation agent has significant role during the synthesis of ZrO₂ and CeO₂ particles. The base KOH and NaOH are appropriate catalyst for ZrO₂ and CeO₂ nano particles respectively. The dissociation of OH⁻ ions is minimum and maximum for KOH and NaOH respectively. It enhances crystallinity and morphology of ZrO₂ and CeO₂ nano particles. Further, pH of the solute media has dictated that the crystallite size, which has been decreased upon increasing pH for both ceramic particles. The OH⁻ ions are highly involved in the aggregation process which would strongly affect the super saturation degree of initial precipitate. Henceforth, the particle size decreased upon increasing the pH during synthesis. Furtherance, on elevating the concentration of Zr(NO₃)₂.6H₂O and Ce(NO₃)₃.6H₂O, the

crystallinity increases up to 0.2 M. Further addition of raw material content causes decrease in crystallinity. Finally, the particle size decreases upon the increased concentration of precipitation agent. The particle evolution is described by Oswald ripening mechanism. It is optimized that the concentration of 1.5M KOH and 2M NaOH would enhance the particles in a homogeneous spherical morphology with the size of 170 nm and less than 20 nm respectively. Decreasing the size of the particle to nanosize would enrich the properties of the prepared materials in many aspects, especially, the lithium ion battery applications. Hence, this material will be anticipated to have better electrochemical properties while using this as a composite based polymer electrolyte, which will then be employed in lithium battery fabrication.

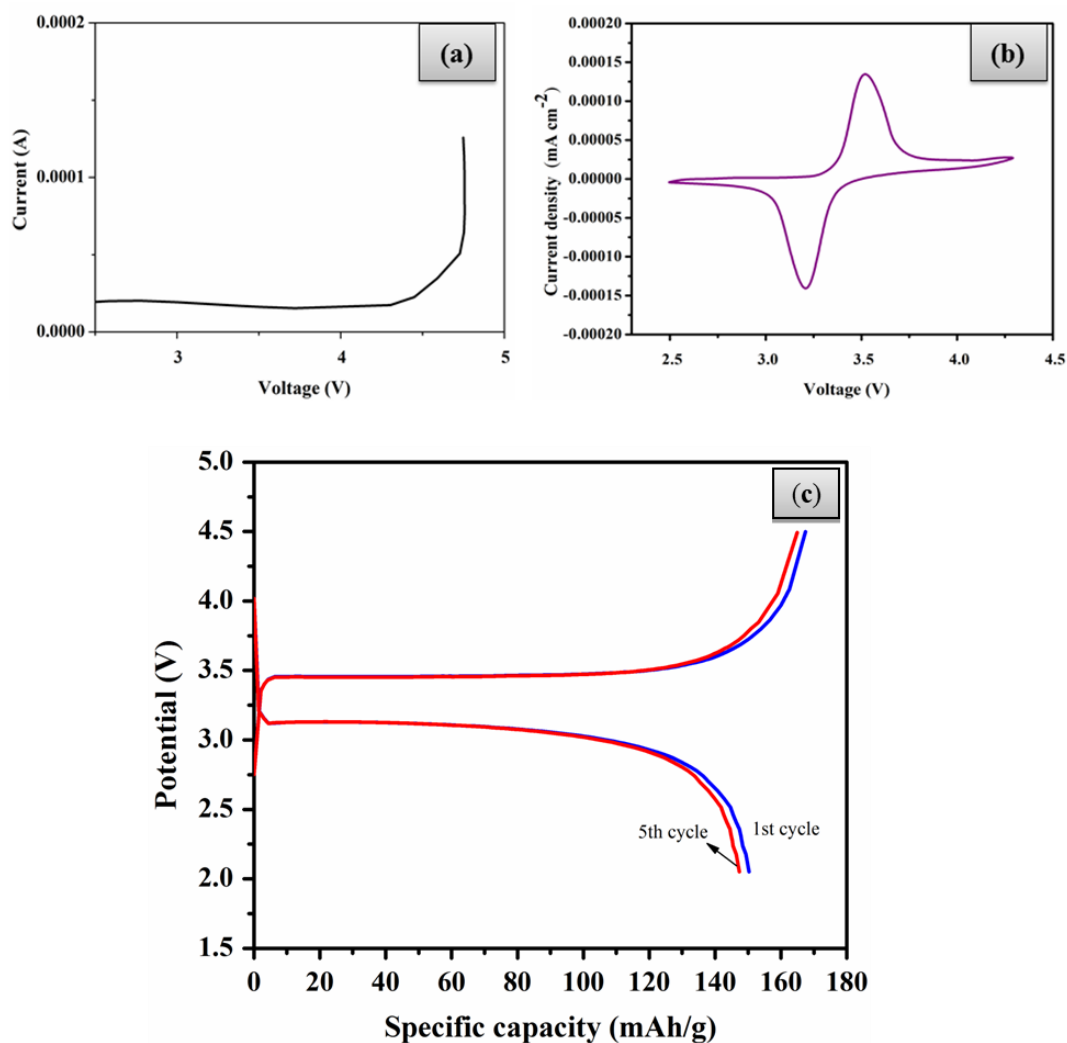


a) TEM image b) SAED pattern c) SEM image of CeO₂ nano particles

The as-prepared ZrO₂ filler (0, 3, 6, 9 and 12) wt.% has been dispersed into the prepared P(S-MMA)-PVdF(25:75 of 27wt.%) -LiClO₄ (8 wt.%) -EC+PC (1:1 of 65wt.%) complex. The highest ionic conductivity has been obtained 1.2×10^{-2} S/cm at room temperature for the 6wt% ZrO₂ based system. The addition of ceramic filler enhanced the free volume, which leads to higher salt dissociation, and also creates more mobile paths for the lithium ions because of an interaction of the polymer and the filler. It also found that the film containing 6 wt. % of ZrO₂ combination exhibited maximum ionic conductivity and thermal stability up to 270°C. This decomposition of the electrolyte is observed around 4.9 V, indicates the oxidative stability of the electrolyte. This is important parameter for the application of electrolyte in high voltage battery fabrication. Therefore, substantial

enrichment in the conductivity has been obtained for the electrolyte system.

The as-prepared CeO₂ composites (0, 3, 6, 9 and 12 wt.%) dispersed P(S-MMA)-PVdF (25:75) of 27wt.%-LiClO₄ (8wt.%) - EC+PC (1;1 of 65 wt.%) based polymer blend gel electrolyte. The 6wt% of CeO₂ based P(S-MMA)- PVdF(25:75) of 27wt.%-LiClO₄(8wt.%) - EC+PC (1;1 of 65 wt.%) electrolyte exhibits the highest ionic conductivity of 2.51×10^{-2} S/cm at room temperature. It is due to the high electronegativity, high dielectric constant (ϵ -26), high basic nature and the particle size is nearly 20 nm of the CeO₂. It dictates the ionic conductivity in turn, the discharge capacity of 153 mAh/g at 0.1 C rate. The ionic conductivity of the electrolyte directly depends on the local viscosity of electrolyte sample because the ionic conductivity is directly coupled with the viscosity. Fluorescence emission intensity is reciprocal to the local free volume of the electrolyte medium. The prepared film is thermally stable up to 315°C. From the above studies, one who supplement that the optimized nano composite polymer blend gel electrolyte system can be used for the potential electrolyte in lithium polymer batteries.



a) Linear sweep voltammogram b) cyclic voltammogram of LiFePO₄/ (CB₃)/Li Cell
 c) Charge-discharge profile for Li/CB₃/LiFePO₄ at 303 K cut-off voltage 4.5-2 V.

14. SUMMARY OF THE FINDINGS

(IN 500 WORDS)

The polymer electrolyte based on PVdF-co-HFP (as a host) has been prepared and characterized with Li/PE/LiFePO₄ cell couple. The Lithium cation (LiTFSI) based SPE exhibited ionic conductivity of 1.93×10^{-5} S/cm at 303 K, whereas in GPE (60 wt% of EC and PC), the ionic conductivity value has been increased to 1.72×10^{-3} S/cm at 303K and exhibits a discharge capacity of 117 mAh/g at 0.1C rate. When incorporating 6 wt% of dispersoid (ZrO₂) into the CGPE, ionic conductivity has been increased to 4.46×10^{-3} S/cm at 303K, which is higher than the solid and gel based polymer electrolytes. It exhibits a discharge

capacity of 126 mAh/g. In order to improve the electrochemical properties of electrolytes, the incorporation of ionic liquid was tried in the polymer matrix in absence of alkali salts. The sulfonium cation based SPE possesses ionic conductivity of 6.93×10^{-5} S/cm at 303 K and offers discharge capacity of 133mAh/g at 0.1C. The ionic conductivity value has been increased to 1.13×10^{-3} S/cm at 303 K in GPE and exhibited a discharge capacity of 138mAh/g. However, the addition of LiTFSI salt in ILPE system, reduces the conductivity value to 4.26×10^{-4} S/cm at 303 K. The sulfonium cation based CGPE possessed ionic conductivity value of 3.42×10^{-3} S/cm at 303 K with an initial discharge capacity of 145 mAh/g. To rectify the corrosion effect of sulfonium cation, phosphonium cation based ILPE has been prepared. The SPE and GPE based on phosphonium cation shows an ionic conductivity value of 3.2×10^{-6} S/cm and 3.4×10^{-4} S/cm at 303K respectively. The optimized gelled sample revealed an excellent discharge capacity of 146 mAh/g. As from the CI plot the prepared CGPE film based on phosphonium cation has conductivity value of 1.15×10^{-3} S/cm at 303K and initial discharge capacity of 149 mAh/g at 0.1C rate. Hence, the phosphonium based CGPE electrolytes exhibits better performances among the systems studied and this could be used as a potential candidate for the lithium battery fabrication.

The synthesis and optimization of zirconia (ZrO_2) and ceria (CeO_2) nano particles have been carried out using modified co-precipitation method. The following parameters are varied to optimize both the ceramic particles such as (i) precipitation agent (ii) pH (iii) concentration of raw material (iv) concentration of precipitation agent. The as prepared ZrO_2 and CeO_2 nano particles have been characterized using XRD, FTIR, RAMAN, SEM, TEM and XPS analyses. It is optimized that the concentration of 1.5M KOH and 2M NaOH would enhance the particles in a homogeneous spherical morphology with the size of 170 nm and less than 20 nm respectively for ZrO_2 and CeO_2 nano particles. The as-prepared ZrO_2 and CeO_2 filler (0, 3, 6, 9 and 12) wt % has been dispersed separately into the prepared P(S-

MMA)-PVdF(25:75 of 27wt %)-LiClO₄ (8 wt %)-EC+PC (1:1 of 65wt.%) complex. The 6wt% of CeO₂ based P(S-MMA)- PVdF(25:75) of 27wt.%-LiClO₄(8wt %)-EC+PC (1;1 of 65 wt %) electrolyte exhibits the highest ionic conductivity of 2.51×10^{-2} S /cm at room temperature and the discharge capacity of 153 mAh/g at 0.1 C rate. The prepared film is thermally stable up to 315°C. From the above studies, one who supplement that the optimized nano composite polymer blend gel electrolyte system can be used for the potential electrolyte in lithium polymer batteries.

15. CONTRIBUTION TO THE SOCIETY

(GIVE DETAILS)

- Recently, the stringent power demand is being neutralized by means of lot of portable energy storage devices, namely, batteries, supercapacitors, electrochromic devices, etc., out of which batteries have dominated the focus of energy storage systems. The major part of any battery is the electrolyte and those electrolytes should be played vital role in all energy storage devices. Those electrolytes need the favorable ionic conductivity and other physical properties.
- Based on the above requirement, PVdF-HFP, P(S-MMA) based copolymer electrolytes have been prepared with the most appreciable ionic conductivity and optimized with lot of other beneficial properties in terms of surface, structure, and thermal stability. Also, the nanocomposites were prepared and used as a filler materials in the co-polymer based polymer electrolytes to enhance the kinetics in the polymer electrolyte complexes through which it was obtained few order(s) of increment in the ionic conductivity. This enlightened the easy approach in using the mentioned co-polymers and filler materials for fabricating the Lithium rechargeable batteries to the society, which is very needed one in the present scenario.
- The outcome of the present project has been arrived as 07 International papers in the

peer reviewed journal and few more works were communicated to the relevant journals. One can go for the fabrication of Lithium batteries, these outcomes are the most helpful.

16. WHETHER ANY Ph.D. ENROLLED/PRODUCED OUT OF THE PROJECT

PhD produced : **02**

Manpower trained : **04**

17. NO. OF PUBLICATIONS OUT OF THE PROJECT - **07**

(List and full papers attached)

| S.No | Title of the Article | Authors | Name of the journal Vol. No. &Page | Impact factor |
|------|--|---|--|---------------|
| 1 | Physical and electrochemical characteristics of phosphonium ionic liquid based solid and gel-polymer electrolyte for lithium secondary batteries | R.Muthupradeepa, M.Sivakumar* , R.Subadevi, V.Suryanarayanan, M.Ramachandran, P.Rajkumar, R.Yuvakkumar | J.Materials Science: Materials in Electronics DOI: 10.1007/s10854-020-04820-7 | 2.220 |
| 2 | Effect of dispersoid on sulfonium ionic liquid based gel polymer electrolyte for lithium secondary battery | R.Muthupradeepa, M.Sivakumar* , R.Subadevi, V. Suryanarayanan, Wei-Ren Liu | Journal of Nanoscience and Nanotechnology. 18 (2018) 215-222 | 1.134 |
| 3 | Sulfonium cation based ionic liquid incorporated polymer electrolyte for lithium ion battery | R. Muthupradeepa, M. Sivakumar* , R. Subadevi and V. Suryanarayanan | <i>Polymer Bulletin</i> , 74 (2017) 1677-1691. | 2.014 |
| 4 | Studies On The Effect Of Dispersoid (ZrO ₂) In PVdF-co-HFP Based Gel Polymer Electrolytes | M.Sivakumar* , R.Subadevi and R.Muthupradeepa | AIP Conference Proceedings, 1536 (2013) 857-858. | --- |
| 5 | Role of pH on synthesis and characterization of cerium oxide (CeO ₂) nanoparticles by modified co-precipitation method | M. Ramachandran, R. Subadevi, M. Sivakumar* | Vacuum, 161 (2019) 220-224. | 2.906 |
| 6. | Facile synthesis and characterization of ZrO ₂ nanoparticles via modified co-precipitation method | M. Ramachandran, R. Subadevi, Wei-Ren Liu and M. Sivakumar* | Journal of Nanoscience and Nanotechnology, 18 (2018) 368-373. | 1.134 |
| 7 | Structural, morphology | M.Ramachandran, | International | --- |

| | | | | |
|--|--|--|--|--|
| | and ionic conductivity studies on composite PS-MMA -ZrO ₂ polymer electrolyte for lithium polymer battery | R.Subadevi, Fu-Ming Wang, Wei-Ren Liu, M.Sivakumar | Journal of ChemTech Research 6 (2014) 1687-1689. | |
|--|--|--|--|--|

(PRINCIPAL INVESTIGATOR)

(REGISTRAR/PRINCIPAL)


(Seal)

(CO-INVESTIGATOR)

Published Papers



Physical and electrochemical characteristics of phosphonium ionic liquid-based solid and gel-polymer electrolyte for lithium secondary batteries

R. Muthupradeepa^{1,2}, M. Sivakumar^{1,*} , R. Subadevi¹, V. Suriyanarayanan³, M. Ramachandran^{1,4}, P. Rajkumar¹, and R. Yuvakkumar¹

¹#120, Energy Materials Lab, Department of Physics, Alagappa University, Science Block, Karaikudi, Tamil Nadu 630003, India

²Sree Sastha Institute of Engineering and Technology, Chennai, Tamil Nadu 600123, India

³Electro-Organic Division, Central Electrochemical Research Institute, Karaikudi, Tamil Nadu 630 006, India

⁴Department of Physics, Arumugam Pillai Seethai Ammal College, Tiruppathur, Tamil Nadu 630211, India

Received: 25 July 2020

Accepted: 3 November 2020

© Springer Science+Business Media, LLC, part of Springer Nature 2020

ABSTRACT

In this work, a methodical study on the influence of ionic conductivity on polymer electrolyte with different weight percentages of ionic liquid and plasticizers had been investigated in detail. Solution casting method has been employed for preparing polymer electrolyte (PE) blend having poly(vinylidene fluoride-co-hexafluoropropylene) P(VdF-co-HFP) as polymer, trihexyltetradecylphosphonium bis(trifluoromethylsulfonyl) amide [P_{14,6,6,6}][Tf₂N] as ionic liquid and ethylene carbonate (EC) as well as propylene carbonate (PC) in 1: 1 ratio as plasticizers. The polymer electrolyte has been found out stable up to 450 °C, as measured from Thermal gravimetric analysis (TGA). Impedance spectral analysis reveals that the ionic conductivity of SPEs is 3.209×10^{-6} S/cm at 303 K with 25 wt% of ionic liquid. The addition of plasticizers (EC + PC (60 wt%)) results in two orders of magnitude of higher ionic conductivity (3.40×10^{-4} S/cm at 303 K), than that of SPEs. X-ray diffraction (XRD), Fourier transform infrared spectroscopy (FTIR) and scanning electron microscope (SEM) are performed to study the physico-chemical characteristics of polymer electrolytes. Electrochemical stability, potential window and discharge characteristics of the coin cell containing the electrolytes and LiFePO₄ electrode were investigated using linear and cyclic voltammetry.

Address correspondence to E-mail: sivakumarm@alagappauniversity.ac.in; susiva73@yahoo.co.in

1 Introduction

The lithium batteries are the utmost choice for high energy consuming devices because of their properties which relate to their high working voltage, high energy density, long cycle life, better mechanical property and size effective [1–3]. Electrolytes with electro active properties such as ionic conductivity, electro chemical window, cyclic shall play a vital role in electrochemical devices. Electrolytes belonging to polymer electrolytes have higher conductivity, high thermal and mechanical stability, wide electro chemical window and so on [4–6]. Whereas Organic electrolytes as well as solid polymer electrolytes fails in these properties such as flammability, volatility, lithium dendrites, leakage, hazards to nature and poor contact between electrodes, [7]. On the other hand, ionic liquid incorporated polymer electrolyte matrix provides mechanical support, whereas ionic liquid itself gives the anion and cation for ionic conductivity [8]. However, selection of suitable polymer host and an ionic liquid is very important. High chemical stability and strong electron withdrawing functional groups are the most desirable property of a polymer. One of the polymer widely investigated is poly(vinylidene fluoride-*co*-hexafluoropropylene) P(VdF-*co*-HFP) for its high dielectric constant ($\epsilon = 8.4$) and facilitation of high number of charge carriers. The crystallinity present in the semi-crystalline polymer retains adequate mechanical stability to activate as a separator for the electrodes, while the amorphous phase provides sufficient conducting nature [9–12]. On the other hand, P(VdF-*co*-HFP) retains more electrolyte solutions due to its low crystallinity associated with excellent chemical resistance, mechanical and thermal properties, etc., [13, 14].

Molten salts have the appearance of liquid at room temperature are called as ionic liquid. Ionic liquids have received great attention from researchers due to their potential applications with excellent physical and chemical properties. Ionic liquids have very interesting property such as low vapor pressure, non-volatility, high thermal stability, high electro chemical window [15, 16]. With the prevailing properties, ionic liquids are considered as one of the best choice of materials for lithium battery fabrication in modern world technology [17, 18]. Organic or inorganic anions and organic cations which are poorly bonded are known as ionic liquids. This asymmetric structure

makes them hard to crystallize; hence they have liquid nature with wide temperature range [19]. In the first generation of ionic liquids, attention is being paid in imidazolium-based cation for its high conductivity and low viscosity. But in the view of its low electrochemical window due to its acidic proton, it has limited applications. Phosphonium ionic liquids have particular strong property of negligible vapor pressure, high thermal capacity, and wide liquid range [20]. Phosphonium architecture-based ionic liquids have particular property compared to ammonium, pyridinium and imidazolium cationic counter parts, as it does not have acidic proton [21, 22]. Phosphonium cation has four different substituents and good chance to bonding with large number of anions [23]. Phosphonium-based ionic liquids exhibit high thermal stability and high electrochemical stability window. Due to its high viscosity (295.91 mPa s at 25 °C), it restricts the ionic mobility and offers low ionic conductivity (0.89 mS/cm) compared to other ionic liquids. Columbic interaction between anion and cation results in high viscosity and highly delocalized cation compose the ionic liquid as liquid at room temperature [24]. Ionic liquids with Tf₂N exhibit low viscosity and wide electrochemical stability due to the delocalized charge in Tf₂N, which leads to flexible structure and weak interaction with other charges [25].

Ethylene and propylene carbonate (EC and PC) plasticizer in 1:1 ratio was added to the IL to improve its poor ionic conductivity caused by high viscosity of phosphonium cation. The gel polymer electrolyte formed with organic carbonate provides necessary viscosity to the cationic phosphonium leads to swamped viscosity. Organic carbonates (EC and PC) dissociate the columbic interaction in ionic liquids because of their high dielectric constant such as $\epsilon = 89.78$ at 40 °C and 64.93 at 25 °C, respectively [26].

In this framework, solid and gel polymer electrolytes (SPEs and GPE) were prepared using solution casting method; P(VdF-*co*-HFP) polymer has been modified using of trihexyltetradecylphosphonium bis(trifluoromethylsulfonyl) amide [P_{14,6,6,6}] [Tf₂N] ionic liquid. For energy storage applications, the optimized electrolyte has been elucidated respectively from different ratios of polymer to ionic liquid such as (95–5 wt%, 90–10 wt%, 85–15 wt%, 80–20 wt% and 75–25 wt%). The GPE has been prepared by adding EC and PC in SPE. The maximum

conductivity and the physical as well as electrochemical properties of the polymer matrix have been found out from their optimum ratio for lithium battery application. The effect of ionic liquid and plasticizer in PE has been studied by subjecting them for different characterizations. The physical property has been studied using X-ray diffraction measurements (XRD), Fourier transform infrared spectrometer (FTIR), thermo gravimetric and differential thermal analysis (TG/DTA), and scanning electron microscopy (SEM), while the electrochemical properties have been analyzed using AC impedance, linear sweep voltammetry (LSV), cyclic voltammetry (CV) and charge-discharge (C/D) analyses.

2 Experimental

Poly(vinylidene fluoride-co-hexafluoropropylene) P(VdF-co-HFP) as polymer matrix, trihexyltetradecylphosphonium bis(trifluoromethylsulfonyl) amide [P_{14,6,6,6}][Tf₂N] ionic liquid, ethylene carbonate (Merck, India) and propylene carbonate are the basic chemicals used in this work. Solution casting method has been employed to prepare the polymer electrolytes in the ratios mentioned in Table 1. The polymer PVdF-co-HFP and ionic liquid [P_{14,6,6,6}][Tf₂N] both were received from Sigma Aldrich USA and used without further purification. Tetrahydrofuran (THF) was used as a solvent to dissolve the polymer and to prepare the polymer matrix. Organic solvents were purchased from SRL India and used as received. As mentioned in Table 1, the calculated amount of polymer was dried in vacuum under 1×10^{-3} Torr pressure in a temperature-controlled vacuum oven at 100 °C for 10 h. The

moisture and impurity present in the polymer was removed by the vacuum heating process. An efficient amount of solvent THF was poured in the polymer to make polymer solution by stirring. The calculated amount of ionic liquid or ionic liquid with EC and PC was added to the above polymer solution, which was stirred continuously to obtain homogeneity. A flat bottom petri plate has been used to cast the mixture of polymer ionic liquid solution to obtain thin electrolyte film. Finally, freestanding films were dried at 60 °C under vacuum for 5 h.

The PANalytical X'Pert PRO powder X-ray diffractometer using Cu-K α radiation as source and operated at 40 kV had been used to study the variation of crystalline nature as the function of ionic liquid ratio. The FTIR Thermo Nicolet 380 spectrometer was used to study the interactions of different fundamental vibrational groups in the range of 4000 to 400 cm⁻¹. Thermal analysis was performed using STA 409 PL Luxxat a heat rate of 10 °C/min within the temperature range from room temperature to 900 °C under Nitrogen atmosphere. The surface nature has been studied with SEM Model JEOL-JSM-6500F at an accelerating voltage of 5 kV and 15 kV after sputtering platinum over the samples.

AC impedance technique has been performed to find out the conductivity of the ionic liquid polymer electrolytes sandwiched between stainless steel (SS) blocking electrodes. A computer-controlled micro Autolab III Potentiostat/Galvanostat with frequency range from 1 Hz to 500 kHz with a signal amplitude of 10 mV, were used to study the conducting behavior at different temperature ranging from 303 to 353 K. The bulk resistance obtained from the complex impedance plot has been employed for ionic conductivity calculation. For other electrochemical

Table 1 The calculated weight percentage, ionic conductivity and activation energy values of solid and gel polymer electrolytes PVdF-co-HFP, [P_{14,6,6,6}][Tf₂N], EC + PC

| PVdF-co-HFP + [P _{14,6,6,6}][Tf ₂ N] (wt%) | EC + PC (wt%) | Sample code/temperature | Conductivity $\times 10^{-6}$ S/cm | | | | | | E_a values (eV) |
|---|---------------|-------------------------|------------------------------------|--------|--------|--------|---------|---------|-------------------|
| | | | 303 K | 313 K | 323 K | 333 K | 343 K | 353 K | |
| 95 + 5 | 0 | K1 | 0.0470 | 0.0581 | 0.1303 | 0.1740 | 0.1942 | 0.2525 | 0.429 |
| 90 + 10 | 0 | K2 | 0.0974 | 0.2429 | 0.4507 | 0.7026 | 1.1541 | 2.4014 | 0.390 |
| 85 + 15 | 0 | K3 | 1.1506 | 1.5145 | 2.4737 | 4.4781 | 12.143 | 22.463 | 0.334 |
| 80 + 20 | 0 | K4 | 1.7375 | 2.2175 | 3.6032 | 6.9046 | 25.502 | 40.345 | 0.321 |
| 75 + 25 | 0 | K5 | 3.2090 | 4.1876 | 6.8012 | 19.249 | 31.483 | 58.813 | 0.305 |
| 75 + 25 | 60 | K6 | 340.23 | 388.32 | 484.87 | 676.36 | 1205.36 | 1579.76 | 0.197 |

analysis, coin cells have been fabricated for high ionic conducting electrolyte sample. Li has been used as reference and counter electrode. Working electrode has been fabricated with 80:10:10 ratios of LiFePO₄:PVdF:Super P carbon. The above combination was prepared as slurry using NMP solvent and coated on Alumina foil and then dried at 80 °C for 6 h. Then the coin cells (CR 2032) have been fabricated for electrochemical characterization. The electrochemical studies were carried out using Autolab electrochemical workstation (GPES, PGSTAT 302N).

3 Results and discussion

3.1 X-ray diffraction

Figure 1 shows X-ray diffraction pattern of pure P(VdF-co-HFP) and mixed SPEs and GPE in the ratio as mentioned in Table 1. It is clearly visible that the pure polymer P(VdF-co-HFP) has semi-crystalline nature, where the crystalline peaks with 2θ angle at 18.44°, 20.13° and 39.04° reflect the α phase of crystalline plane [27]. The representation of these peaks makes the atoms to arrange in lattice and remaining amorphous nature is responsible for ionic conductivity [28]. However, in SPEs and GPE, the appeared peaks corresponding to P(VdF-co-HFP) are wider and reduce the crystalline domains and try to form an

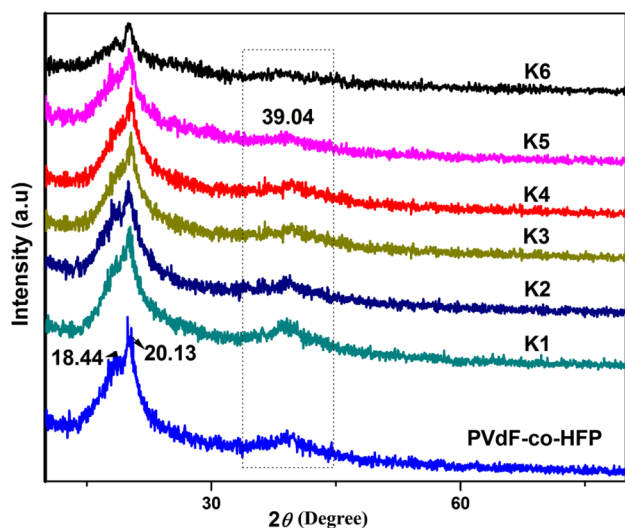


Fig. 1 X-ray diffraction pattern of pure P(VdF-co-HFP), different SPE K1-(95:5), K2- (90:10), K3- (85:15), K4- (80:20), K5- (75:25) of P(VdF-co-HFP) + [P_{14,6,6,6}][Tf₂N] and GPE K6- PVdF-co-HFP + [P_{14,6,6,6}][Tf₂N] (75:25) + EC + PC (60) wt%

amorphous system. Here, intensity of the resultant peaks for P(VdF-co-HFP) polymer matrix blended with [P_{14,6,6,6}][Tf₂N] as well as [P_{14,6,6,6}][Tf₂N] + EC + PC decreases drastically, which shows weak peaks with wide nature in all cases. From the patterns, it is noted that intensities of the peak decreases upon increasing IL content. When compared to the SPEs, the diffraction pattern of electrolyte with EC + PC shows nearly a flat pattern. This peak is representing high amorphous nature, which is responsible for high ionic conductivity.

3.2 FTIR analysis

Figure 2 represents the FTIR spectra in the region of 4000 to 400 cm⁻¹ of pure P(VdF-co-HFP) and IL imported PEs. The wavenumber between 1000 and 400 cm⁻¹ have been magnified to view the spectrum more clearly. A crystalline phase of P(VdF-co-HFP) obtained at 490 cm⁻¹, 512 cm⁻¹, 531 cm⁻¹, 614 cm⁻¹, 761 cm⁻¹, 796 cm⁻¹, 976 cm⁻¹ represent the presence of the P(VdF-co-HFP) in the complex system. The vibrations at 490 cm⁻¹ and 512 cm⁻¹ represent the bending and wagging modes of CF₂ group, whereas the wave number at 531 cm⁻¹ and 976 cm⁻¹ ascribe to nonpolar TGTG trans gauche conformation [29]. The CF₂ bending and CCC skeletal vibration are noted from the wave number at 614 cm⁻¹. The vibrational peak at 796 cm⁻¹ stands for CF₃ stretching for polymer. Here, peaks 839 cm⁻¹ and 879 cm⁻¹ represent the β amorphous phase of polymer (represented by * in Fig. 2), where, the mixed mode of CH₂ rocking and CF₂ asymmetric stretching appears at 839 cm⁻¹ and 879 cm⁻¹ corresponding to CF₂ and CC symmetric stretching vibrations. The appearance of peaks at 2960 cm⁻¹ and 3024 cm⁻¹ represent the C-H stretching polymer [11]. The Tf₂N anion has been confirmed from the obtained peaks at 1348 cm⁻¹, 1196 cm⁻¹, 1136 cm⁻¹ and 1055 cm⁻¹, and the peaks in the complexes are shifted to 1344 cm⁻¹, 1055 cm⁻¹. The remaining peaks combine together and form may be due to more thickness of the film a single band. A band existing at 1150 cm⁻¹ represent the P = O group in [P_{14,6,6,6}] of IL. The appearance of peaks at 2855 cm⁻¹ and 2950 cm⁻¹ represent the CH₂ bonds of the aliphatic chains presented in phosphonium cation [30]. The shifting and disappearance of peaks confirms the formation of complexation between the polymer and ionic liquid. While increasing the ionic liquid content, most of the

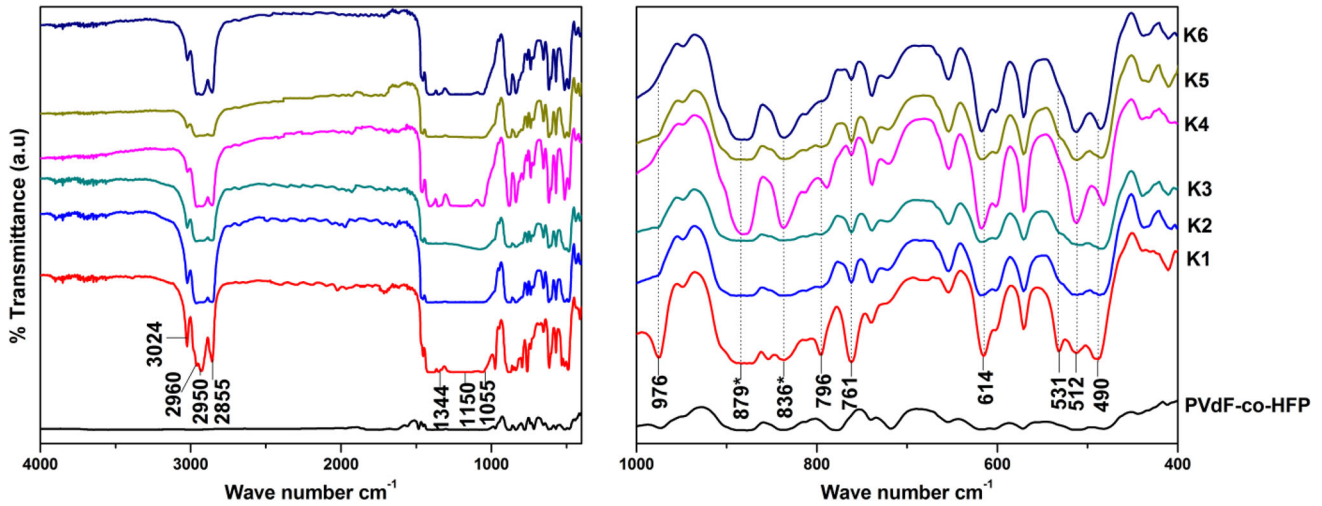


Fig. 2 FTIR spectra of pure P(VdF-co-HFP), different SPE K1-(95:5), K2- (90:10), K3- (85:15), K4- (80:20), K5- (75:25) of P(VdF-co-HFP) + [P_{14,6,6,6}][Tf₂N] and GPE K6-PVdF-co-HFP + [P_{14,6,6,6}][Tf₂N] (75:25) + EC + PC (60) wt% system

crystalline peaks become weaker and amorphous peak becomes broader. This shows that the high content of ionic liquid tries to form an amorphous phase.

3.3 Ionic conductivity

The ionic conductivity values of the electrolytes have been estimated through AC impedance studies by observing real and imaginary parts for plotting CI plot. Figure 3a displays the complex impedance (CI) plot of P(VdF-co-HFP) polymer electrolyte with different [P_{14,6,6,6}][Tf₂N] contents and GPE at room temperature. It is noted that the CI plots of SPEs reflect the general of ionic solids with a typical semicircle and a spike behavior, whereas, only spike is appeared in GPE [30, 31]. The intercept of the semicircle or the spike with higher frequency in Z' real axis gives the information about bulk resistance (*R_b*) of the polymer electrolyte [32, 33]. The conductivity values were calculated using the following equation:

$$\sigma = \frac{l}{AR_b} \tag{1}$$

where σ is the ionic conductivity value, *l* is thickness of the electrolyte, *A* is the area of the film and *R_b* is the bulk resistance. It is observed that from Fig. 3a the size of semicircle portion of CI plot at room temperature decreases upon the addition of IL; at one stage, the semicircle has been disappeared. Also it is noted that the incorporation of the plasticizer causes a

complete elimination of the semicircle [34]. The ionic conductivity values are proportional to [P_{14,6,6,6}][Tf₂N] content (Table 1). The higher content of [P_{14,6,6,6}][Tf₂N] suggests more amount of liquid electrolyte with maximum ionic conductivity of 3.209×10^{-6} S/cm at 303 K with 25 wt% of IL. These can be simply explained as follows: high content of [P_{14,6,6,6}][Tf₂N] in electrolyte has more number of free ions and these ions have very weak interaction with the polymer compared to the metallic salts [35]. These free ions found in polymer electrolyte have migrated easily through their free volume and results in higher conductivity. The addition of high amount of ionic liquid (beyond 25 wt%) produces higher conductivity among the polymer electrolyte studied. It is comparable with the earlier reports that the 100% of [P_{14,6,6,6}][Tf₂N] has ionic conductivity of the order of 8.9×10^{-4} S/cm at 303 K [24] and 1.34×10^{-4} S/cm at 303 K as reported by Battez et al. [30]. The major disadvantage with ionic liquid limits their use in industrial application due to its high cost. Because of this, the content of ionic liquid is restricted to 25% in SPEs. The concept of GPE has been introduced to reduce the viscosity of IL in polymer electrolytes. However, the plasticizer selection is made with EC + PC plasticizer with 60 wt%. The inclusion of plasticizer in SPE has found to increase the ionic conductivity up to two orders of magnitude. The prepared gel polymer electrolyte has ionic conductivity of 3.40×10^{-4} S/cm at 303 K. Hence, it is concluded that, the inclusion of plasticizer induces the conductivity in ILPE.

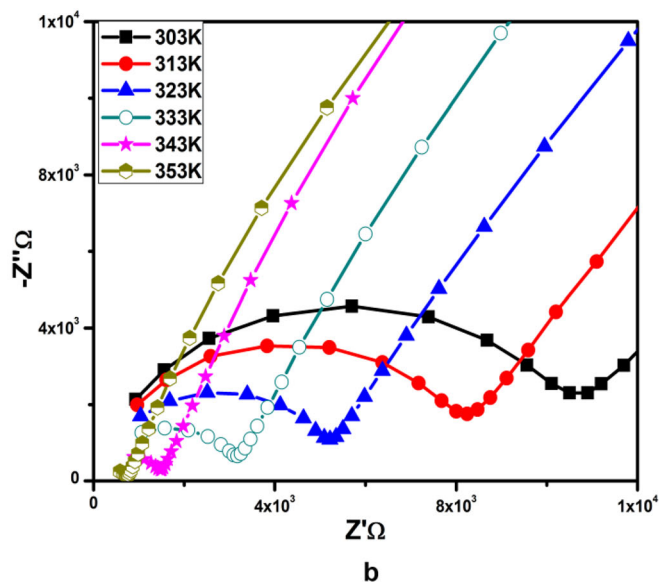
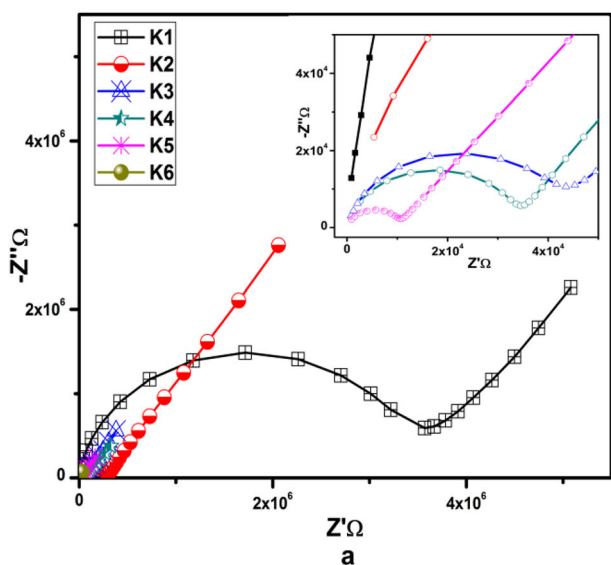


Fig. 3 a Complex impedance plot for SPE K1-(95:5), K2- (90:10), K3- (85:15), K4- (80:20), K5- (75:25) of P(VdF-co-HFP) + [P_{14,6,6,6}][Tf₂N] and GPE K6 P(VdF-co-HFP) + [P_{14,6,6,6}][Tf₂N] (75:25) + EC + PC (60) wt% in the

SS/GPE/SS cell at room temperature, **b** Complex impedance plot of K5 P(VdF-co-HFP) + [P_{14,6,6,6}][Tf₂N] (75:25) at different temperatures

In order to understand ionic conducting behavior at different temperatures, the ionic conductivity of K1–K6 has been studied between 303 and 353 K and Fig. 3b shows the CI plot of K5 at various temperatures. In phosphonium-based ionic liquids, the higher viscosity with huge number of ions does not form a completely amorphous system leading to poor ionic conductivity, than sulphonium IL-based system.

The temperature-dependent ionic conductivity plot of all electrolytes in the variation of ionic conductivity values as a function of temperature has been plotted and shown in Fig. 4. The ion conducting behavior of the prepared electrolytes, (K1–K6) obeys the Arrhenius behavior and satisfies the Arrhenius relation given below:

$$\sigma = \sigma_0 \exp(E_a/kT) \tag{2}$$

where σ is the conductivity, σ_0 is the pre exponential factor, E_a activation energy, k is the Boltzmann constant and T is the absolute temperature. From the slope of the straight line, the activation energy values have been calculated and listed in Table 1. The activation energies of SPE (K5) and GPE (K6) with and without plasticizers are 0.305 eV and 0.197 eV, respectively. The maximum conducting sample in SPE category, it requires minimum activation energy. Still the requirement of energy is reduced upon adding plasticizer 60 wt%.

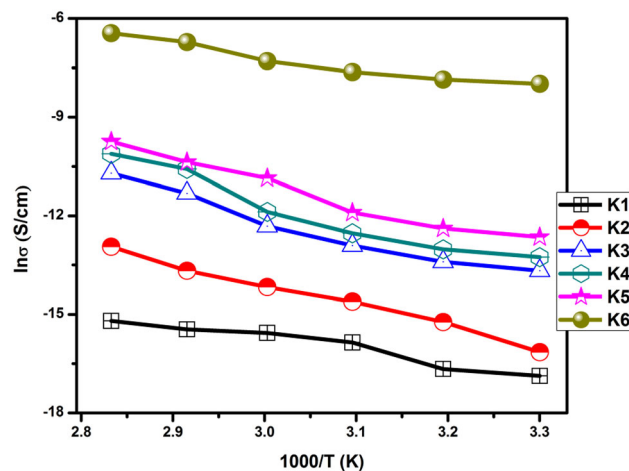


Fig. 4 Arrhenius plot of samples SPE K1-(95:5), K2- (90:10), K3- (85:15), K4- (80:20), K5- (75:25) of P(VdF-co-HFP) + [P_{14,6,6,6}][Tf₂N] and GPE K6 P(VdF-co-HFP) + [P_{14,6,6,6}][Tf₂N] (75:25) + EC + PC (60) wt% between the temperature 303 K to 353 K

The conductivity of 5 wt% of IL has lower value of conductivity, which is almost non-conducting due to the lesser number of charge carriers and due to the semi-crystalline nature of P(VdF-co-HFP). With the increase of the temperature, the polymer chains are more flexible and produce larger number of free volumes, which helps for easy ionic migration leading to higher ionic conductivity. The increase of

temperature also lowers the crystalline nature. At high ionic liquid and plasticizer content, the numbers of charge carriers are more and produce simply more pathways for cation and anions.

3.4 Scanning electron microscope (SEM) studies

The surface morphology of the prepared P(VdF-co-HFP) + [P_{14,6,6,6}][Tf₂N] electrolytes was studied using SEM. Figure 5 represents the surface structure of pure P(VdF-co-HFP) as well as P(VdF-co-HFP) + [P_{14,6,6,6}][Tf₂N] or P(VdF-co-HFP) + [P_{14,6,6,6}][Tf₂N] + EC + PC electrolytes with the magnification of 1 K. The pure P(VdF-co-HFP) electrolyte shows many spherical balls like structure and they are uniformly distributed though out the matrix. These balls are responsible for the crystalline nature of the polymer matrix [27]. The addition of [P_{14,6,6,6}][Tf₂N] reduces the size of the spherical balls and produces flat surface with lesser number of pores. Adding 25 wt% of [P_{14,6,6,6}][Tf₂N] produces maximum pores in prepared SPEs, while GPE has more number of pores than that. These pores were responsible for ionic conduction and reduced spherical balls forms more amorphous network which results in high ionic conductivity, as discussed in XRD and ionic conductivity studies.

3.5 Thermal studies

The thermo gravimetric and differential thermal analysis (TGDTA) was used to study the thermal stability of the prepared electrolyte samples. Generally, the pure [P_{14,6,6,6}][Tf₂N] ionic liquid has the thermal stability of 350 °C as reported by Battez et al. [29], whereas the ionic liquid incorporated polymer electrolyte has maintained the maximum thermal stability of 300 °C with 22% weight loss. The thermal stability of prepared electrolytes was measured from 32 to 900 °C having two weight loss regions. The first degradation temperature has been found nearly at 320 °C corresponding to the decomposition of the ionic liquid medium with the weight loss of 20 wt%. The complete decomposition temperature of polymer electrolyte has appeared around 500 °C showing the melting of the polymer electrolyte in nitrogen controlled atmosphere. The deep weight loss of about 60% is also noted indicating the decomposition temperature of polymer electrolyte. Among the samples studied, the electrolyte with higher ionic conductivity has maximum thermal stability of 260 °C. Compared to SPEs, the GPE has less stability around 260 °C, due to the evaporation of molecular solvents. The maximized region in Fig. 6 clearly shows the weight loss region of the individual polymer electrolytes. The remaining weight percentage may be due to the presence of residual carbon in the polymer electrolytes. A typical DTA curve for the polymer

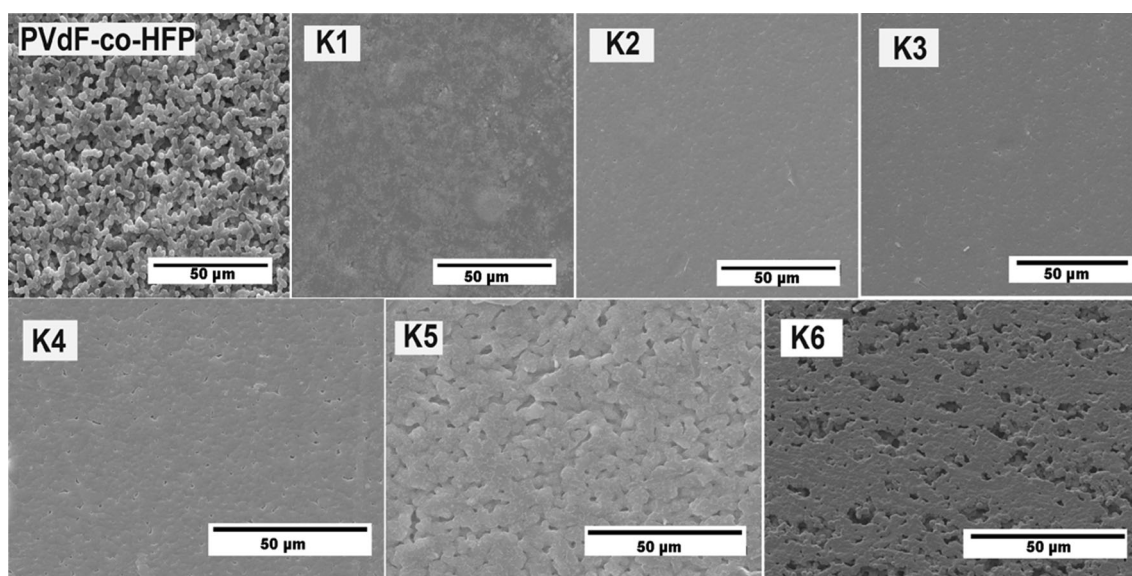


Fig. 5 SEM image of pure P(VdF-co-HFP), SPE K1-(95:5), K2- (90:10), K3- (85:15), K4- (80:20), K5- (75:25) of P(VdF-co-HFP) + [P_{14,6,6,6}][Tf₂N] and GPE K6-PVdF-co-HFP + [P_{14,6,6,6}][Tf₂N] (75:25) + EC + PC (60) wt% magnification of 1 K

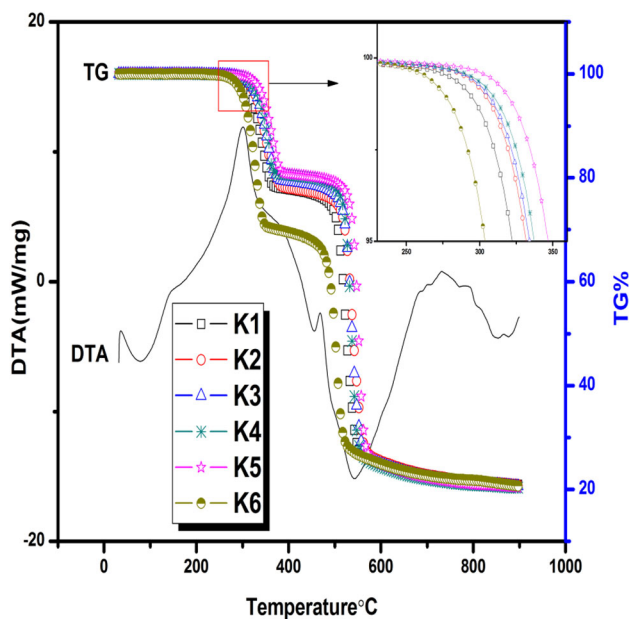


Fig. 6 TGDTA graph of SPE K1-(95:5), K2- (90:10), K3- (85:15), K4- (80:20), K5- (75:25) of P(VdF-co-HFP) + [P_{14,6,6,6}][Tf₂N] and GPE K6 P(VdF-co-HFP) + [P_{14,6,6,6}][Tf₂N] (75:25) + EC + PC (60) wt% and typical DTA plot of SPE

electrolytes (SPE) has also been displayed. Corresponding exothermic curves also noted around 300 °C, 470 °C and 720 °C shows the inline behavior of the TG and DTA. The higher ionic conducting sample has been found as a suitable electrolyte for further electrochemical studies.

3.6 Linear sweep voltammetry

The linear sweep voltammetry technique (LSV) was used to find the electrochemical stability of polymer electrolyte and presented in Fig. 7. It is noted that the present polymer electrolyte samples shows no observable current through the working electrode from open circuit 4.8 V. Gradually increasing electrode potential above 4.8 V shows the electrochemical stability of polymer electrolyte. A significant electrochemical stability upto 4.8 V (K5) and 5 V (K6) were noted with a scanning rate of 5 mV/s. This stability is higher than the commercially available electrolytes for lithium batteries with the working voltage of 4.2 V. Also the electrolytes with plasticizer (GPE) have electrochemical stability slightly higher than the SPE. The anodic current is stable upto 4.8 V and after that, a sharp increase in anodic current is noted and the current that is related to the decomposition of the

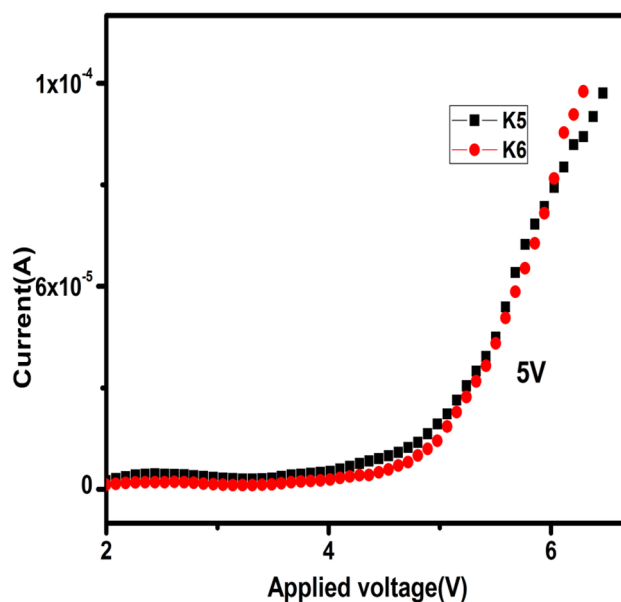


Fig. 7 LSV of SPE K5 P(VdF-co-HFP) + [P_{14,6,6,6}][Tf₂N] (75:25) and GPE K6 P(VdF-co-HFP) + [P_{14,6,6,6}][Tf₂N] (75:25) + EC + PC (60) wt% at a scan rate of 5 mV/s

polymer electrolyte. This represents the electrochemical reaction of the electrode with the polymer electrolyte [34].

3.7 Cyclic voltammetry

Cyclic voltammetry of coin cell with P(VdF-co-HFP) (75 wt%) + [P_{14,6,6,6}][Tf₂N] (25 wt%) and (75:25) of P(VdF-co-HFP): [P_{14,6,6,6}][Tf₂N] (40 wt%) + EC + PC (60 wt%) as electrolytes with LiFePO₄ cathode taken at room temperature for the first three consecutive cycles at a scan rate of 5 mV s⁻¹ is shown in Fig. 8a, b. The first scan starts with an oxidation peak (3.42 for K5 and 3.57 for K6) followed by a reduction peak (3.2 V). The appearance of oxidation and reduction peaks suggests the strong reversible behavior of electrolyte material. Repeated scan for the consecutive cycles shows the overlapping of the curves, and this is mainly related with the reversibility. The increasing oxidation peak indicates the decompositions of the polymer electrolyte. The formation of solid electrolyte interface (SEI) on the electrode surface are identified by the decreasing the current in the second and third cycles. The SEI formation prevents further reaction of ionic liquid with lithium electrode. It is also noted that the oxidation happens within clear and high current conduction for the phosphonium-based sample. However, a feeble current

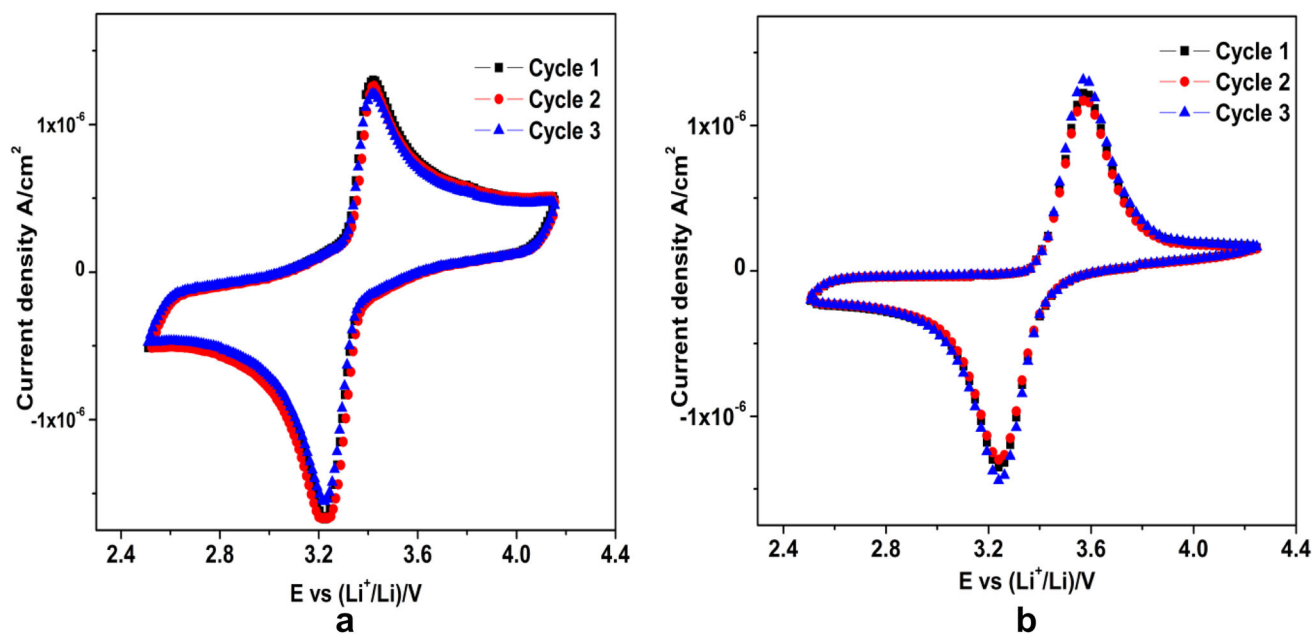


Fig. 8 Cyclic voltammetry of **a** SPE K5 P(VdF-co-HFP) + [P_{14,6,6,6}][Tf₂N] (75:25) and **b** GPE K6 P(VdF-co-HFP) + [P_{14,6,6,6}][Tf₂N] (75:25) + EC + PC (60 wt%) at a scan rate of 5 mV/s

conduction was observed for sulfonium-based electrolytes which is due to the lesser corrosive nature of phosphonium IL with the electrode in the cell.

3.8 Charge discharge studies

Coin cells have been assembled with Li metal/LiFePO₄ electrodes containing P(VdF-co-HFP) (75 wt%) + [P_{14,6,6,6}][Tf₂N] (25 wt%) and (75:25) ratio of P(VdF-co-HFP) + [P_{14,6,6,6}][Tf₂N] (40 wt%) – EC + PC (60 wt%) electrolyte to investigate the charge/discharge performance. Figure 9a, b show the cyclic voltage profile of first, fifth and tenth cycles. A flat voltage plateau has been obtained with voltage range of 3.4 V. A coulombic efficiency of above 85% has been obtained in the first cycle for both samples. The coin cell fabricated with K5 sample delivers a discharge value of about 137 mAh/g, whereas, the plasticizer embedded system delivers 146 mAh/g [36]. The discharge capacity in the multiple cycles decreases with the increase of cycle numbers. The decrease in discharge capacity is mainly due to the formation of passive layer on the cathode material. Finally, in the tenth cycle, the capacity values of charge/discharge reached to 142/131 mAh/g (K5) and 157/136 mAh/g (K6) respectively. Comparing with the previous literature reports [37–39], the present work revealed a better discharge capacity due to the phosphonium-

based ionic liquids. From the above studies, it is concluded that the plasticizer embedded system has more discharge capacity and it is suitable as electrolyte for lithium secondary batteries.

4 Conclusion

This study reports the physical and electrochemical properties of polymer electrolytes composed of phosphonium ionic liquid incorporated with P(VdF-co-HFP) solid and gel polymer electrolytes. All the electrolytes were characterized using XRD, FTIR, TG-DTA and SEM. It is concluded that the 75:25 wt% of P(VdF-co-HFP): Phosphonium IL electrolytes exhibit maximum conductivity and this drives the properties too. Also using this ratio of polymer and IL the effect of addition of plasticizer has been tested and concluded with the appreciable properties in all aspects. The addition of plasticizer would result in higher ionic conductivity and wide working voltage, however affects the thermal stability. From the experimental studies, it is observed that all the electrolytes follow Arrhenius behavior, where the best ionic conductivity of 3.40×10^{-4} S/cm at 303 K has been achieved for the GPE with minimal activation energy value of 0.197 eV. Samples containing maximum ionic conductivity have necessary porosity with

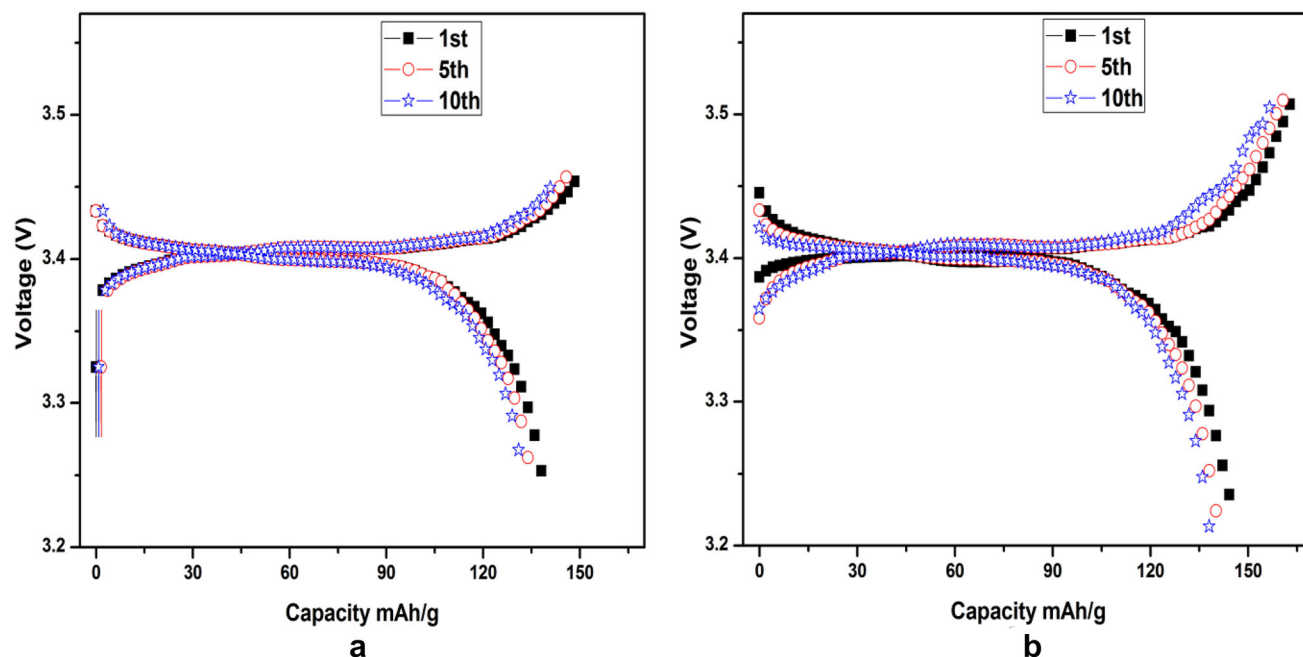


Fig. 9 Charge discharge profile of **a** SPE K5 P(VdF-co-HFP) + $[P_{14,6,6,6}][Tf_2N]$ (75:25), **b** GPE K6 P(VdF-co-HFP) + $[P_{14,6,6,6}][Tf_2N]$ (75:25) + EC + PC (60) wt% for first, fifth and tenth cycles

network structure, which is revealed by SEM images. The sample K6 is found to have thermal stability upto 260 °C with a wide electrochemical window of 5 V and discharge capacity of 146 mAh/g in lithium battery. Further, phosphonium ionic liquid-based polymer electrolyte incorporated with inorganic filler will be studied to improve the performance of composite gel polymer electrolyte.

Acknowledgements

The author M. Sivakumar gratefully acknowledges for the financial support to carry out this work by University Grants Commission (UGC), New Delhi, Govt. India, under major research project (F.No.41-839/2012(SR)). Also, all the authors gratefully acknowledge for extending the analytical facilities in the Department of Physics, Alagappa University under the PURSE programme, sponsored by Department of Science and Technology (DST) New Delhi, Govt. of India and Ministry of Human Resource Development RUSA- Phase 2.0 Grant sanctioned vide Lt.No.F-24-51/2014 U Policy (TN Multi Gen), Dept. of Education, Govt. of India.

References

1. M. Osinska, M. Walkowiak, A. Zalewska, T. Jesionowski, Study of the role of ceramic filler in composite gel electrolytes based on microporous polymer membranes. *J. Membr. Sci.* **326**(2), 582–588 (2009). <https://doi.org/10.1016/j.memsci.2008.10.036>
2. Y. Xia, T. Fujieda, K. Tatsumi, P.P. Prosini, T. Sakai, Thermal and electrochemical stability of cathode materials in solid polymer electrolyte. *J. Power Sources* **92**(1–2), 234–243 (2001). [https://doi.org/10.1016/S0378-7753\(00\)00533-4](https://doi.org/10.1016/S0378-7753(00)00533-4)
3. G. Li, Z. Li, P. Zhang, H. Zhang, Y. Wu, Research on a gel polymer electrolyte for Li-ion batteries. *Pure Appl. Chem.* **80**(11), 2553–2563 (2008). <https://doi.org/10.1351/pac200880112553>
4. C.S. Kim, S.M. Oh, Importance of donor number in determining solvating ability of polymers and transport properties in gel-type polymer electrolytes. *Electrochim. Acta* **45**(13), 2101–2109 (2000). [https://doi.org/10.1016/S0013-4686\(99\)0426-0](https://doi.org/10.1016/S0013-4686(99)0426-0)
5. F.B. Dias, L. Plomp, J.B. Veldhuis, Trends in polymer electrolytes for secondary lithium batteries. *J. Power Sources* **88**(2), 169–191 (2000). [https://doi.org/10.1016/S0378-7753\(99\)00529-7](https://doi.org/10.1016/S0378-7753(99)00529-7)
6. O.V. Bushkova, S.E. Popov, T.V. Yaroslavl'tseva, V.M. Zhukovsky, A.E. Nikiforov, Ion–molecular and ion–ion interactions in solvent-free polymer electrolytes based on amorphous butadiene–acrylonitrile copolymer and LiAsF₆. *Solid State*

- Ion. **178**(35–36), 1817–1830 (2008). <https://doi.org/10.1016/j.ssi.2007.11.023>
7. S. Ferrari, E. Quartarone, P. Mustarelli, A. Magistris, M. Fagnoni, S. Protti, C. Gerbaldi, A. Spinella, Lithium ion conducting PVdF-HFP composite gel electrolytes based on N-methoxyethyl-N-methylpyrrolidinium bis (trifluoromethanesulfonyl)-imide ionic liquid. *J. Power Sources* **195**(2), 559–566 (2010). <https://doi.org/10.1016/j.jpowsour.2009.08.015>
 8. J.P. Tafur, F. Santos, A.J. Romero, Influence of the ionic liquid type on the gel polymer electrolytes properties. *Membranes* **5**(4), 752–771 (2015). <https://doi.org/10.3390/membranes5040752>
 9. D. Saikia, Y.W. Chen-Yang, Y.T. Chen, Y.K. Li, S.I. Lin, Li NMR spectroscopy and ion conduction mechanism of composite gel polymer electrolyte: A comparative study with variation of salt and plasticizer with filler. *Electrochim Acta* **54**(4), 1218–1227 (2009). <https://doi.org/10.1016/j.electacta.2008.09.001>
 10. S.K. Chaurasia, R.K. Singh, Crystallization behaviour of a polymeric membrane based on the polymer PVdF-HFP and the ionic liquid BMIMBF 4. *RSC Adv.* **4**(92), 50914–50924 (2014). <https://doi.org/10.1039/C4RA07085B>
 11. D. Saikia, Y.W. Chen-Yang, Y.T. Chen, Y.K. Li, S.I. Lin, Investigation of ionic conductivity of composite gel polymer electrolyte membranes based on P (VDF-HFP), LiClO₄ and silica aerogel for lithium ion battery. *Desalination* **234**(1–3), 24–32 (2008). <https://doi.org/10.1016/j.desal.0000.00.000>
 12. L.N. Sim, S.R. Majid, A.K. Arof, Effects of 1-butyl-3-methyl imidazolium trifluoromethanesulfonate ionic liquid in poly (ethyl methacrylate)/poly (vinylidene fluoride-co-hexafluoropropylene) blend based polymer electrolyte system. *Electrochim Acta* **123**, 190–197 (2014). <https://doi.org/10.1016/j.electacta.2014.01.017>
 13. T. Michot, A. Nishimoto, M. Watanabe, Electrochemical properties of polymer gel electrolytes based on poly (vinylidene fluoride) copolymer and homopolymer. *Electrochim Acta* **45**(8–9), 1347–1360 (2000). [https://doi.org/10.1016/S0013-4686\(99\)00343-6](https://doi.org/10.1016/S0013-4686(99)00343-6)
 14. B.G. Soares, K. Pontes, J.A. Marins, L.F. Calheiros, S. Livi, G.M. Barra, Poly (vinylidene fluoride-co-hexafluoropropylene)/polyaniline blends assisted by phosphonium-based ionic liquid: dielectric properties and β -phase formation. *Eur. Polym. J.* **73**, 65–74 (2015). <https://doi.org/10.1016/j.eurpolymj.2015.10.003>
 15. R.E. Ramírez, L.C. Torres-González, E.M. Sánchez, Electrochemical aspects of asymmetric phosphonium ionic liquids. *J. Electrochem. Soc.* **154**(2), 229–233 (2007). <https://doi.org/10.1149/1.2404789>
 16. E.H. Cha, J.Y. Mun, E. Cho, T.E. Yim, Y.G. Kim, S.M. Oh, S.A. Lim, J.W. Lim, The corrosion study of Al current collector in phosphonium ionic liquid as solvent for lithium ion battery. *J. Korean Electrochem. Soc.* **14**(3), 152–156 (2011). <https://doi.org/10.5229/JKES.2011.14.3.152>
 17. M. Taige, D. Hilbert, T.J. Schubert, Mixtures of ionic liquids as possible electrolytes for lithium ion batteries. *Int. J. Res. Phys. Chem. Chem. Phys.* **226**(2), 129–139 (2012). <https://doi.org/10.1524/zpch.2012.0161>
 18. H.L. WuTY, P.R. Chen, J.W. Liao, Ionic conductivity and transporting properties in LiTFSI-doped bis (trifluoromethanesulfonyl) imide-based ionic liquid electrolyte. *Int. J. Electrochem. Sci.* **8**, 2606–2624 (2013)
 19. S.S. Keskar, L.A. Edey, C.M. Fellows, W.O.S. Doherty, ATR-FTIR measurement of biomass components in phosphonium ionic liquids. *J. Wood Chem. Technol.* **32**, 175–186 (2012). <https://doi.org/10.1080/02773813.2011.631718>
 20. S.R. Sarda, W.N. Jadhav, A.S. Shete, K.B. Dhopte, S.M. Sadawarte, P.J. Gadge, R.P. Pawar, Phosphonium ionic liquid-catalyzed Michael addition of mercaptans to α , β -unsaturated ketones. *Synth. Commun.* **40**(14), 2178–2184 (2010). <https://doi.org/10.1080/00397910903221050>
 21. J.W. Vaughan, D. Dreisinger, J. Haggins, Density, viscosity, and conductivity of tetraalkyl phosphonium ionic liquids. *ECS Trans.* **2**(3), 381–392 (2006). <https://doi.org/10.1149/1.2196027>
 22. A.F. Ferreira, P.N. Simoes, A.G. Ferreira, Quaternary phosphonium-based ionic liquids: thermal stability and heat capacity of the liquid phase. *J. Chem. Thermodyn.* **45**(1), 16–27 (2012). <https://doi.org/10.1016/j.jct.2011.08.019>
 23. M. Nadhera, J. Reiter, J. Moskon, R. Dominko, Lithium bis (fluorosulfonyl) imide-PYR14TFSI ionic liquid electrolyte compatible with graphite. *J. Power Sources* **196**(18), 7700–7706 (2011). <https://doi.org/10.1016/j.jpowsour.2011.04.033>
 24. P.A. Thomas, B.B. Marvey, Room temperature ionic liquids as green solvent alternatives in the metathesis of oleochemical feedstocks. *Molecules* **21**(2), 184 (2016). <https://doi.org/10.3390/molecules21020184>
 25. A.J. Rennie, N. Sanchez-Ramirez, R.M. Torresi, P.J. Hall, Ether-bond-containing ionic liquids as supercapacitor electrolytes. *J Phys Chem Lett* **4**(17), 2970–2974 (2013). <https://doi.org/10.1021/jz4016553>
 26. R. Zhang, Y. Chen, R. Montazami, Ionic liquid-doped gel polymer electrolyte for flexible lithium-ion polymer batteries. *Materials* **8**(5), 2735–2748 (2015). <https://doi.org/10.3390/ma8052735>
 27. S.K. Chaurasia, R.K. Singh, S. Chandra, Thermal stability, complexing behavior, and ionic transport of polymeric gel membranes based on polymer PVdF-HFP and ionic

- liquid,[BMIM][BF₄]. *J. Phys. Chem. B* **117**(3), 897–906 (2013). <https://doi.org/10.1021/jp307694q>
28. P.K. Singh, K.C. Sabin, X. Chen, Ionic liquidsolid polymer electrolyte blends for supercapacitor applications. *Polym. Bull.* **73**, 255–263 (2016). <https://doi.org/10.1007/s00289-015-1484-3>
 29. M. Wang, S.A. Vail, A.E. Keirstead, M. Marquez, D. Gust, A.A. Garcia, Preparation of photochromic poly (vinylidene fluoride-co-hexafluoropropylene) fibers by electrospinning. *Polymer* **50**(16), 3974–3980 (2009). <https://doi.org/10.1016/j.polymer.2009.06.044>
 30. A.H. Battez, M. Bartolome, D. Blanco, J.L. Viesca, A. Fernandez-Gonzalez, R. Gonzalez, Phosphonium cation-based ionic liquids as neat lubricants: physicochemical and tribological performance. *Tribol. Int.* **95**, 118–131 (2016). <https://doi.org/10.1016/j.triboint.2015.11.015>
 31. M. Dobbelin, I. Azcune, M. Bedu, A. Ruiz de Luzuriaga, A. Genua, V. Jovanovski, G. Cabanero, I. Odriozola, Synthesis of pyrrolidinium-based poly (ionic liquid) electrolytes with poly (ethylene glycol) side chains. *Chem. Mater.* **24**(9), 1583–1590 (2012). <https://doi.org/10.1021/cm203790z>
 32. A.R. Polu, D.K. Kim, H.W. Rhee, Poly (ethylene oxide)-lithium difluoro (oxalato) borate new solid polymer electrolytes: ion–polymer interaction, structural, thermal, and ionic conductivity studies. *Ionics* **21**(10), 2771–2780 (2015). <https://doi.org/10.1007/s11581-015-1474-1483>
 33. F. Deng, X. Wang, D. He, J. Hu, C. Gong, Y.S. Ye, X. Xie, Z. Xue, Microporous polymer electrolyte based on PVDF/PEO star polymer blends for lithium ion batteries. *J. Membr. Sci.* **491**, 82–89 (2015). <https://doi.org/10.1016/j.memsci.2015.05.021>
 34. M. Ravi, S. Song, J. Wang, T. Wang, R. Nadimicherla, Ionic liquid incorporated biodegradable gel polymer electrolyte for lithium ion battery applications. *J. Mater. Sci.: Mater. Electron.* **27**(2), 1370–1377 (2016). <https://doi.org/10.1007/s10854-015-3899-x>
 35. J.H. Shin, W.A. Henderson, C. Tizzani, S. Passerini, S.S. Jeong, K.W. Kim, Characterization of solvent-free polymer electrolytes consisting of ternary PEO–LiTFSI–PYR14 TFSI. *J. Electrochem. Soc.* **153**(9), A1649–1654 (2006). <https://doi.org/10.1149/1.2211928>
 36. K. Tsunashima, F. Yonekawa, M. Kikuchi, M. Sugiya, Tributylmethylphosphonium Bis (trifluoromethylsulfonyl) amide as an effective electrolyte additive for lithium secondary batteries. *J. Electrochem. Soc.* **157**(11), A1274–1278 (2010). <https://doi.org/10.1149/1.3490662>
 37. K. Xu, Nonaqueous liquid electrolytes for lithium-based rechargeable batteries. *Chem. Rev.* **104**(10), 4303–4418 (2004). <https://doi.org/10.1021/cr030203g>
 38. S. Seki, Y. Ohno, Y. Mita, N. Serizawa, K. Takei, H. Miyashiro, Imidazolium-based room-temperature ionic liquid for lithium secondary batteries: relationships between lithium salt concentration and battery performance characteristics. *ECS Electrochem. Lett.* **1**(6), A77 (2012). <https://doi.org/10.1149/2.003206eel>
 39. A. Swiderska-Mocek, Electrolyte based on 1-ethyl-3-vinylimidazolium bis (trifluoromethanesulphonyl) imide for Li-ion batteries. *Electrochim Acta* **132**, 504–511 (2014). <https://doi.org/10.1016/j.electacta.2014.03.185>

Publisher's Note Springer Nature remains neutral with regard to jurisdictional claims in published maps and institutional affiliations.

Effect of Dispersoid on Sulfonium Ionic Liquid Based Gel Polymer Electrolyte for Lithium Secondary Battery

R. Muthupradeepa¹, M. Sivakumar^{1,*}, R. Subadevi¹, V. Suryanarayanan², and Wei-Ren Liu^{3,*}

¹Energy Materials Lab, School of Physics, Alagappa University, Science Block, Karaikudi 630004, India

²Electroorganic Division, CSIR-Central Electrochemical Research Institute, Karaikudi 630006 Tamil Nadu, India

³Department of Chemical Engineering, Chung-Yuan Christian University, Chung-Li, Taiwan, 32023, R.O.C.

The present study emphasizes on the effect of toting of TiO₂ filler on the electrochemical enactment of polymer electrolyte containing PVdF-co-HFP(30) + SEt₃TFSI(10) + EC/PC(60) + TiO₂(x) wt% (Poly (vinylidene fluoride-co-hexafluoropropylene + Triethylsulfoniumbis(trifluoromethylsulfonyl)imide + Ethylene carbonate/Propylene carbonate (1:1 ratio) + Titanium dioxide) for lithium battery applications. Composite electrolytes with different weight percentages of TiO₂ were prepared and characterized by different surface analytical, thermal and electrochemical techniques. With gradual increase of the amount of TiO₂ upto 6 wt%, broadening of the prominent peak has been noted, suggesting a decrease in the degree of crystallinity upon the addition of TiO₂, as revealed by X-ray diffraction (XRD). Raman and FT-IR studies confirm the presence of various functional groups, present in the matrix. The electrolyte with TiO₂ (6 wt%) has maximum stability of 460 °C, as confirmed by thermal analysis. Conductivity of the composite polymer electrolytes increases upto 6 wt% of TiO₂ (3.42×10^{-3} S/cm at 303 K) and further addition, causes a dip down in conductivity, indicating an improvement in the ionic conductivity and thermal stability with the incorporation of TiO₂ filler. Surface morphologic images show the presence of surface and cavity in the polymer matrix, filled with the filler uniformly. Voltammetric studies confirm the electrochemical stability of films upto 4.62 V. Coin cell containing Li anode and LiFePO₄ cathode along with polymer electrolyte/6 wt% TiO₂ filler, delivers a first discharge capacity of 145 mAh/g with the working voltage of 3.4 V.

Keywords: Ionic Liquid, Polymer Electrolyte, Cyclic Voltammetry, Linear Voltammetry, Discharge Capacity.

1. INTRODUCTION

Polymeric, organic materials have significant advantages over inorganic materials in their easily scalable dimensions, processability with shapes and possibility for molecular design through synthesis.^{1,2} Recently, many studies performed on the oxide polymer electrolyte attracts great attention in the field of energy device owing to its high ionic conductivity, as well as enormous thermal, mechanical and electrochemical stabilities.³⁻⁵ Polymer materials are preferable and alternative to liquid electrolytes on account of their high ionic conductivity, ease of formation of thin film along the electrode-electrolyte interface, compact and no leakage characteristics etc. With these above backgrounds, they have become ideal candidates

as electrolytes for various electrochemical devices such as batteries,⁶⁻⁸ fuel cells^{9,10} and super capacitors.¹¹ The ionic conductivity of polymer electrolytes have been improved in several ways like polymer blending, addition of plasticizers as well as ionic liquids and incorporation of fillers. Among those methods, dispersion of inorganic fillers in polymer electrolytes is one of the best approaches and have been extensively studied.¹²⁻¹⁴ Weston and Steele firstly developed the composite polymer electrolytes comprising of a polymer host, doping salt and inorganic/ceramic fillers in 1982.¹⁵ Typically, the composite polymer electrolytes are prepared by incorporation of inorganic fillers or metal oxides in polymer matrix, resulting in enhanced chemical and electrochemical properties.¹⁶ Dispersion of fillers such as TiO₂, SiO₂, Al₂O₃ etc., shows positive effects in polymer electrolytes. The inorganic

*Authors to whom correspondence should be addressed.

fillers in polymer electrolytes have no contribution in enhancing their conductivity, but do improve the interfacial property and help to retain large amount of liquid electrolytes in their pores.¹⁷ Liu et al. has found that the introduction of nano SiO₂ in PP13TFSI and PEO18LiTFSI ionic liquid electrolytes helps to suppress the formation of dendrite enhances the electrical conductivity and decreases the interface resistance between Li and the polymer electrolyte.¹⁸

It is important to note that most of the studies have focused on composite polymer electrolytes incorporated with salts and a little attention is paid to study the filler effect in ionic liquid based polymer electrolytes. It is generally accepted that the ionic liquid has excellent properties such as high ionic conduction, non-volatility, good thermal stability for high temperature application.^{19–21} As noted in the literature, Wei et al.²² has reported that triethyl sulfonium bis(trifluoro methylsulfonyl) imide (SEt₃TFSI) ionic liquid has very high specific capacitance value with large electro chemical widow, when compared to the imidazolium and ammonium analogues.

In our previous work, it has been established that the electrolyte composed of poly(vinylidene fluoride-co-hexafluoro propylene) P(VdF-co-HFP), triethyl sulfonium bis(trifluoro methylsulfonyl) imide (SEt₃TFSI) and ethylene carbonate and propylene carbonate (EC + PC) (1:1 ratio) (PVdF-co-HFP(30) + SEt₃TFSI(10) + EC/PC(60) wt% composition) provides excellent conductivity and high thermal stability [un published results]. The plasticizers added in above system reduce the mechanical properties of the polymer electrolyte.²³ Inclusion of inorganic fillers in such polymer electrolytes induces amorphous nature with better mechanical strength. The main objective of this work is to harvest the combined effect of ionic liquid/polymer electrolytes and fillers in improving the performance of lithium battery containing those electrolytes. The composite polymer electrolytes are obtained by dispersing various amounts of TiO₂ (X = 3, 6, 9, 12, 15 wt%) in PVdF-co-HFP + SEt₃TFSI + EC/PC. Significant improvement in terms of ionic conductivity, thermal and electrochemical stability of the polymer electrolytes has been reported and discussed in the present work.

2. MATERIAL AND METHOD

Poly(vinylidene fluoride-co-hexafluoro propylene) (PVdF-co-HFP), triethyl sulfonium bis(trifluoro methyl sulfonyl) imide SEt₃TFSI (Aldrich USA), ethylene carbonate (EC) (Merck Germany), propylene carbonate (PC) (SRL India) was purchased and used as such. The PVdF-co-HFP(30):SEt₃TFSI(10) + EC/PC(60) wt% composition was obtained as per the procedure, reported in the previous literature, which shows higher ionic conductivity than the other compositions. Titanium dioxide (with different wt.% such as 3, 6, 9, 12 and 15) incorporated composite polymer electrolytes were prepared by solution casting method.

Table I. Ionic conductivity values and activation energy values of the CPE F1–F5 in the temperature range of 303–353 K.

| PVdF-co-HFP(30)+SEt ₃ TFSI(10)+EC/PC(60)+TiO ₂ (X) wt% | Conductivity × 10 ⁻³ S/cm | | | | | | E _a values (eV) |
|--|--------------------------------------|-------|-------|-------|-------|-------|----------------------------|
| | 303 K | 313 K | 323 K | 333 K | 343 K | 353 K | |
| F1 (X = 3) | 2.29 | 2.79 | 2.89 | 3.20 | 4.52 | 5.98 | 0.165 |
| F2 (X = 6) | 3.42 | 3.51 | 4.07 | 4.52 | 5.62 | 6.70 | 0.127 |
| F3 (X = 9) | 1.05 | 1.25 | 1.75 | 2.64 | 3.32 | 5.43 | 0.173 |
| F4 (X = 12) | 0.85 | 0.95 | 1.14 | 1.26 | 1.51 | 2.12 | 0.194 |
| F5 (X = 15) | 0.46 | 0.57 | 0.59 | 0.68 | 0.93 | 1.32 | 0.2043 |

Appropriate amount of polymer composite was dissolved in tetrahydrofuran (THF) (SRL India). The above mixture was stirred continually for a day to obtain a homogeneous solution. Finally, predetermined amount of TiO₂ was dispersed in the homogeneous solution under a magnetic stirrer. This viscous solution was casted on flat bottom petri plates and kept at room temperature for overnight. In order to remove the excess solvent present in the electrolytes, the films were dried under vacuum at 60 °C for 5 h. The compositions for each sample are listed in Table I. The crystalline structure of the pure PVdF-co-HFP, TiO₂ and prepared electrolyte samples was verified by X-ray diffraction analysis using the PANalytical X'Pert PRO powder X-ray Diffractometer using Cu-K α radiation as source and operated at 40 kV. Laser Raman Spectra was studied with STR500 Laser Raman spectrometer, SEKI, Japan. The chemical composition and vibrational groups have been studied through the FTIR Thermo Nicolet 380 spectrometer within the range of 400 to 4000 cm⁻¹. Thermal studies of the prepared electrolytes had been carried out with STA 409 PL Luxx at a heat rate of 10 k/min within the temperature range from room temperature to 900 °C under nitrogen atmosphere. The scanning electron microscope images were obtained from JEOL-JSM-6500F at an accelerating voltage of 5 and 15 kV after sputtering platinum over the samples.

Blocking stainless steel SS electrodes were used to perform the conductivity measurements of composite polymer electrolytes. The electrolytes are sandwiched between stainless steel electrodes, and the sample analysed using micro Autolab III Potentiostat/Galvanostat instrument with a frequency range from 1 Hz–500 kHz in the temperature ranges of 303–353 K. A CR2032 coin cell was fabricated for voltammetric studies. The charge/discharge life cycle was carried out using WonAtech (WBCS3000S) automatic charge/discharge testing system. The electrode composition of 80:10:10(LiFePO₄: PVdF: Super p carbon) were used for the coin cell fabrication. The slurry was made using NMP solvent and was coated on Alumina foil. After coating, the electrodes were dried at 80 °C for about 6 h. The mass of the active substance was nearly 1 mg. All the electrochemical studies had been done with quasi-equilibrated coin cell.

3. RESULTS AND DISCUSSION

X-ray diffraction pattern of composite polymer electrolyte (CPE) with different amounts of TiO_2 are shown in Figure 1. The pure PVdF-co-HFP with a crystalline peak at 20.1° shows its semi-crystalline nature. Moreover the XRD patterns of TiO_2 shows several crystalline peaks at $2\theta = 25.27^\circ, 36.9^\circ, 37.7^\circ, 38.5^\circ, 48^\circ, 53.8^\circ, 55^\circ, 62.6^\circ, 68.7^\circ, 70.2^\circ, 75^\circ$ with the (h, k, l) values of (101), (103), (004), (112), (200), (105), (211), (204), (116), (220), (215) matches with JCPDS No. 894203. The reproduced peaks in prepared electrolyte samples confirm the presence of anatase TiO_2 . From this pattern, it is clearly seen that with an increase of TiO_2 concentration, the intensity of the peaks corresponding to TiO_2 increases. It is noted that in sample with gradual increase of the amount of TiO_2 , broadening of the prominent peak and a decrease in the intensity of a 2θ value at 20.1° has been noted, which suggests a decrease in the degree of crystallinity of the polymer matrix upon the addition of TiO_2 .^{24,25} High content of TiO_2 leads low degree of crystallinity of polymer matrix. The high intensity crystalline region restricts the cation motion for ionic conduction. From Figure 1, it was concluded that the sample F2 with TiO_2 (6 wt%) possesses maximum amorphous and high ionic conductivity characteristics.²⁶

Raman analysis can provide key information of chemical composition, structure, vibrational, rotational in a system. Figure 2 shows Raman spectra of titanium dioxide incorporated polymer electrolytes at room temperature. According to the group theory analysis, the lattice dynamics of the anatase TiO_2 has normal modes of $A_{1g} + 2B_{1g} + 3E_g + A_{2u} + B_{2u} + 2E_u$ where the A_{1g} , B_{1g} and $3E_g$

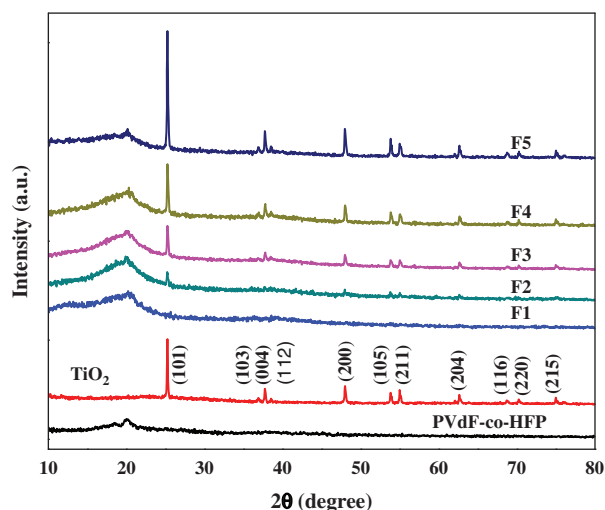


Figure 1. XRD diagram for F1:PVdF-co-HFP(75) + SEt_3TFSI (25) + EC/PC(60) wt% + TiO_2 (3 wt%), F2:PVdF-co-HFP(75) + SEt_3TFSI (25) + EC/PC(60) wt% + TiO_2 (6 wt%), F3:PVdF-co-HFP (75) + SEt_3TFSI (25) + EC/PC(60) wt% + TiO_2 (9 wt%), F4:PVdF-co-HFP(75) + SEt_3TFSI (25) + EC/PC(60) wt% + TiO_2 (12 wt%), F5 = PVdF-co-HFP(75) + SEt_3TFSI (25) + EC/PC(60) wt% + TiO_2 (15 wt%).

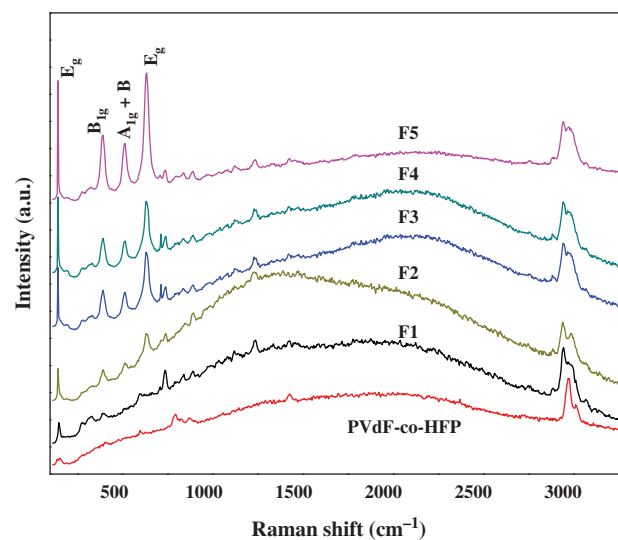


Figure 2. Raman spectra of CPE F1, F2, F3, F4, F5, the CPE composition are same as in Figure 1.

are Raman active modes.²⁷ The observed Raman peaks at 142 cm^{-1} (E_g), 393 cm^{-1} (B_{1g}), 514 cm^{-1} ($A_{1g} + B_{1g}$), and 636 cm^{-1} (E_g) confirms the presence of tetragonal anatase phase. The presence of these peaks indicates that the TiO_2 does not involve in any chemical bonding in the prepared polymer electrolytes. E_g mode at 142 cm^{-1} and 636 cm^{-1} is a characteristic peak of anatase mode.²⁸ There are two E_g modes observed at around 142 cm^{-1} and 636 cm^{-1} , B_{1g} modes at 393 cm^{-1} and 514 cm^{-1} , which are referred as $A_{1g} + B_{1g}$ mode. The symmetric stretching vibration (E_g), symmetric bending vibration (B_{1g}) and antisymmetric bending vibration (A_{1g}) stands for O–Ti–O respectively.^{29–31}

The peak assignment for TFSI anion was discussed in many literatures. The bis(trifluoro methane sulfonyl) imide anion, $\text{N}(\text{SO}_2\text{CF}_3)_2$ (TFSI^-) present in the SEt_3TFSI has two conformational stage C1 and C2 theoretically. The C1(transoid) and C2(cisoid) have symmetry with the CH_3 ($\delta_s\text{CH}_3$) on the same and opposite sides of S–N–S plane. But experimentally, it is difficult to assign these modes. The most prominent vibration of TFSI is found around 740 cm^{-1} , which is the complex assignment of TFSI expanded and cataract mode. Most of the Raman modes of polymer and liquid plasticizers are vanished due to the high intensity TiO_2 Raman peaks. The single peak at 740 cm^{-1} confirms the free ions, whereas shifting of high frequency denotes the ionic pairs. The 1137 cm^{-1} of free imide ion has been shifted to lower wavenumber of 1123 cm^{-1} due to polymer complexes attributed to the symmetric out-of-phase stretching mode of the $\nu_s\text{SO}_2$ group.^{32,33} The peak represented in 1407 cm^{-1} assigned to rocking mode of PVDF-co-HFP.³⁴

The FTIR spectra of polymer electrolyte shows the complexation and interaction between their components. The typical FTIR spectra of composite polymer

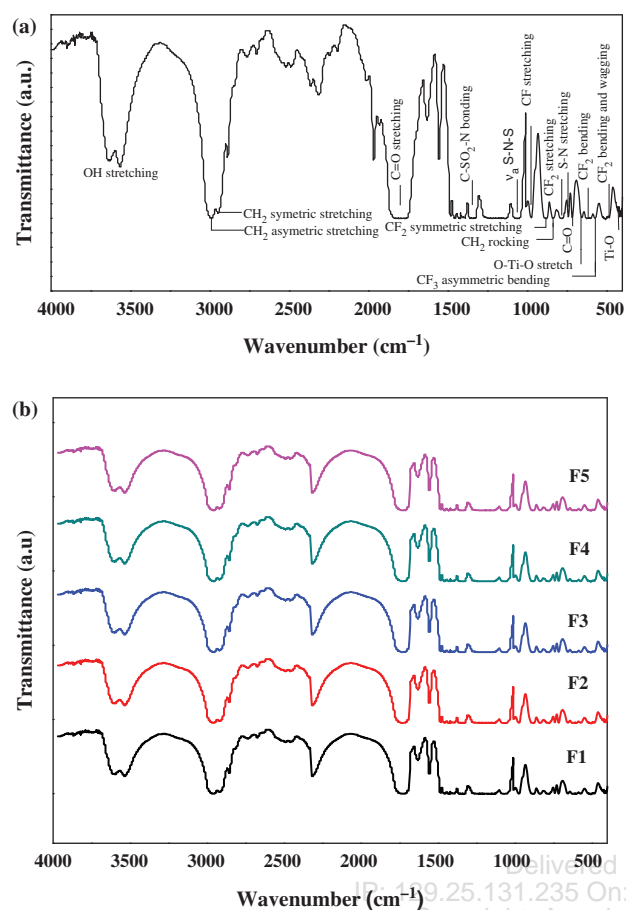


Figure 3. (a) FTIR spectrum of F2 sample; (b) FTIR spectra of F1, F2, F3, F4 and F5.

electrolytes PVdF-co-HFP + SEt₃TFSI + TiO₂ in the range of 4000–400 cm⁻¹ are shown in Figures 3(a) and (b). The α phase of PVdF-co-HFP occurring at 489, 534, 614, 762, 796 and 976 cm⁻¹ has been shifted over to lower numbers such as 482, 523, 614, 762, 785, 974 cm⁻¹ respectively due to complex formation, where, 482 cm⁻¹ belongs to bending and wagging vibration of CF₂, 613 cm⁻¹ corresponds to the CF₂ bending mode, 762 cm⁻¹ associates with CH₂ rocking vibration, 785 cm⁻¹ relates to CF₃ stretching vibration, 976 cm⁻¹ leads to CF stretching mode. Observed peaks at 836 cm⁻¹ (CH₂ rocking) and 880 cm⁻¹ (CF₂ symmetric stretching vibration) represent the amorphous phase of polymer. The PVdF-co-HFP symmetrical and asymmetrical stretching modes of CH₂ groups at 2980 cm⁻¹ and 3022 cm⁻¹ has been shifted to 2947 cm⁻¹, 2990 cm⁻¹ in the complexes.^{35,36} It is noted that the band positions of C=O stretching, symmetric ring deformation and ring deformation of PC molecule are located at 1791 cm⁻¹, 712 cm⁻¹ and 777 cm⁻¹, respectively.³⁷ The doublet peak of ethylene carbonate at 1774 cm⁻¹ and 1803 cm⁻¹ are merged and appeared as a single band between 1747 to 1844 cm⁻¹ representing the C=O bending.^{38,39} The peaks at 667 cm⁻¹, 505 cm⁻¹ and 447 cm⁻¹ are attributed to Ti–O bond. The peak at 667 cm⁻¹ refers to symmetric

O–Ti–O stretch, while peak at 446 cm⁻¹ and 505 cm⁻¹ are due to the vibration of Ti–O bond.⁴⁰ A characteristic peak appeared around 1060 cm⁻¹ represents ν_a S–N–S of TFSI anion.⁴¹ Other peaks at 1335 cm⁻¹ represents C–SO₂–N bonding mode, whereas 574 cm⁻¹ belongs to the CF₃ asymmetric bending mode, band between 601 and 625 cm⁻¹ stands for deformation mode of SO₂. Frequencies at 740, 785 cm⁻¹ correspond to S–N stretching vibration of SEt₃TFSI.³⁶ The band appears between 3400 and 3600 cm⁻¹ represents the OH stretching mode at the time of sample loading.

The ionic conducting performance of the samples at different temperatures had been studied using AC impedance. The ionic conductivity of the ionic liquid/polymer electrolyte containing different amounts of TiO₂ was analyzed using SS/CPE/SS cell at various temperatures ranging from 303 K to 353 K. The bulk resistance was evaluated from the complex impedance plot, obtained by the intercept of the real axis at high frequency region. Figure 4(a) represents the complex impedance plot of the prepared electrolyte samples with Z' Ω in X axis and Z'' Ω in Y axis. The room temperature ionic conductivity value and the activation energy values for five different compositions are reported in Table I. Ionic conductivity value for prepared composite polymer electrolytes are measured using the formula given below

$$\sigma = \frac{l}{AR_b} \quad (1)$$

where, σ is the ionic conductivity, l —thickness of the electrolyte sample, A —area of the prepared electrolyte, R_b —bulk resistance.

It is found that, the ionic conductivity of the composite polymer electrolyte increases upto a maximum and there is a dip down in the conductivity at a high content of TiO₂. The influence of filler material in the ionic liquid containing polymer electrolyte has a positive effect in terms of ionic conductivity. The best result with high value of ionic conductivity had been obtained for the sample containing 6 wt% of TiO₂. The dispersion of TiO₂ filler in ionic liquid polymer electrolyte not only increases the ionic conductivity, but also enhances the thermal and electrochemical stability of the electrolyte.

The ionic conductivity (σ) of sample F2 ($X = 6$ wt%) is 3.42×10^{-3} S/cm at room temperature which increases with the increase of temperature, as recorded in Table I. This increase in ionic conductivity with temperature results in the decreases in viscosity, leading to enhanced ionic mobility, as reported by Shalu et al.³⁶ As expected, the ionic conductivity initially increases with the addition of TiO₂, attains maximum, and starts to decrease with further incorporation of TiO₂ fillers. The addition of inorganic filler reduces the degree of crystallization in semi crystalline CPE and also improves the polymer inorganic interface.³ As observed in the XRD analysis, sample with

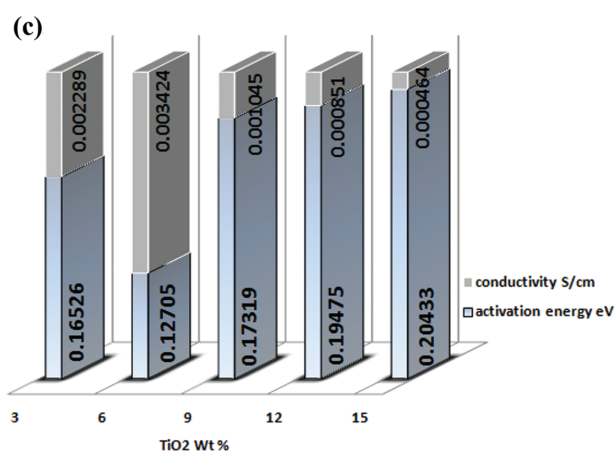
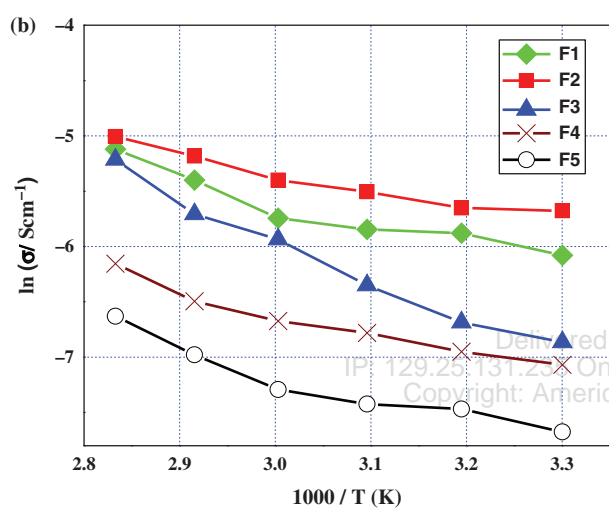
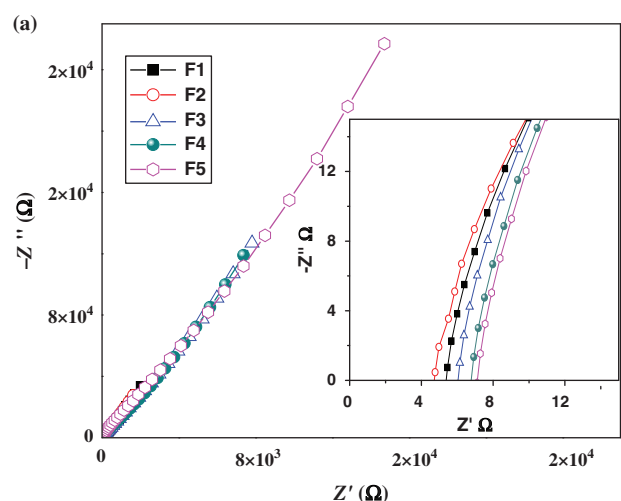


Figure 4. (a) The room temperature complex impedance plot CPE F1, F2, F3, F4, F5; (b) Arrhenius plot CPE F1, F2, F3, F4, F5; (c) Activation energy (E_a) versus room temperature ionic conductivity plot the CPE composition are same as in Figure 1.

6 wt% of TiO₂ is highly amorphous in nature. Sohaimy et al. observed that the amorphous nature provided better ionic diffusion and reduced the energy barrier for segmental motion in polymer.⁴² The above study shows that the

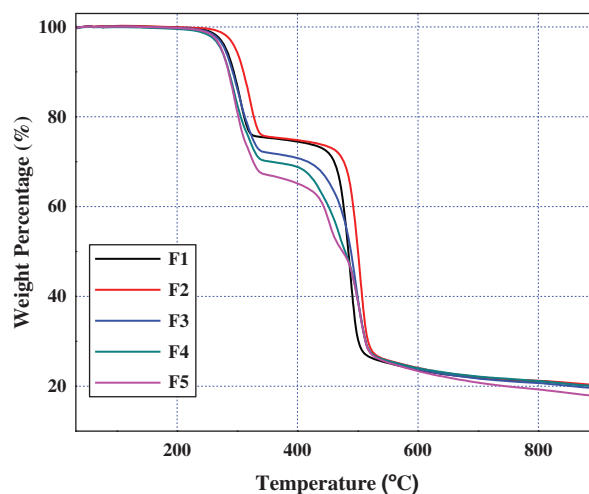


Figure 5. TGA curves of CPE F1, F2, F3, F4, F5, the CPE composition are same as in Figure 1.

XRD results correlates well with the ionic conductivity, where the composite polymer electrolyte F2 ($X = 6$ wt%) has high ionic conductivity and is amorphous in nature, when compared to other samples prepared.

$$\sigma = \sigma_0 \exp(-E_a/kT) \quad (2)$$

Equation (2) express the Arrhenius relation where σ_0 is the pre exponential factor, E_a the activation energy, k is the Boltzmann constant and T is the absolute temperature. Figure 4(b) shows the Arrhenius behavior of the prepared CPE. The ionic conductivity of the composite polymer electrolyte depends on temperature and can be explained by the free volume model. According to free volume theory, ionic conductivity increases with temperature due to the lattice vibration which in turn increases the ions mobility, inter and intra chain hopping, resulting in an enhanced value at high temperatures.

The diagram in Figure 4(c) depicts the activation energy (E_a) as well as the room temperature ionic conductivity values as a function of various compositions of TiO₂. The analysis of these results shows that the sample with maximum ionic conductivity possesses minimum activation energy. The activation energy initially decreases with the addition of TiO₂ and reaches a minimum value at 6 wt.%, beyond that it gradually increases. This investigation shows that activation energy E_a (in eV) is inversely proportional to the ionic conductivity, as noted from the graph obtained between activation energy and room temperature ionic conductivity.

The thermal behavior of ionic liquid polymer electrolyte containing different contents of filler is shown in Figure 5. The prepared electrolytes have decomposition behavior in two steps. The first step is the weight loss occurred around 250 °C for every sample, corresponding to the thermal stability of ionic liquid.⁴³ It is remarkably noted that there is no mass loss for the samples upto 250 °C, confirming no thermal degradation. The second step weight loss has

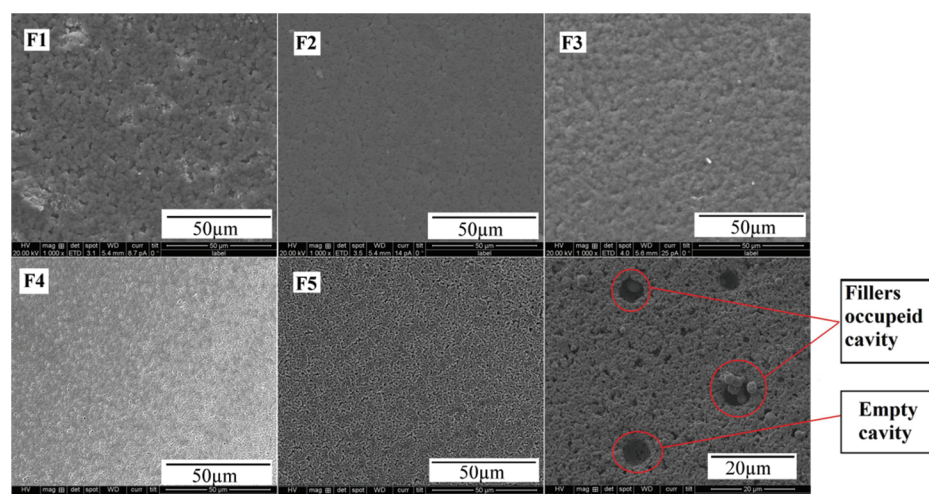


Figure 6. SEM images of CPE F1, F2, F3, F4, F5, the CPE composition are same as in Figure 1. Last image Less than 1% of TiO_2 (trial sample image).

various values according to the filler content. At low filler content, the electrolytes behave thermally active medium, especially, the sample with 6 wt% of TiO_2 follows the best thermal behavior upto 460 °C. Significant weight loss at 460 °C illustrates the decomposition of the polymer electrolytes. The recorded thermal behavior of the polymer electrolyte suggests that the operating thermal range is suitable for stable working of lithium battery.⁴⁴

Figure 6 shows the SEM images of the composite polymer electrolyte containing TiO_2 at 1 K. It is evidently seen that the surface textures of the polymer matrix crams with TiO_2 particles.⁴⁵ The dispersed TiO_2 filler has been distributed uniformly throughout the electrolyte in every sample. It is evident that as the amount of filler increases, the polymer matrix becomes more amorphous. The size of the cavity reduces in more amorphous system and the distributed pores are varied between 200 μm to 600 nm.

The large number of nano size pores is responsible to store higher quantity of liquid electrolyte. The fillers occupied the surface and cavity which can enhance the ionic conductivity. However, excess amount of filler agglomerates on the surface of the polymer matrix, which almost fills the formed cavity and restricts the motion of the cations. The scanned image of polymer electrolyte containing less than 1% of TiO_2 is displayed. Empty cavity, fillers occupied cavity and dispersed fillers are also clearly visible on the surface of the polymer matrix.^{46, 47}

The electrochemical stability window of polymer matrix with TiO_2 (6) wt% has been studied using LSV. From Figure 7, it is observed that anodic current has negligible value below 4 V. Above 4.0 V, the anodic current increases gradually to high values. The current onset detected at 4.62 V versus Li, corresponds to the decomposition of the composite electrolyte.^{48, 49}

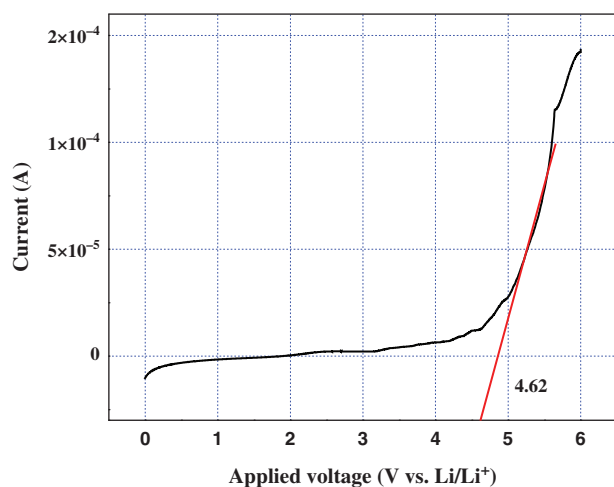


Figure 7. LSV of the coin cell containing F2 and Li anode as well as Li cathode recorded at a scan rate of 5 mV/s.

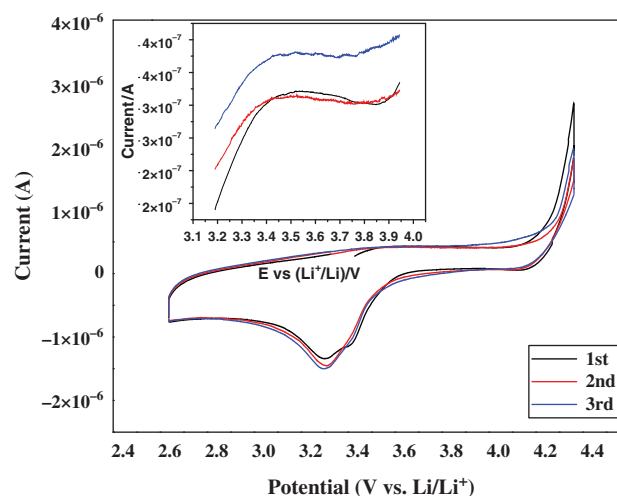


Figure 8. CV of the coin cell containing F2 and Li anode as well as Li cathode recorded at a scan rate of 5 mV/s.

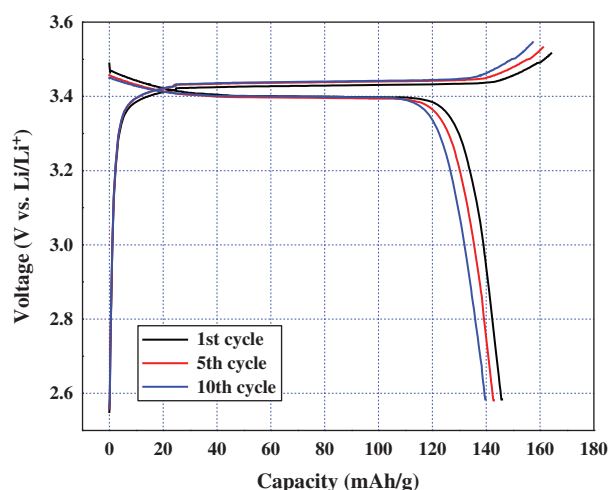


Figure 9. Charge–discharge characteristics of the coin cell containing F2 and LiFePO₄ as the cathode and Li as the anode.

Figure 8 shows the first, second and third cycles of the CV of the coin cell containing composite polymer electrolyte with TiO₂ (6%) at a scan rate of 5 mV/s between the voltage range of 2.2 to 4.6 V versus Li. Redox behaviour with an anodic and cathodic potential at 3.5 V and 3.2 V versus Li is noted.⁵⁰ Magnified anodic peak is put as an inset in CV graph. The anodic peak corresponds to the decomposition process of electrolyte resulting in the formation of the solid electrolyte interface film (SEI passivation film) on the electrode surface and the cathodic peak belongs to Li deposition. With subsequent cycles, the oxidation and reduction peaks shifted towards the lower value and the peak current increases further.

Figure 9 displays the first ten charge–discharge cycles of the fabricated coin cell containing with Li/CPE + TiO₂ (6 wt%)/LiFePO₄ within the potential range of 2.4 to 3.6 V. The CPE based coin cell maintains above 90% of the initial discharge capacity upto 10 cycles. The cell delivers initial discharge capacity of 145 mAh/g. The cycling efficiency is more than 88% and after 10th, cycles, the cell retains a discharge capacity of 145 mAh/g, reveals the suitability of this polymer electrolyte for Li battery applications.

4. CONCLUSIONS

The ionic liquid based polymer electrolyte PVdF-co-HFP + SEt₃TFSI + EC/PC (30/10/60) wt% with various compositions of TiO₂ such as 3, 6, 9, 12 and 15% as a filler had been prepared and characterized by different surface analytical techniques. XRD analysis shows that sample with gradual increase of the amount of TiO₂, broadening of the prominent peak and a decrease in the intensity of 2θ value at 20.1° has been noted, suggesting a decrease in the degree of crystallinity of the polymer matrix upon the addition of TiO₂. Raman and FT-IR studies confirm the presence of various functional groups, present in the

matrix. Thermal analysis reveal that the electrolyte with TiO₂ (6 wt%) has maximum stability of 460 °C. Complex impedance plot proclaim that the conductivity of the composite polymer electrolytes increases upto 6 wt% of TiO₂ (3.42×10^{-3} S/cm at 303 K) and further addition, causes a dip down in conductivity, indicating an improvement in the ionic conductivity and thermal stability with the incorporation of TiO₂ filler in the polymer matrix. The Arrhenius behaviour study reveals that minimum activation energy for ionic conduction is found to be 0.2 eV. Furthermore, the SEM images show the surface and cavity in the polymer matrix, filled with the filler uniformly. Cyclic and linear voltammetry reveal that the films are electrochemically stable upto about 4.62 V. The first discharge capacity of 145 mAh/g with the working voltage of 3.4 V had been achieved for the coin cell containing Li as anode and LiFePO₄ as cathode along with polymer electrolyte 6% TiO₂ filler as the electrolyte, where the cell delivers good reversibility with discharge capacity of 145 mAh/g at 10th cycle.

Acknowledgment: The author M. Sivakumar gratefully acknowledges for the financial support to carry out this work by University Grants Commission (UGC), New Delhi, Government India under major research project (F. No. 41-839/2012(SR)).

References and Notes

1. S. Wu, T. Tsuruoka, K. Terabe, T. Hasegawa, J. P. Hill, K. Ariga, and M. Aono, *Proc. SPIE* 7493, 749364 (2009).
2. S. Wu, T. Tsuruoka, K. Terabe, T. Hasegawa, J. P. Hill, K. Ariga, and M. Aono, *Adv. Mater.* 21, 93 (2011).
3. J. W. Fergus, *J. Power Sources* 195, 4554 (2010).
4. S. Abada, G. Marlair, A. Lecocq, M. Petit, V. Sauvart-Moynot, and F. Huet, *J. Power Sources* 306, 178 (2016).
5. S. Zhang, J. Cao, Y. Shang, L. Wang, X. He, J. Li, P. Zhao, and Y. Wang, *J. Mater. Chem A* 3, 17697 (2015).
6. Y. Imada, T. Kukita, H. Nakano, and Y. Yamamoto, *Bull. Chem. Soc. Jap.* 89, 546 (2016).
7. J. Patra, P. P. Dahiya, C.-J. Tseng, J. Fang, Y.-W. Lin, S. Basu, S. B. Majumder, and J.-K. Chang, *J. Power Sources* 294, 22 (2015).
8. J. H. Kim, B. R. Min, C. K. Kim, J. Won, and Y. S. Kang, *J. Phys. Chem. B* 106, 2786 (2002).
9. M. Guo, J. Fang, H. Xu, W. Li, X. Lu, C. Lan, and K. Li, *J. Memb. Sci.* 362, 97 (2010).
10. J. T.-W. Wang and S. L.-C. Hsu, *Electrochim. Acta.* 56, 2842 (2011).
11. R. Kotz and M. Carlen, *Electrochim. Acta.* 45, 2483 (2000).
12. C. Karlsson, A. S. Best, J. Swenson, J. Kohlbrecher, and L. Borjesson, *Macromolecules* 38, 6666 (2005).
13. J. C. Bachman, S. Muy, A. Grimaud, H. H. Chang, N. Pour, S. F. Lux, O. Paschos, F. Maglia, S. Lupart, P. Lamp, and L. Giordano, *Chem. Rev.* 116, 140 (2015).
14. R. H. Y. Subban and A. K. Arof, *J. New. Mat. Electrochem. Systems* 6, 197 (2003).
15. J. E. Weston and B. C. H. Steele, *Solid State Ionics* 7, 75 (1982).
16. L. M. Bronstein, R. L. Karlinsey, B. Stein, Z. Yi, J. Carini, and J. W. Zwanzige, *Chem. Mater.* 18, 708 (2006).
17. S. Ferrari, E. Quartarone, P. Mustarelli, A. Magistris, M. Fagnoni, S. Protti, C. Gerbaldi, and A. Spinella, *J. Power Sources* 195, 559 (2010).

18. S. Liu, H. Wang, N. Imanishi, T. Zhang, A. Hirano, Y. Takeda, O. Yamamoto, and J. Yang, *J. Power Sources* 196, 7681 (2011).
19. J. Park, Y. Jung, P. Kusumah, J. Lee, K. Kwon, and C. K. Lee, *Int. J. Mol. Sci.* 15, 15320 (2014).
20. W. Ogihara, N. Suzuki, N. Nakamura, and H. Ohno, *Polym J.* 38, 117 (2006).
21. K. Sakaushi and M. Antonietti, *Bull. Chem. Soc. Jpn.* 88, 386 (2015).
22. D. Wei and T. W. Ng, *Electrochem. Commun.* 11, 1996 (2009).
23. J. R. Nair, L. Porcarelli, F. Bella, and C. Gerbaldi, *ACS Appl. Mater. Interfaces* 7, 12961 (2015).
24. R. Miao, B. Liu, Z. Z. Zhu, Y. Liu, J. Li, X. Wang, and Q. Li, *J. Power Sources* 184, 420 (2008).
25. D. Shanmukaraj and R. Murugan, *J. Power Sources* 149, 90 (2005).
26. R. Yogamalar, R. Srinivasan, A. Vinu, K. Ariga, and A. C. Bose, *Solid State Commun.* 149, 1919 (2009).
27. W. Xijun, Z. Ming-Sheng, Y. Zhen, J. Xiaoli, and C. Qiang, *Chinese Phys. Lett.* 11, 685 (1994).
28. C.-A. Chen, Y.-M. Chen, Y.-S. Huang, D.-S. Tsai, K.-K. Tiongchand, and P.-C. Liao, *Cryst. Eng. Comm.* 11, 2313 (2009).
29. W. F. Zhang, Y. L. He, M. S. Zhang, Z. Yin, and Q. Chen, *J. Phys. D: Appl. Phys.* 33, 912 (2000).
30. H. C. Choi, Y. M. Jung, and S. B. Kim, *Vib. Spectrosc.* 37, 33 (2005).
31. F. Tian, Y. Zhang, J. Zhang, and C. Pan, *J. Phys. Chem. C* 116, 7515 (2012).
32. S. C. Nunes, V. D. Z. Bermudez, D. Ostrovskii, P. C. Barbosa, M. M. Silva, and M. J. Smith, *Chem. Phys.* 345, 32 (2008).
33. A. Martinelli and L. Nordstierna, *Phys. Chem. Chem. Phys.* 14, 13216 (2012).
34. B. N. Sahoo and K. Balasubramanian, *RSC Adv.* 5, 6743 (2015).
35. R. A. Senthil, J. Theerthagiri, J. Madhavan, and A. K. Arof, *Ionics* 22, 425 (2016).
36. V. K. Shalu and R. K. Singh, *J. Mater. Chem. C* 3, 7305 (2015).
37. B. Zhang, Y. Zhou, X. Li, X. Ren, H. Nian, Y. Shen, and Q. Yun, *Spectrochim. Acta. A* 122, 59 (2014).
38. Z. Osman and A. K. Arof, *Electrochim. Acta.* 48, 993 (2003).
39. J. S. Gnanaraj, E. Zinigrad, L. Asraf, H. E. Gottlieb, M. Sprecher, M. Schmidt, W. Geissler, and D. Aurbach, *J. Electrochem. Soc.* 150, A1533 (2003).
40. M. A. Hamza, F. N. Saiof, A. S. Al-ithawi, M. A. Ameen, and H. M. Yaseen, *Adv. Mater. Phys. Chem.* 3, 174 (2013).
41. L. J. Hardwick, J. A. Saint, I. T. Lucas, M. M. Doeff, and R. Kosteckia, *J. Electrochem. Soc.* 156, A120 (2009).
42. M. I. H. Sohaimy and M. I. N. Isa, *Fiber. Polym.* 16, 1031 (2015).
43. K. M. Abraham and M. Alamgir, *J. Power Sources* 43, 195 (1993).
44. S. Rajendran, M. Sivakumar, R. Subadevi, and J. M. Leonora, *Bull. Electrochemi.* 20, 87 (2004).
45. Z. Tian, X. He, W. Pu, C. Wan, and C. Jiang, *Electrochim. Acta.* 52, 688 (2006).
46. F. Caruso, D. N. Furlong, K. Ariga, I. Ichinose, and T. Kunitake, *Langmuir* 14, 4559 (1998).
47. M. Sivakumar, R. Subadevi, and R. Muthupradeepa, *AIP Conf. Proc.* 1536, 857 (2013).
48. R. Subadevi, M. Sivakumar, S. Rajendran, and H.-C. Wu, *Ionics* 18, 283 (2012).
49. N. Ataollahi, A. Ahmad, H. Hamzah, M. Y. A. Rahman, and N. S. Mohamed, *Russ J. Electrochem.* 51, 227 (2015).
50. H. Ye, J. Huang, J. J. Xu, A. Khalfan, and S. G. Greenbaum, *J. Electrochem. Soc.* 154, A1048 (2007).

Delivered by Ingenta to:
Received: 6 December 2016. Accepted: 3 January 2017.
IP: 129.25.131.235 On: Thu, 21 Dec 2017 00:36:19
Copyright: American Scientific Publishers

*Sulfonium cation based ionic liquid
incorporated polymer electrolyte for lithium
ion battery*

**R. Muthupradeepa, M. Sivakumar,
R. Subadevi & V. Suryanarayanan**

Polymer Bulletin

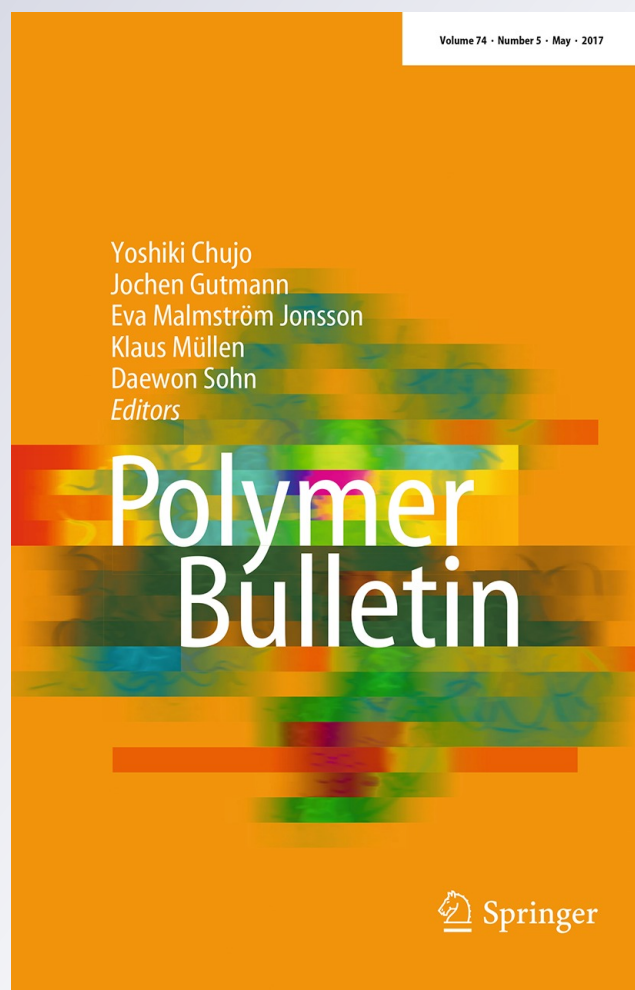
ISSN 0170-0839

Volume 74

Number 5

Polym. Bull. (2017) 74:1677-1691

DOI 10.1007/s00289-016-1796-y



Your article is protected by copyright and all rights are held exclusively by Springer-Verlag Berlin Heidelberg. This e-offprint is for personal use only and shall not be self-archived in electronic repositories. If you wish to self-archive your article, please use the accepted manuscript version for posting on your own website. You may further deposit the accepted manuscript version in any repository, provided it is only made publicly available 12 months after official publication or later and provided acknowledgement is given to the original source of publication and a link is inserted to the published article on Springer's website. The link must be accompanied by the following text: "The final publication is available at link.springer.com".

Sulfonium cation based ionic liquid incorporated polymer electrolyte for lithium ion battery

R. Muthupradeepa¹ · M. Sivakumar¹ ·
R. Subadevi¹ · V. Suryanarayanan²

Received: 25 May 2016 / Revised: 20 August 2016 / Accepted: 29 August 2016 /
Published online: 7 September 2016
© Springer-Verlag Berlin Heidelberg 2016

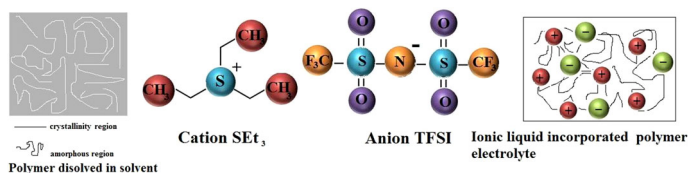
Abstract Polymer electrolyte (PE) composed of poly(vinylidene fluoride-*co*-hexafluoropropylene) P(VdF-*co*-HFP) and triethylsulfonium bis(trifluoromethylsulfonyl)imide (SEt₃TFSI) ionic liquid (IL) had been evaluated in lithium ion battery for the first time in order to improve its performance and cycle life. X-ray diffraction analysis (XRD) reveals that incorporation of the IL (20 and 25 wt%) into the polymer matrix results in the change of state of the material from semi-crystalline to amorphous nature. Thermogravimetric and differential thermal analysis (TG/DTA) of the PE sample with 25 wt% of the IL shows high thermal stability. The nature of functional groups present in the PE was investigated by Raman spectrum. Surface morphological characteristics indicate that increase in the loading of the IL into the polymer matrix leads to maximum number of pores with good interconnected network. Polymer/IL electrolyte (wt. ratio of 75:25) having a maximum ionic conductivity of 6.93×10^{-5} S/cm at 303 K with an activation energy of 0.23 eV shows excellent electrochemical potential stability of 4.4 V vs Li, as revealed by cyclic voltammetry (CV). Charge–discharge characteristics of the coin cell containing the above optimized ratio of PE with LiFePO₄ cathode and Li anode shows a discharge capacity of 133 mAh/g, which is stable up to ten cycles.

✉ M. Sivakumar
susiva73@yahoo.co.in

¹ School of Physics, Alagappa University, #120, Science Block, Karaikudi, Tamil Nadu 630004, India

² Electroorganic Division, CSIR-Central Electrochemical Research Institute, Karaikudi, Tamil Nadu 630006, India

Graphical abstract



Keywords Polymer electrolyte · Sulfonium ionic liquid · Cyclic voltammetry · Charge discharge

Introduction

Employment of polymer electrolytes in lithium ion battery has been widely investigated as an alternative to liquid combustible systems for their particular properties such as high mechanical stability, non-inflammability and non-leakage [1–5] and their usage avoids the evolution of gaseous materials during solvent decomposition. Further, Li ion battery can be made very compact, lightweight and highly reliable with the incorporation of thin film electrolytes. It is important to note that lithium ion polymer batteries had been proposed since early 1980s as being a potential solution to the safety issues. On the other hand, these polymer electrolyte materials have very poor ionic conductivities at room temperature (i.e. $<10^{-5}$ S/cm), resulting in the limitations on their viability by significantly lowering the amount of current that can be drawn from a battery. In order to improve their room temperature ionic conductivity, alternative approaches have been developed by the incorporation of liquid plasticizers or low molecular weight polymers [6, 7], block copolymers [8], high conductivity inorganic nanofillers [9] and room temperature ionic liquids (RTILs) [10–12]. Among these, RTILs offer a promising approach for overcoming these drawbacks, which can act both as solvent and electrolyte, into the polymer electrolytes.

The RTILs have recently been considered as alternative electrolytes to carbonate based systems because they possess high oxidation potential, non-flammability, a low vapor pressure, good thermal stability, low toxicity and affordable boiling points [13–15]. Additionally, ionic liquids play dual character as electrolyte salts and organic liquids and are eco friendly in nature [16]. The absence of volatility is one of the most important benefits of ionic liquids, offering less toxicity, when compared to low boiling solvents. Hence, these salts are indeed extraordinary safety assets and the replacement of the conventional, flammable and volatile organic solvents by ionic liquid based electrolytes may greatly reduce the risk of thermal runaways. Imidazolium [17–20], piperidinium [21–24] and pyrrolidinium cation [25–28] based ILs are highly conducting and used as electrolytes for Li ion battery. However, problems associated with these ILs are their instability at low voltages and intercalation into the graphite anode resulting in exfoliation as well as rapid capacity fade. Moreover, pyrrolidinium cation based ILs are poor solvents for

lithium and show limited lithium conductivity values. Hence, a different strategy has been adopted by the incorporation of IL into polymer matrix, thereby enhancing their ionic conductivity and electrochemical stability and this can meet performance standards of a battery electrolyte with good capacity and cycle life. Among the different polymers employed so far, fluorinated polymer namely PVDF-*co*-HFP [poly(vinylidene fluoride-*co*-hexafluoropropylene)] has been widely employed as an excellent polymer matrix, on account of their good thermal and oxidative stability. Moreover, it has good mechanical stability and film formation ability and concomitant low surface energy, due to presence of fluorine network, justifying it is choice for IL-based polymer electrolyte (PE). Recently, Hwang et al. have reviewed the employment of PVDF-*co*-HFP PE matrices incorporated with different imidazolium cations based ILs on their synthetic pathways, ion sources, IL contents and proton conductivities [29]. The mechanical and dimensionally stable solid electrolyte containing ionic liquid has comparable conductivity and electrochemical stability with that of liquid electrolytes [30–32]. Literature studies clearly reveal that most of the research work involving ILs incorporated into PVDF–HFP matrix are restricted to nitrogen based structures and recent investigations demonstrate that sulfur and phosphorous based systems have showed superior electrochemical stability and conductivity values, when compared to latter [33, 34]. In particular, sulfonium based ionic liquids received great attention owing to their low viscosity, high conductivity and electrochemical stability [35, 36]. Zhang et al. [31] reported that the ethyl based sulfonium ionic liquid possessed higher conductivity, when compared to methyl and butyl alkyl groups. Further, the nature of the anion influences the viscosity of the ionic liquid. For example, TFSI anion exhibits high charge delocalization within the S–N–S backbone, resulting in low viscosity [37, 38]. Moreover, ionic liquid containing TFSI anion is highly hydrophobic in nature and has low moisture sensitive and exhibits high thermal stability, molar conductivity and electrochemical stability with low viscosity, and much safer than the conventional organic electrolytes [39, 40].

In the present work, PE containing PVdF-*co*-HFP incorporated with triethylsulfonium bis(trifluoromethylsulfonyl) imide (SEt₃TFSI) ionic liquid, which has not been reported previously for Li battery application, has been tried as the electrolyte for improving its performance. The physico-chemical properties and electrochemical characteristics of the thin film are presented. The optimal ratio of PVDF-*co*-HFP and ILs are carefully investigated which facilitates the improvement of the interphase stability between the electrolyte and anode material.

Experimental

Preparation of IL incorporated polymer electrolyte (PE)

All the electrolytes have been prepared using the solution casting technique. PVdF-*co*-HFP and ionic liquid SEt₃TFSI were purchased from Aldrich USA. Tetrahydrofuran (THF) and *N*-methyl 2 pyrrolidone (NMP) was purchased from SRL India and used without further purification. Required quantity of polymer was dried under

Table 1 Ionic conductivity values of the PE (PE-IL1 to PE-IL5) in the temperature range of 303–353 K

| Sample | PVdF-co-HFP (wt%) | SEt ₃ TFSI (wt%) | Conductivity $\times 10^{-5}$ S/cm | | | | | E_a values (eV) | |
|--------|-------------------|-----------------------------|------------------------------------|-------|-------|-------|-------|-------------------|-------|
| | | | 303 K | 313 K | 323 K | 333 K | 343 K | | 353 K |
| PE-IL1 | 95 | 5 | 0.005 | 0.009 | 0.023 | 0.037 | 0.155 | 0.345 | 0.40 |
| PE-IL2 | 90 | 10 | 0.010 | 0.019 | 0.055 | 0.176 | 0.276 | 0.668 | 0.37 |
| PE-IL3 | 85 | 15 | 0.732 | 1.110 | 1.779 | 2.833 | 3.123 | 4.365 | 0.29 |
| PE-IL4 | 80 | 20 | 3.371 | 5.743 | 6.877 | 7.556 | 9.825 | 13.87 | 0.25 |
| PE-IL5 | 75 | 25 | 6.938 | 7.362 | 9.578 | 14.57 | 24.33 | 45.35 | 0.23 |

vacuum (1×10^{-3} Torr) at 100 °C for 10 h in order to remove the moisture. It was completely dissolved in THF and calculated amount of ionic liquid was mixed with the polymer solution, which was stirred continuously in order to obtain homogeneity. The homogeneous solution was casted onto flat bottom petri plates. Then the solution was dried to form film at 30 °C in the vacuum oven for overnight. Further, the films were dried at 60 °C under vacuum for 5 h in order to get the flexible freestanding film. Table 1 shows the different wt% of IL incorporated PE.

Characterizations of thin film PE

The film was characterized for its crystal structure by X-ray diffraction analysis using the PANalytical X'Pert PRO powder X-ray Diffractometer using Cu-K α radiation as source and operated at 40 kV. Laser Raman spectra were done with STR 500 Laser Raman spectrometer, SEKI, Japan. Thermo-gravimetric analysis of the gel electrolyte was performed using STA 409 PL Luxx at a heat rate of 10 K/min within the temperature range from room temperature to 900 °C under nitrogen atmosphere. The surface morphology of the electrolytes was characterized by SEM Model JEOL-JSM-6500F scanning electron microscope at an accelerating voltage of 5 and 15 kV after sputtering platinum over the samples and AFM with Agilent Technology Inc., (A100SGS).

Electrochemical studies

Two stainless electrodes (2 cm \times 2 cm) were used for conductivity measurement, where the electrolyte was sandwiched between the parallel blocking electrodes. The impedance spectra were measured in the frequency and the temperature ranges from 1 Hz to 500 kHz and 303 to 353 K, respectively, using a computer-controlled micro Autolab III Potentiostat/Galvanostat. The evaluated ohmic resistance value was converted into conductivity. The electrochemical studies were carried out using Autolab electrochemical workstation (GPES, PGSTAT 302 N) and the charge/discharge life cycle was carried out using WonAtech (WBSC3000S) automatic charge/discharge testing system. For linear voltammetric studies, a CR-2032 coin cell was fabricated with Li metal as counter as well as reference electrodes and

stainless steel as working with the IL-incorporated PE. The coin cell for the electrochemical characterization had been assembled with the electrode composed of 80:10:10(LiFePO₄: PVdF: Super p carbon). The slurry was made using NMP and was coated on alumina foil. After coating, the electrodes were dried at 80 °C for about 6 h. The mass of the active substance was nearly 1 mg.

Results and discussion

X-ray diffraction (XRD)

The crystalline peak properties of IL incorporated PVdF-*co*-HFP were characterized by XRD. Figure 1 shows the XRD diffraction pattern of the prepared polymer electrolyte (PE) samples containing different wt% of IL such as 5, 10, 15, 20, 25, denoted as PE-IL1, PE-IL2, PE-IL3, PE-IL4 and PE-IL5. The pure PVdF-*co*-HFP is a semi-crystalline polymer and there are two broad peaks at 20.4° and 39.4° corresponding to its crystalline planes [41]. With the incorporation of IL into the polymer matrix, the peak intensity of both the peaks decreases (sample IL1). Further addition of IL makes the peak weak and wide (PE-IL2 and PE-IL3). For both PE-IL4 and PE-IL5 samples, the high-intensity region peak disappears and the peak noted at a 2θ value of 20.4 becomes low, which reveals that the high amount of

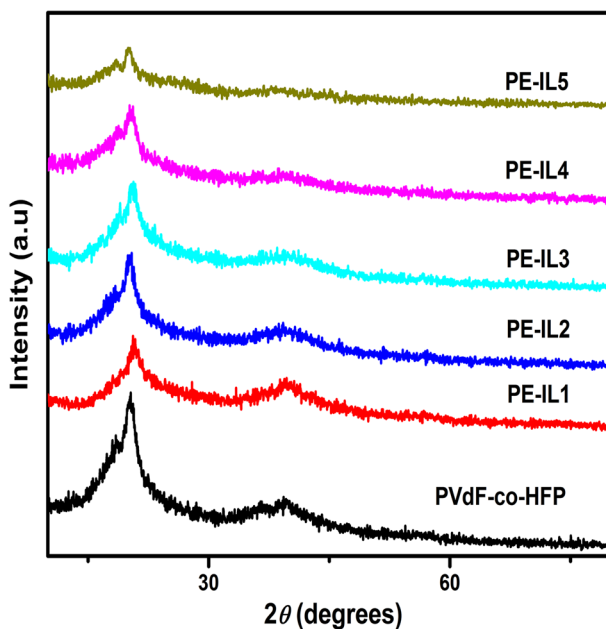


Fig. 1 X-ray diffraction patterns of pure P(VdF-*co*-HFP), PE-IL1—PVdF-*co*-HFP(95 %) + SEt₃TFSI(5 %), PE-IL2—PVdF-*co*-HFP(90 %) + SEt₃TFSI(10 %), PE-IL3—PVdF-*co*-HFP(85 %) + SEt₃TFSI(15 %), PE-IL4—PVdF-*co*-HFP(80 %) + SEt₃TFSI(20 %), PE-IL5—PVdF-*co*-HFP(75 %) + SEt₃TFSI(25 %)

ionic liquid plasticizers the electrolyte and produces more amorphous phase in the polymer network [42, 43].

Raman spectroscopy

Raman spectroscopy is particularly appropriate to characterize PE and the bond present in the spectrum corresponds to vibrational frequency of the molecules. Figure 2 represents such spectra for different PE samples. Pure polymer PVdF-co-HFP shows the major Raman peak at 795 cm^{-1} assigned to CH_2 ν rocking and the rocking mode of CF_2 and CH_2 at 413 cm^{-1} disappears in all the electrolyte samples, as a result of the effect of addition of the SEt_3TFSI [44]. Another major peak of 877 cm^{-1} corresponds to the combination of symmetric C–C and $\text{CCC}\delta$ skeletal bending of $\text{C(F)}\text{--C(H)}\text{--C(F)}$ of the host polymer PVdF-co-HFP is shifted to high frequency value of 886 cm^{-1} reflecting the major change in the bare polymer. A peak at 600 cm^{-1} indicates the CF scissoring $\text{CCC}\delta$ skeletal bending of $\text{C(H)}\text{--C(H)}\text{--C(F)}$ [40]. The CH_2 ν rocking (832 cm^{-1}), ν_s symmetric stretching (1424 , 2976 cm^{-1}) and ν_a anti-symmetric stretching (3011) are also noted in the Raman spectrum. The most intense band of the anion appearing at 741 cm^{-1} was attributed to the CF_3 bending of the SCF_3 group of TFSI [45]. The SO_2 band of NSO_2CF_3 is out of phase anti-symmetric stretching, located at 1335 cm^{-1} . Bands specifically associated with TFSI^- are still observed at 1125 cm^{-1} with ν_s symmetric stretching. The peak at 1046 cm^{-1} has been noted as ν_a SNS anti-symmetric stretching vibration of triflate anion [46].

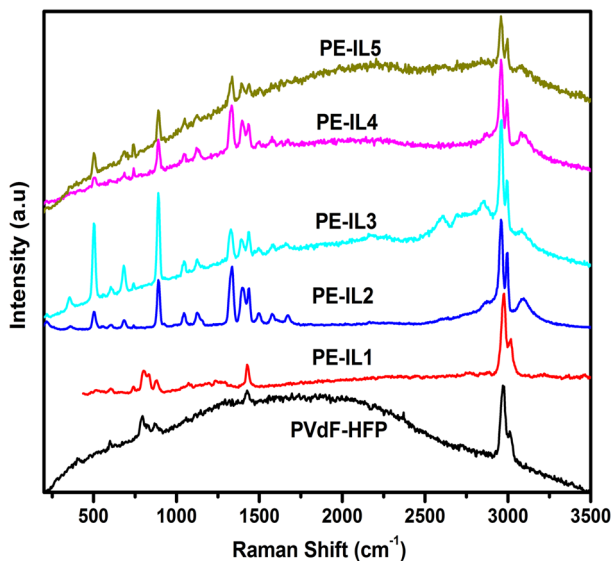


Fig. 2 Raman spectra of pure PVdF-co-HFP, the PEs namely PE-IL1, PE-IL2, PE-IL3, PE-IL4 and PE-IL5. The PE compositions are the same as in Fig. 1

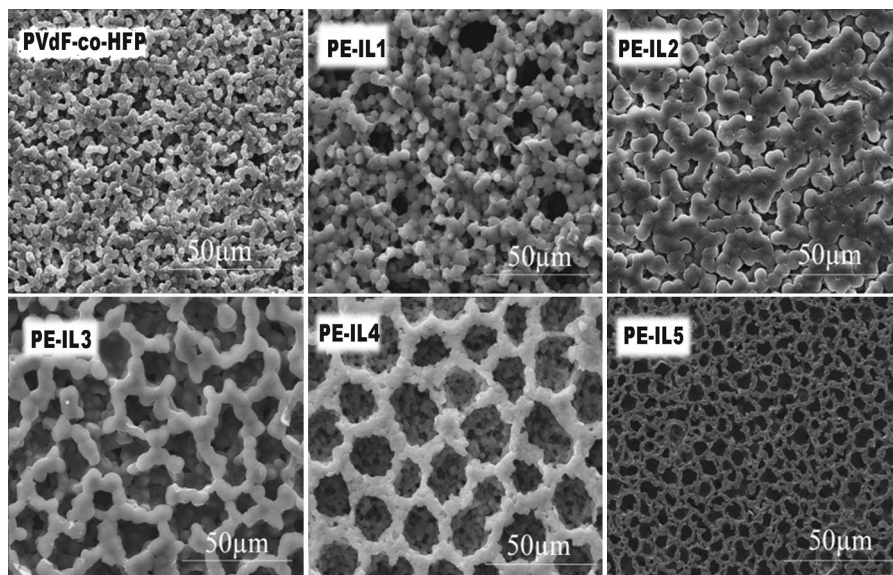


Fig. 3 SEM images of the PEs namely PE-IL1, PE-IL2, PE-IL3, PE-IL4 and PE-IL5 with the magnification of 1 K. The PE compositions are the same as in Fig. 1

Surface morphologic studies using scanning electron microscope (SEM) and atomic force microscope (AFM)

Figure 3 shows the SEM images obtained for different PE samples containing various IL contents. The micropores noted in the SEM images are directly related to its conductivity values. The scanning images of the PE samples differ from their number of pores, pore size and uniform distribution of micropores. The appearance of pores corresponds to the process associated with the evaporation of the THF solvent during vacuum oven drying. The increased number of pores enhances the absorption of non-volatile liquid electrolyte, leading to high conductivity of PE [12, 47]. The sample PE-IL1 [PVDF-co-HFP:SEt₃TFSI (95:5 wt%)] shows granular shape indicating the semiconducting nature of the polymer. Further incorporation of the IL content into the polymer results in the decrease of the pore size as well increase of number of pores with interconnected network and increase of amorphous nature of the PE [48]. Highly amorphous nature leads to high conductivity and large amount of absorbed IL. From the SEM pictures, it is observed that the PE-IL5 (PVDF-co-HFP:SEt₃TFSI (75:25 wt%)) provides a well closed interconnected network with maximum number of pores.

Based on the SEM analysis, surface topography of the sample PE-IL5 was characterized by AFM and is shown in Fig. 4. From the figure, it appears that homogeneous nature of the PE had been found to be enhanced with the addition of IL electrolyte [49], where this can increase the contact between the electrolyte and electrode. The topographical image shows large number of pores, which is responsible for the ion migration.

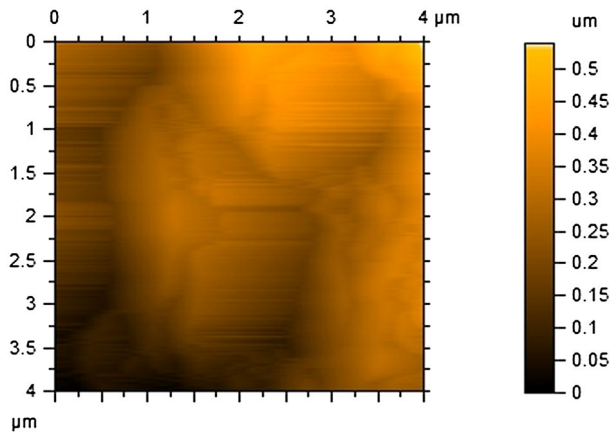


Fig. 4 AFM image of PE-IL5

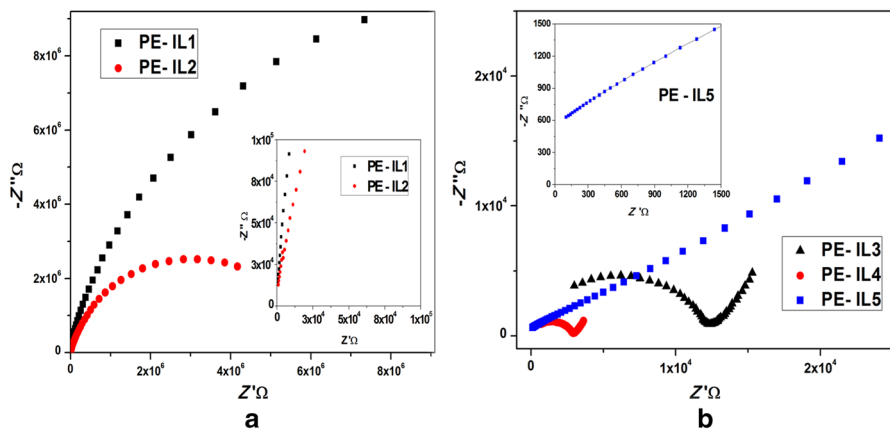


Fig. 5 Room temperature complex impedance plot of PEs namely PE-IL1, PE-IL2, PE-IL3, PE-IL4 and PE-IL5. The PE compositions are the same as in Fig. 1

Conductivity studies

Impedance measurement was performed for finding out the ionic conductivity of the polymer electrolytes starting from PE-IL1 to PE-IL5 films at different temperatures starting from 303 to 353 K with an increment of 10 K and the spectra are shown in Fig. 5. For both PE-IL1 and PE-IL2, the impedance spectra shows a semicircle, which is due to the effect of bulk resistance [50]. It is noted that for the PE with low ionic liquid content (5 and 10 wt%) follows a solid polymer electrolyte (SPE) behavior. The increase of the ionic liquid (15 and 20 wt%) results in a depressed semicircle with a spike. This is due to the effect of electrolyte/blocking electrode interface. Further increase of the ionic liquid content (25 wt%) results in a complex impedance plot with a spike. Low-frequency straight line towards the real axis is caused by the effect of the capacitive electrode behavior. The disappearance of

semicircle in high content of ionic liquid is due to the decrease of ionic resistance of the electrolyte. This causes high degree of disorder in the polymer electrolyte, favoring high ionic transport. The semicircle in the high-frequency range is related to the conduction process in the bulk of the complex and the linearity in the low-frequency region is due to the effect of blocking electrode.

Conductivity values of the different contents IL incorporated polymer had been measured from the following equation:

$$\sigma = \frac{l}{AR_b} \quad (1)$$

where σ is the ionic conductivity, l is the thickness of the electrolyte sample, A is the area of the prepared electrolyte, R_b is the bulk resistance. The conductivity values for the samples from PE-IL1 to PE-IL5 at different temperatures are shown in Table 1. From the table, it is noted that with the increase of ionic liquid content, the conductivity of the PE increases linearly and the polymer electrolyte with 25 wt% ionic liquid (PE-IL5) has the maximum ionic conductivity of 6.93×10^{-5} S/cm. Further the conductivity also increases with the increase of temperature from 303 to 353 K, as revealed from the plot of log conductivity versus inverse temperature ($1000/T$) for different contents of IL (Fig. 6) and this may be correlated with the influence of internal activation of molecules [48]. The activation energy (E_a) values were calculated from the slope of the straight line. A low activation energy ($E_a = 0.23$ eV) had been obtained for the sample having maximum ionic conductivity. Decrease in the E_a value suggests more amorphous nature of the polymer electrolyte, as shown in Table 1. A similar trend in the increase of conductivity value with temperature is also noted for the IL incorporated polymers [29].

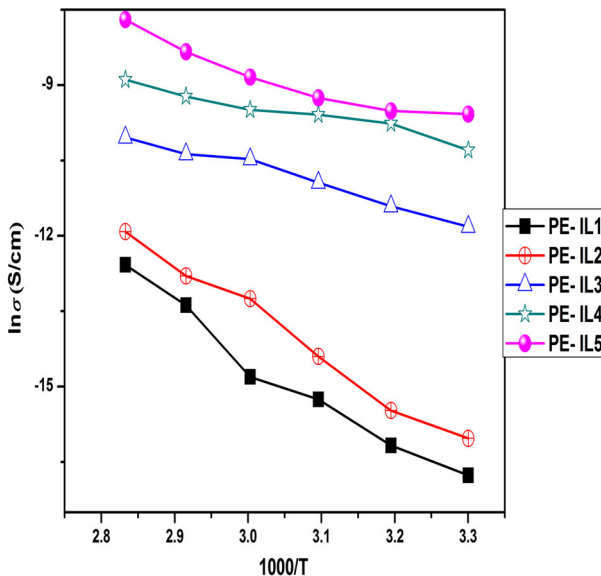


Fig. 6 Temperature dependent ionic conductivity plot

Typically, the addition of polymers to liquid electrolytes containing lithium salts to form gels results in a significant drop in the ionic conductivity [51, 52]. It is noted that the increase in the electrolyte conductivity is due to the addition of a liquid salt with ions possessing plasticizing nature that have only a weak interaction with the polymer, leading to easy migration of ions. Further, the enhanced conductivity may also be associated with large number of charge carriers for the ionic transport, where the large size of imide anion discourages the ion pair formation [53]. Ionic transport is caused by the diffusion of carrier ions through the free volume of polymer matrix so that the large size of the imide disperses the carrier ions in the polymer domain at the molecular level, inducing high conductivity.

Thermal analysis

Thermo-gravimetric and differential thermal analysis (TG/DTA) of the samples of pure PVdF-co-HFP, Pure IL, PE-IL4 and PE-IL5, having higher conductivity than the others, are shown in Fig. 7. Thermal analysis shows three types of response in the temperature range between room temperature and 900 °C. At first stage, a small weight loss around 70 °C is responsible for the evaporation of the moisture at the time of loading of the sample. It is well known from the literature that the IL is stable up to 240 °C. The TG graph of the polymer electrolyte confirms its stability up to 440 °C. Significant decomposition at 240 °C represents the thermal stability of IL with the mass change of 19 wt%. After 500 °C, a gradual decrease of weight is observed and at 900 °C, a residual mass of 19 wt% remains due to the presence of carbon in the polymer electrolyte. When compared to PE-IL4 electrolyte, PE-IL5 however, shows better thermal stability. The results noted in the DTA results are in good agreement with the TG [54]. In the temperature regions of 250, 450 and 600 °C, the exothermic curve shows the decomposition of the PE. The TGA and DTA results infer that PE containing PVdF-co-HFP:SEt₃TFSI (75:25, PE-IL5) possess high thermal stability [55] and this composition had been investigated for further characterization related to voltammetry and charge–discharge studies.

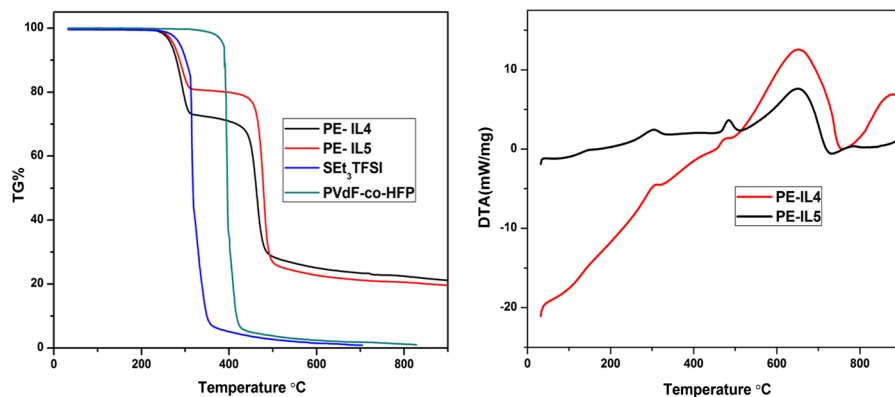


Fig. 7 TG/DTA plot for the PEs namely PE-IL4 and PE-IL5. The PE compositions are the same as in Fig. 1

Electrochemical characterization

Linear sweep voltammetry

The electrochemical stability window of the PE (PE-IL5) was studied using linear sweep voltammetry (LSV) and the voltammogram recorded at a scan rate of 5 mV/s is shown in Fig. 8. From the figure, it can be seen that until 4.5 V vs Li, the current flow is found to be negligible and after that it increases sharply with applied voltage, indicating the decomposition of the PE. [56]. This shows that the PE is stable up to the potential region of 4.4 V vs Li.

Cyclic voltammetry (CV)

The electrochemical characteristics of the coin cell containing LiFePO_4 and the PE (PE-IL5) were studied using CV. Figure 9 shows the first, second and third cycle of the CV for the polymer electrolyte at a scan rate of 5 mV/s within a voltage range of 2.4–4.4 V vs Li. An anodic and a cathodic peak appear at a potential of 3.55 and 3.3 V vs Li [57], respectively, indicating the strong reversible behavior of the electrochemical system. The insert shows the magnified view of anodic peak. Multiple scan for the three cycles shows the overlapping of the curves, which may be associated with the reversibility [58]. Beyond 4.5 V, the anodic current rises due to the decompositions of the polymer electrolyte and further decrease in the current for the second and third cycle indicates the formation of solid electrolyte interface (SEI) on the electrode surface [59]. The SEI formation prevents further reaction of SEt_3TFSI with the lithium electrode.

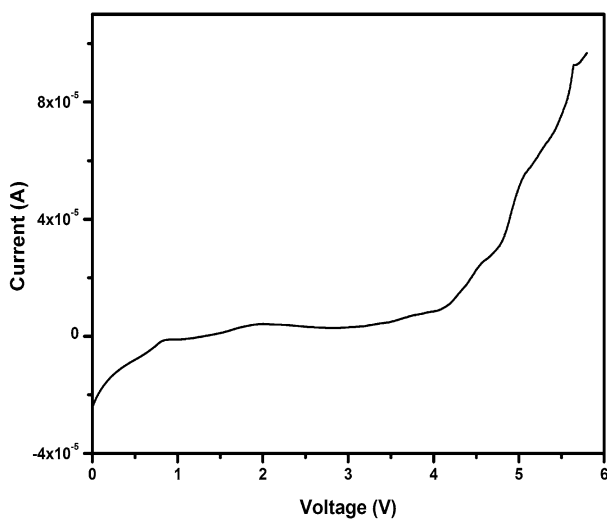


Fig. 8 LSV of the coin cell containing PE-IL5 and Li anode as well as Li cathode recorded at a scan rate of 5 mV/s

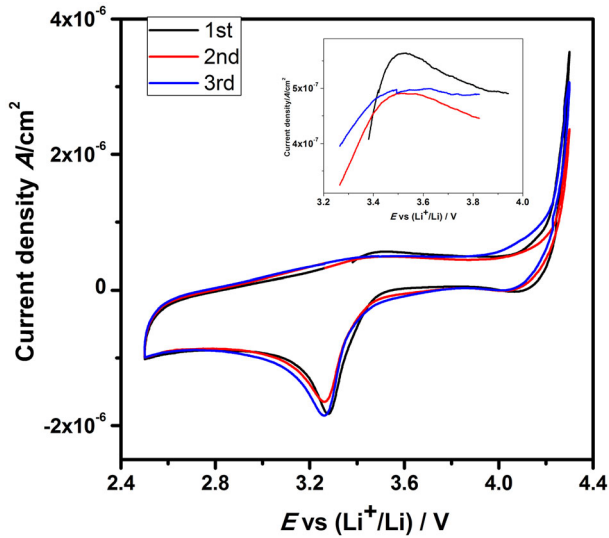


Fig. 9 CV of the coin cell containing PE-IL5 and Li anode as well as Li cathode recorded at a scan rate of 5 mV/s

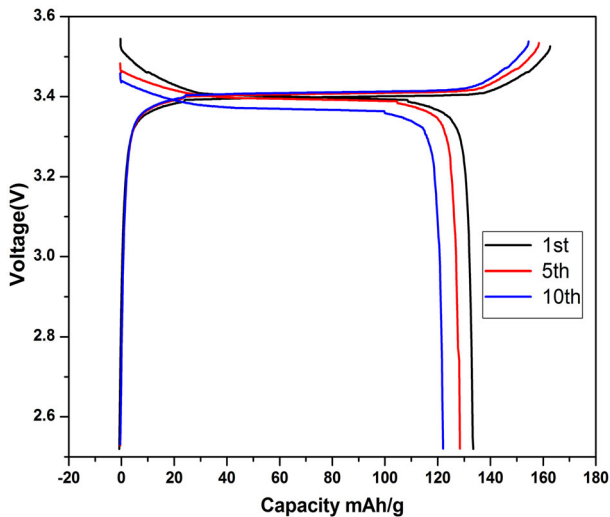


Fig. 10 Charge–discharge characteristics of the coin cell containing PE-IL5 and LiFePO₄ as the cathode and Li as the anode

Charge–discharge profile

The charge–discharge characteristics of the coin cell containing LiFePO₄ cathode and the PE (PE-IL5) were investigated and capacity vs voltage curves recorded for ten cycles for such cell is shown in Fig. 10. The cell gives excellent initial discharge

capacity of 133 mAh/g with the working voltage of 3.40 V. The charge–discharge profile shows very flat voltage range of 3.39 V in the first cycle and a similar pattern is followed for other cycles, reflecting good electrochemical properties. The discharge capacity in the subsequent cycles slowly decreases with the increase of cycle numbers. The capacity decrease is mainly attributed to the formation of passive layer on the cathode material. The cell delivers good reversibility with discharge capacity of 122 mAh/g at 10th cycle.

Conclusions

The PVdF-*co*-HFP containing different weight percentages of IL, SET₃TFSI had been prepared and characterized. The XRD results confirm the appearance of amorphous nature of the substance with the addition of IL (20 and 25 wt %) to the polymer matrix and the PE is stable up to 450 °C, as revealed by TG/DTA analysis. The nature of different functional groups present PE had been identified using Raman spectroscopy. The maximum number of pores with good interconnected network leads to high ionic conductivity, as evidenced by SEM and AFM images. Polymer/IL electrolyte (wt. ratio of 75:25, PE-IL5) with a maximum ionic conductivity of 6.93×10^{-5} S/cm and activation energy of 0.23 eV shows an excellent electrochemical potential stability of 4.4 V vs Li, as revealed from LSV and CV. A discharge capacity of 133 mAh/g was obtained for the coin cell containing PE-IL5 electrolyte and LiFePO₄ as the cathode, which is stable up to ten cycles.

Acknowledgments The author M. Sivakumar gratefully acknowledges for the financial support to carry out this work by University Grants Commission (UGC), New Delhi, Govt. India, under major research project (F.No.41-839/2012(SR)).

References

1. Tarascon JM, Armand M (2001) Issues and challenges facing rechargeable lithium batteries. *Nature* 414:359–367
2. Yuan F, Chen HZ, Yang HY, Li HY, Wang M (2005) PAN–PEO solid polymer electrolytes with high ionic conductivity. *Mater Chem Phys* 89:390
3. An YX, Zuo PJ, Cheng XQ, Liao LX, Yin GP (2011) The effects of LiBOB additive for stable SEI formation of PP13TFSI-organic mixed electrolyte in lithium ion batteries. *Electrochim Acta* 56:4841–4848
4. Brissot C, Rosso M, Chazalviel J-N, Lascaud S (1999) Dendritic growth mechanisms in lithium/polymer cells. *J Power Sources* 81–82:925–929
5. Farrington MD (2001) Safety of lithium batteries in transportation. *J Power Sources* 96:260–265
6. Chintapalli S, Frech R (1996) Effect of plasticizers on ionic association and conductivity in the (PEO) 9LiCF₃SO₃ system. *Macromolecules* 29:3499
7. Saito Y, Stephan AM, Kataoka H (2003) Ionic conduction mechanisms of lithium gel polymer electrolytes investigated by the conductivity and diffusion coefficient. *Solid State Ionics* 160:149
8. Ghosh A, Kofinas P (2008) Nanostructured block copolymer dry electrolyte. *J Electrochem Soc* 155:A428–A431
9. Croce F, Appetecchi GB, Persi L, Scrosati B (1998) Nanocomposite polymer electrolytes for lithium batteries. *Nature* 394:456

10. Shin JH, Henderson WA, Passerini S (2005) PEO-based polymer electrolytes with ionic liquids and their use in lithium metal-polymer electrolyte batteries. *J Electrochem Soc* 152:A978–A983
11. Shin JH, Henderson WA, Passerini S (2005) An elegant fix for polymer electrolytes. *Electrochem Solid State* 8:A125–A127
12. Shin JH, Henderson WA, Passerini S (2003) Ionic liquids to the rescue? Overcoming the ionic conductivity limitations of polymer electrolytes. *Electrochem Commun* 5:1016–1020
13. Goodenough JB, Kim Y (2010) Challenges for rechargeable Li batteries. *Chem Mater* 22:587–603
14. Fisher AS, Khalid MB, Widstrom M, Kofinas P (2012) Anion effects on solid polymer electrolytes containing sulfur based ionic liquid for lithium batteries. *J Electrochem Soc* 159(5):A592–A597
15. Xiong S, Xie K, Blomberg E, Jacobsson P, Matic A (2014) Analysis of the solid electrolyte interphase formed with an ionic liquid electrolyte for lithium–sulfur batteries. *J Power Sources* 252:150–155
16. Deraman K, Mohamed NS, Subban RHY (2013) Conductivity and electrochemical studies on polymer electrolytes based on poly vinyl (chloride)–ammonium triflate–ionic liquid for proton battery. *Int J Electrochem Sci* 8:1459–1468
17. Yang P, Cui W, Li L, Liu L, An M (2012) Characterization and properties of ternary P (VdF–HFP)–LiTFSI–EMITFSI ionic liquid polymer electrolytes. *Solid State Sci* 14:598–606
18. Sekhon SS, Lalia BS, Park J-S, Kim CS, Yamada K (2006) Physicochemical properties of proton conducting membranes based on ionic liquid impregnated polymer for fuel cells. *J Mater Chem* 16:2256
19. Fericola A, Panero S, Scrosati B, Tamada M, Ohno H (2007) New types of Brønsted acid-base ionic liquids-based membranes for applications in PEMFCs. *Chem Phys Chem* 8:1103
20. Sutto TE (2007) Hydrophobic and hydrophilic interactions of ionic liquids and polymers in solid polymer gel electrolytes. *J Electrochem Soc* 154:P101–P107
21. Kim K, Cho Y-H, Shin H-C (2013) 1-Ethyl-1-methyl piperidinium bis(trifluoromethanesulfonyl)imide as a co-solvent in Li-ion batteries. *J Power Sources* 225:113–118
22. Baranchugov V, Markevich E, Pollak E, Salitra G, Aurbach D (2007) Amorphous silicon thin films as a high capacity anodes for Li-ion batteries in ionic liquid electrolytes. *Electrochem Commun* 9:796–800
23. Markevich E, Baranchugov V, Salitra G, Aurbach D, Schmidt MA (2008) Behavior of graphite electrodes in solutions based on ionic liquids in in situ Raman studies. *J Electrochem Soc* 155(2):A132–A137
24. Gao K, Song X-H, Shi Y, Li S-D (2013) Electrochemical performances and interfacial properties of graphite electrodes with ionic liquid and alkyl-carbonate hybrid electrolytes. *Electrochim Acta* 114:736–744
25. Kaga Y, Katayama Y, Miura T, Komaba S (2010) Anode reactions of a tin thin film electrode modified with an ion-conductive polymer in a room-temperature ionic liquid electrolyte. *ECS Trans* 25(36):91–98
26. Hassoun J, Fericola A, Navarra MA, Panero S, Scrosati B (2010) An advanced lithium-ion battery based on a nanostructured Sn–C anode and an electrochemically stable LiTFSI–Py 24 TFSI ionic liquid electrolyte. *J Power Sources* 195:574–579
27. Lux SF, Schmuck M, Jeong S, Passerini S, Winter M, Balducci A (2010) Li-ion anodes in air-stable and hydrophobic ionic liquid-based electrolyte for safer and greener batteries. *Int J Energy Res* 34:97–106
28. Lewandowski A, Swiderska-Mocek A (2009) Properties of the lithium and graphite–lithium anodes in *N*-methyl-*N*-propylpyrrolidinium bis (trifluoromethanesulfonyl) imide. *J Power Sources* 194:502–507
29. Ye Y-S, Rick J, Hwang B-J (2013) Ionic liquid polymer electrolytes. *J Mater Chem A* 1:2719
30. Singh PK, Bhattacharya B, Mehra RM, Rhee HW (2011) Plasticizer doped ionic liquid incorporated solid polymer electrolytes for photovoltaic application. *Curr Appl Phys* 11:616–619
31. Zhang Q, Liu S, Li Z, Li J, Chen Z, Wang R, Lu L, Deng Y (2009) Novel cyclic sulfonium-based ionic liquids: synthesis, characterization, and physicochemical properties. *Chem Eur J* 15:765–778
32. Anuar NK, Subban RHY, Mohamed NS (2012) Properties of PEMA–NH₄CF₃SO₃ added to BMATFSI ionic liquid. *Materials* 5:2609–2620
33. Matsumoto H, Matsuda T, Miyazaki Y (2000) Room temperature molten salts based on trialkyl-sulfonium cations and bis(trifluoromethylsulfonyl) imide. *Chem Lett* 29:1430–1431
34. Tsunashima K, Sugiya M (2007) Physical and electrochemical properties of low-viscosity phosphonium ionic liquids as potential electrolytes. *Electrochem Commun* 9:2353–2358

35. Zhao D, Fei Z, Ang WH, Dyson PJ (2007) Sulfonium-based ionic liquids incorporating the allyl functionality. *Int J Mol Sci* 8:304–315
36. Fisher AS, Khalid MB, Widstrom M, Kofinas P (2011) Solid polymer electrolytes with sulfur based ionic liquid for lithium batteries. *J Power Sources* 196:9767–9773
37. Hapiot P, Lagrost C (2008) Electrochemical reactivity in room-temperature ionic liquids. *Chem Rev* 108:2238–2264
38. Sirisopanaporn C, Fernicola A, Scrosati B (2009) New, ionic liquid-based membranes for lithium battery application. *J Power Sources* 186:490–495
39. Kim GT, Jeong SS, Xue MZ, Balducci A, Winter M, Passerini S, Alessandrini F, Appetecchi GB (2012) Development of ionic liquid-based lithium battery prototypes. *J Power Sources* 199:239–249
40. Liew CW, Ong YS, Lim JY, Lim CS, Teoh KH, Ramesh S (2013) Effect of ionic liquid on semi-crystalline poly(vinylidene fluoride-co-hexafluoropropylene) solid copolymer electrolytes. *Int J Electrochem Sci* 8:7779–7794
41. Wu F, Feng T, Bai Y, Wu C, Ye L, Feng Z (2009) Preparation and characterization of solid polymer electrolytes based on PHEMO and PVDF–HFP. *Solid State Ionics* 180:677–680
42. Yu B, Zhou F, Wang C, Liu W (2007) A novel gel polymer electrolyte based on poly ionic liquid 1-ethyl 3-(2-methacryloyloxy ethyl) imidazolium iodide. *Eur Polym J* 43:2699–2707
43. Singh PK, Sabin KC, Chen X (2016) Ionic liquid–solid polymer electrolyte blends for supercapacitor applications. *Polym Bull* 73:255–263
44. Aravindan V, Vickraman P, Krishnaraj K (2008) Lithium difluoro (oxalate) borate-based novel nanocomposite polymer electrolytes for lithium ion batteries. *Polym Int* 57:932–938
45. Kim JK, Matic A, Ahn JH, Jacobsson P (2010) An imidazolium based ionic liquid electrolyte for lithium batteries. *J Power Sources* 195:7639–7643
46. Duluard S, Grondin J, Bruneel JL, Campet G, Delville M-H, Lassegues J-C (2008) Lithium solvation in a PMMA membrane plasticized by a lithium-conducting ionic liquid based on 1-butyl-3-methylimidazolium bis(trifluoromethanesulfonyl)imide. *J Raman Spectroscopy* 39:1189–1194
47. Han HS, Kang HR, Kim SW, Kim HT (2002) Phase-separated polymer electrolyte based on poly(vinyl chloride)/poly(ethyl methacrylate) blend. *J Power Sources* 112:461–468
48. Ramesh S, Liew C-W, Ramesh K (2011) Evaluation and investigation on the effect of ionic liquid onto PMMA–PVC gel polymer blend electrolytes. *J Non Cryst Solids* 357:2132–2138
49. Jung H-R, Ju D-H, Lee W-J, Zhang X, Kotek R (2009) Electrospun hydrophilic fumed silica/polyacrylonitrile nanofiber-based composite electrolyte membranes. *Electrochem Acta* 54:3630–3637
50. Saikia D, Chen-Yang YW, Chen YT, Li YK, Lin SI (2008) Investigation of ionic conductivity of composite gel polymer electrolyte membranes based on P (VDF–HFP), LiClO₄ and silica aerogel for lithium ion battery. *Desalination* 234:24–32
51. Sekhon SS (2003) Conductivity behaviour of polymer gel electrolytes: role of polymer. *Bull Mater Sci* 26:321–328
52. Abraham KM, Alamgir M (1993) Ambient temperature rechargeable polymer-electrolyte batteries. *J Power Sources* 43:195–208
53. Stephan AM, Kumar SG, Renganathan NG, Kulandainathan MA (2005) Characterization of poly(vinylidene fluoride–hexafluoropropylene)(PVdF–HFP) electrolytes complexed with different lithium salts. *Eur Polym J* 41:15–21
54. Gerbaldi C, Nair JR, Ahmad S, Meligrana G, Bongiovanni R, Bodoardo S, Penazzi N (2010) UV-cured polymer electrolytes encompassing hydrophobic room temperature ionic liquid for lithium batteries. *J Power Sources* 195:1706–1713
55. Missan HPS, Lalia BS, Karan K, Maxwell A (2010) Polymer–ionic liquid nano-composites electrolytes: electrical, thermal and morphological properties. *Mater Sci Eng B* 175:143–149
56. Noor ISM, Majid SR, Arof AK, Djurado D, Neto SC, Pawlicka A (2012) Characteristics of gellan gum–LiCF₃SO₃ polymer electrolytes. *Solid State Ionics* 225:649–653
57. Ye H, Huang J, Xu JJ, Khalfan A, Greenbaum SG (2007) Li ion conducting polymer gel electrolytes based on ionic liquid/PVDF–HFP blends. *J Electrochem Soc* 154:A1048–A1057
58. Raghavan P, Zhao X, Manuel J, Chauhan GS, Ahn JH, Ryu H-S, Ahn H-J, Kim K-W, Nah C (2010) Electrochemical performance of electrospun poly(vinylidene fluoride-co-hexafluoropropylene)-based nanocomposite polymer electrolytes incorporating ceramic fillers and room temperature ionic liquid. *Electrochim Acta* 55:1347–1354
59. Nittani T, Shimada M, Kawamura K, Dokko K, Rho Y-H (2005) Synthesis of Li⁺ ion conductive PEO–PSt block copolymer electrolyte with microphase separation structure. *Electrochem solid State Lett* 8:A385–A388

Studies on the effect of dispersoid(ZrO_2) in PVdF-co-HFP based gel polymer electrolytes

M. Sivakumar, R. Subadevi, and R. Muthupradeepa

Citation: *AIP Conf. Proc.* **1536**, 857 (2013); doi: 10.1063/1.4810498

View online: <http://dx.doi.org/10.1063/1.4810498>

View Table of Contents: <http://proceedings.aip.org/dbt/dbt.jsp?KEY=APCPCS&Volume=1536&Issue=1>

Published by the *AIP Publishing LLC*.

Additional information on AIP Conf. Proc.

Journal Homepage: <http://proceedings.aip.org/>

Journal Information: http://proceedings.aip.org/about/about_the_proceedings

Top downloads: http://proceedings.aip.org/dbt/most_downloaded.jsp?KEY=APCPCS

Information for Authors: http://proceedings.aip.org/authors/information_for_authors

ADVERTISEMENT



AIPAdvances

Submit Now

**Explore AIP's new
open-access journal**

- **Article-level metrics
now available**
- **Join the conversation!
Rate & comment on articles**

Studies On The Effect Of Dispersoid(ZrO_2) In PVdF-co-HFP Based Gel Polymer Electrolytes

M.Sivakumar*, R.Subadevi and R.Muthupradeepa

Department of Physics, Science Block, Alagappa University, Karaikudi-630004. Tamil Nadu, India.

Email susiva73@yahoo.co.in

Abstract. Gel polymer electrolytes containing poly(vinylidene fluoride-co-hexafluoropropylene) (P(VdF-co-HFP)) / Lithium bis(trifluoromethane sulfone)imide (LiTFSI) / mixture of ethylene carbonate and propylene carbonate (EC+PC) with different concentration of ZrO_2 has been prepared using the solution casting technique. The conductivity of the prepared electrolyte sample has been determined by AC impedance technique in the range 303-353K. The temperature dependent ionic conductivity plot seems to obey VTF relation. The maximum ionic conductivity value of $4.46 \times 10^{-3} S/cm$ has been obtained for PVdF-co-HFP(32%) - LiTFSI(8%) - EC+PC (60%) + ZrO_2 (6wt%) based polymer electrolyte. The surface morphology of the prepared electrolyte sample has been studied using SEM.

Keywords: PVdF-co-HFP, LiTFSI, ZrO_2 , Impedance studies, SEM.

PACS: 84

INTRODUCTION

Polymer electrolytes are generally prepared with the incorporation of salt solution in high molecular weight polymer. The ionic conductivity of solid polymer electrolyte is very poor of the order of $10^{-8} S/cm$. In order to improve the ionic conductivity, various methods have been adopted such as using plasticizer, blending, incorporation of fillers, etc.[1].

In the present study, the effect of different concentration of dispersoid ($ZrO_2=0, 3, 6, 9, 12wt\%$) in the gel polymer electrolyte has been studied in the view point of its ionic conductivity and complexation. The gel polymer electrolyte comprises Poly (vinylidene fluoride-co-Hexafluoropropylene) P(VdF-co-HFP), a semi crystalline polymer, the Lithium-bis(trifluoromethane sulfone)imide (LiTFSI) and Ethylene carbonate (EC) and Propylene carbonate (PC) liquid electrolyte in an optimized ratio. The prepared electrolyte films have been subjected to various characterization techniques and the results are discussed.

EXPERIMENTAL

The PVdF-co-HFP, LiTFSI are purchased from Aldrich USA and separately preheated near to their respective melting point for 10h in a vacuum controlled oven under 10^{-3} Torr pressure to remove the impurities. The solvents PC and THF (tetrahydrofuran) are purchased from SRL India and EC purchased from Merck, Germany were used without any further purification. The appropriate amount (as shown in table 1) of polymer and salt are weight up separately. The

predried polymer and salt are separately dissolved in THF; then it is stirred until the solution becomes homogeneous. The solution was casted on a flat bottom petri plate and the solvent was allowed to evaporate in the room temperature for 24h. Finally, the film has been dried at $60^\circ C$ for 12h in order to remove the residual solvent. The conductivity of the prepared electrolyte has been measured using a micro auto lab type III Potentiostat/Galvanostat of frequency range 40Hz–300kHz in the temperature range of 303–353 K stainless steel (SS) was used as a blocking electrode. The surface morphology has been studied using Hitachi 3000-N with the magnification of 250.

RESULTS AND DISCUSSION

Conductivity Studies

The impedance spectroscopy is a powerful tool to analyze the electrical impedance of an electrolyte material. The complex impedance obtained through AC impedance, gives the complete electrical behavior of the electrolyte and the electrolyte-electrode interface as a function of frequency. In general, there are two semicircles appear in a complex impedance (CI) plot. The higher frequency semicircle gives the bulk resistance of the electrolyte and other at lower frequency gives the interfacial impedance [2]. The ionic conductivity has been measured using the following formula

$$\sigma = \frac{l}{AR_b}$$

where, σ – Ionic conductivity, R_b – Bulk resistance
A - Area of the film, l – Thickness of the film

Proceeding of International Conference on Recent Trends in Applied Physics and Material Science

AIP Conf. Proc. 1536, 857-858 (2013); doi: 10.1063/1.4810498

© 2013 AIP Publishing LLC 978-0-7354-1160-9/830.00

The calculated conductivity values are shown in Table 1. From CI plot, the disappearance of semicircle follows many of the plasticized based system [3]. It is observed that the conductivity increases with the increase of temperature which is in agreement with the free volume theory [4]. The bare electrolyte without filler owns the ionic conductivity of 9.72×10^{-4} S/cm at 303K, while adding ZrO_2 into it, the conductivity has been enhanced by one order of magnitude. The conductivity has increased with the increase of ZrO_2 content up to 6wt% ($\sigma = 4.46 \times 10^{-3}$ S/cm at 303K) in bare PVdF-co-HFP(32%) + LiTFSI(8%) + EC+PC (60%) system. The incorporation of fillers enhances the free volume because of the interaction of the polymers and ceramic fillers. The introduction of fillers causes more amorphous phases in the polymer electrolyte. Further increase of ZrO_2 content causes the conductivity dips down. This is because of the crystalline region of the fillers restricted the movement of ions within the electrolyte system.

Fig 1 shows the temperature dependent ionic conductivity plot for the prepared electrolyte sample in the temperature range of 303–353K. The plot seems to obey Arrhenius relation, which generally describes the electrical conductivity versus temperature behavior in polymer electrolytes using the relation

$$\sigma = \sigma_0 \exp (E_a/KT)$$

where σ_0 constant, E_a – activation energy,

K-Boltzmann constant, T-absolute temperature (K).

The activation energy (E_a) of the electrolyte sample has been measured from the slope of the plot and listed in Table 1. The minimum activation energy of 0.213eV has been obtained for the sample possessed maximum ionic conductivity.

TABLE 1. Conductivity values and activation energy of the prepared electrolyte samples PVdF-co-HFP(32%) + LiTFSI(8%) + EC+PC (60%) + ZrO_2 (0%, 3%, 6%, 9%, 12%)

| Sampl e code | Conductivity value $\times 10^{-3}$ S/cm | | | | | | E_a valu eeV |
|-----------------|--|------|------|------|------|------|-------------------|
| | 303K | 313K | 323K | 333K | 343K | 353K | |
| K | 0.97 | 1.11 | 1.43 | 1.62 | 1.95 | 2.23 | 0.235 |
| K1 | 2.55 | 2.59 | 2.77 | 3.03 | 3.4 | 3.73 | 0.219 |
| K2 | 4.46 | 4.61 | 4.95 | 5.22 | 5.71 | 6.21 | 0.213 |
| K3 | 3.55 | 3.74 | 3.85 | 4.06 | 4.52 | 5.29 | 0.223 |
| K4 | 3.31 | 3.4 | 3.51 | 3.72 | 3.82 | 3.97 | 0.228 |

SEM

Fig 2 shows the SEM image of sample K2-6wt % of ZrO_2 contained GPE with the magnification $\times 250$. The micro pores present in the system have the ability to retain the liquid electrolytes and the ionic conductivity of the electrolyte also high. The ZrO_2 particles are distributed uniformly throughout the matrix and form a very good network.

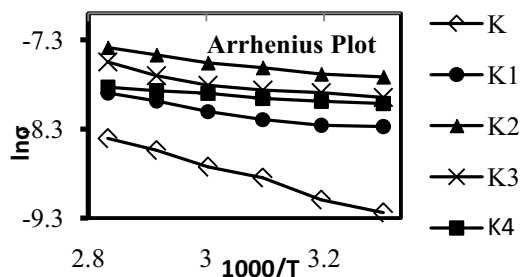


FIGURE 1. Temperature depended conductivity plot of PVdF-co-HFP(32%) + LiTFSI(8%) + EC+PC (60%) + ZrO_2 (0%, 3%, 6%, 9%, 12%)

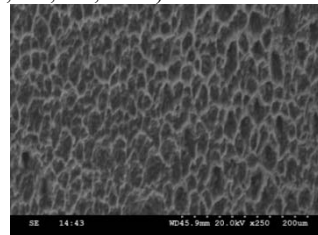


FIGURE 2 SEM image of K2 at X 250

CONCLUSION

The composite polymer electrolyte system has been prepared with different compositions of ZrO_2 filler using solution casting technique. The maximum ionic conductivity value of 4.46×10^{-3} S/cm has been obtained for (K2) PVdF-co-HFP(32%) - LiTFSI(8%) - EC+PC (60%) - ZrO_2 (6%) based electrolyte system. Also, the ionic conductivity increases upon adding ZrO_2 in the bare gel polymer system up to 6 wt%, further addition of ZrO_2 dips down the conductivity which is due to higher crystalline region present in the matrix which restricts the mobility of charge carriers. The temperature dependent ionic conductivity plots seem to obey the Arrhenius relation. The pores have been created while adding ZrO_2 ; it causes good network and it results high ionic conductivity which has been studied using SEM.

REFERENCES

1. Z.H. Li, H.P. Zhang, P. Zhang, G.C. Li, Y.P. Wu, X.D. Zhou, *J. Membrane Sci.*, 322, 416–422 (2008).
2. M. Watnabe, N. Ogata, Ionic conductivity of Poly(propylene oxide) Electrolytes, in: J.R. MacCallum, C.A. Vincent (Eds.), *Polymer Electrolyte Review*, vol.1, Elsevier, New York, 1987, pp. 42.
3. S. Rajendran, M. Sivakumar, R. Subadevi, *J. Appl Polym Sci.*, 90, 2794–2800 (2003).
4. Armand, M. B.; Chabagno, J. M.; Duclot, M. J. In *Fast-Ion Transport in Solids*; Vashishta, P.; Mundy, L. N.; Shenoy, G., Eds.; North Holland: Amsterdam, 1979; p 131.



Role of pH on synthesis and characterization of cerium oxide (CeO₂) nano particles by modified co-precipitation method



M. Ramachandran^{a,b}, R. Subadevi^a, M. Sivakumar^{a,*}

^a #120, Energy Materials Lab, Department of Physics, Science Block, Alagappa University, Karaikudi, 630003, Tamil Nadu, India

^b Department of Physics, Arumugam Pillai Seethai Ammal College, Tiruppattur, 630 211, Tamil Nadu, India

ARTICLE INFO

Keywords:

Cerium oxide
Modified co-precipitation method
Precipitation agent
Nano particles

ABSTRACT

A facile synthesis has been made to prepare cerium oxide (CeO₂) nano particles via modified co-precipitation method using different pH values viz, 9 to 12 in steps of 1. The as prepared powders have been systematically studied to analyze their structure, morphology and photoluminescence properties. The representative samples have been analyzed through TEM and XPS analyses. The crystallite size has been decreased upon increasing the pH of the environment. When pH of the solute reached 12, the particle size is reached to 27 nm, which is ascertained through TEM analysis.

1. Introduction

Cerium is the most excessive among rare earth elements, occupying at about 66 parts per million of the earth crust, and also presently a subject of great care due to its multiple applications, which include materials for catalysis, gas sensors, solid oxide fuel cells, ceramics, and oxygen storage [1,2]. Nowadays, nano materials are playing vital role in many applications due to its outstanding physical and chemical properties, which are significantly different from those bulk materials. Rigorous studies have revealed that the extensive applications of Ceria are associated to its relative abundance, unique acid-base surface properties with the dynamically reversible Ce³⁺/Ce⁴⁺ redox pair. These properties also provide ceria with remarkable catalytic performance [3]. Numerous methods, including precipitation from solution [4], microwave assisted method [5], hydrothermal synthesis [6], sol-gel [7], solvo thermal method [8] and polyol method [9] have been used to prepare ceria nano particles with different morphologies and size such as nano belts, nano spheres, nano fibres and nano flower etc.

Among these, modified co-precipitation method has been an extensively proficient assembly of homogeneous high-purity and crystalline oxide at low cost, also simple procedure allows scaling up for mass production [10]. Zaravkovic et al. [11], synthesized CeO₂ nano particle with irregular morphology and soft agglomeration via chemical route. Guangyu et al. [12], reported yeast adopted CeO₂ with hollow microsphere morphology via bio-template chemical route. However, it is still a challenge to develop the efficient route for fabricating the CeO₂ nanoparticles with preferred morphology. With the specific curiosity to

overrule this issue, an attempt is made to synthesize CeO₂ using cerium nitrate as source material, PVP as surfactant by using modified co-precipitation method by varying the pH as 9, 10, 11 and 12. The as prepared powders were analyzed for their structure, morphology and photoluminescence properties.

2. Materials and methods

The CeO₂ nano particles were synthesized by the modified co-precipitation method. Cerium nitrate hexa hydrate (Ce(NO₃)₃·6H₂O) (434.8 g/mole; 99%, Alpha Aeser), sodium hydroxide (NaOH); (39.99 g/mole, SRL), polyvinyl pyrrolidone (PVP) (Mol.wt.40,000 Merck, Germany) were used as starting materials without further purification. To obtain different morphology, 2.5 wt% of PVP [13] was added separately to 0.01 M of aqueous Ce(NO₃)₃·6H₂O. The resulting aqueous mixture was stirred further for 10 min at room temperature and then the pH value has been varied to the desired value (viz, 9 (CP1), 10 (CP2), 11 (CP3), and 12 (CP4)) by adding the NaOH drop wise into the mixture. The whole mixture was further stirred for 90 min to obtain pale yellow precipitate. The precipitate has centrifuged at 200 rpm and splashed with deionized water and acetone several times to get rid of the residual surfactant. Then the precipitate was dried in vacuum oven at 110 °C for 4 h, milled the sample for 30 m and subsequently calcined in air at 600 °C for 2 h to get CeO₂ powder.

The crystalline structure of the material has been analyzed through X-ray diffraction analysis (XRD) using X-ray diffractometer (Philips X'Pert PRO) with CuKα (45 KV, 50 mA) radiation at room temperature

* Corresponding author.

E-mail address: susiva73@yahoo.co.in (M. Sivakumar).

<https://doi.org/10.1016/j.vacuum.2018.12.002>

Received 9 August 2018; Received in revised form 21 November 2018; Accepted 2 December 2018

Available online 24 December 2018

0042-207X/ © 2018 Elsevier Ltd. All rights reserved.

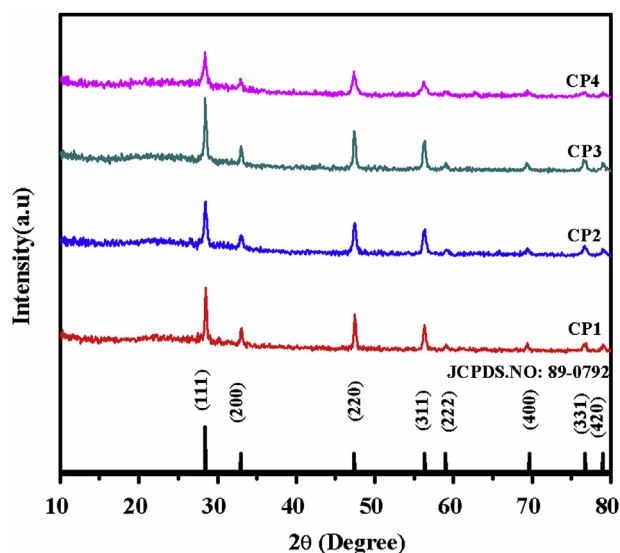


Fig. 1. XRD patterns of CeO₂ nano particles prepared by varying pH as 9(CP1), 10(CP2), 11(CP3), and 12 (CP4).

in the range of $20^\circ \leq 2\theta \leq 80^\circ$. Fourier Transform Infrared (FTIR) study was performed using Thermo Nicolet 380 spectrophotometer in the region $4000\text{--}400\text{ cm}^{-1}$. The surface morphology and size of the as-prepared samples have been observed using scanning electron microscopy (SEM) (Quanta FEG 200 Instrument with EDX) and high resolution transmission electron microscopy (HRTEM, FEI Techno F30 ST equipped with a field emission gun at 300 KV) techniques. The electronic state of the elements has been analyzed by X-ray photon electron spectroscopy (XPS, PHI model 5802). Photoluminescence spectroscopy has been performed using Bruin omega-10 spectrometer.

3. XRD analysis

The purity and crystallinity of the as-synthesized CeO₂ samples have been studied using X-ray powder analysis and Fig. 1 illustrates the X-ray diffraction patterns of CeO₂ particles prepared by varying pH such as 9 (CP1), 10 (CP2), 11 (CP3) and 12 (CP4) respectively. It can be seen from Fig. 1, the diffraction peaks at $2\theta = 28.5, 33.1, 47, 56.3, 59.1, 69.5, 76.7, \text{ and } 79.1^\circ$, which are indexed to (111), (200), (220), (311), (222), (400), (331) and (420) lattice planes of cubic phase of cerium oxide with space group Fm-3m and JCPDS(81–0792). The sharp and strong diffraction peaks in Fig. 1 reveals that the as-prepared samples are well crystallized; also, the diffraction peaks from other species could not be identified. This elucidates the purity of the obtained samples. According to the X-ray diffraction patterns, the crystallite diameters of samples CP1, CP2, CP3 and CP4 have been respectively calculated as 33, 30, 23 and 19 nm using Debye Scherrer equation [14]. The diffraction patterns reveal that the crystallite size has been decreased upon increasing pH. The OH[−] ions are highly involved in the aggregation process which would strongly affect the supersaturation degree of initial precipitate [15,16]. Henceforth, the particle size decreased upon increasing pH during the synthesis.

4. FTIR analysis

Fig. 2 shows the FT-IR spectra of the as-synthesized CeO₂ nano particles (CP1–CP4). The absorption bands at $1554, 1409 \text{ and } 730\text{ cm}^{-1}$ are ascribed to the stretching vibration of O–H absorption and non-bridging of OH groups and characteristic of cubic CeO₂ respectively. This indicates the presence of physisorbed water molecules linked to CeO₂ nanoparticles. Moreover, the lattice vibrational modes appearing at $434 \text{ and } 853\text{ cm}^{-1}$ are recognized to the Ce–O stretching vibration,

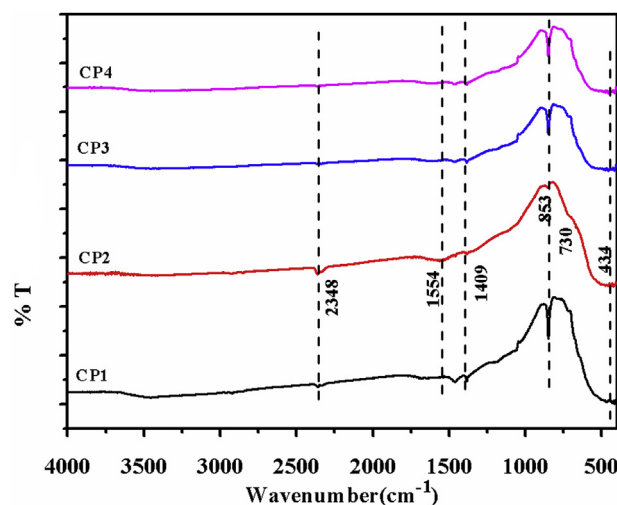


Fig. 2. FTIR spectra of CeO₂ nano particles prepared by varying pH as 9(CP1), 10(CP2), 11(CP3) and 12 (CP4).

which are the characteristic bonds of cubic CeO₂ [17]. The vibrational peak appeared at 2348 cm^{-1} is corresponding to the C=O stretching vibration of CeO₂, which appears weakly when the pH is 9 and 10 and disappears when the pH is > 10 . All the vibrational peaks assigned in the spectra are in agreement with the pure material that has been used in the present study.

5. SEM analysis

The surface morphology of all the samples has been analyzed using SEM analysis and the SEM images are shown in Fig. 3(a–d) along with the EDX spectrum (Fig. 3(inset)) of the sample CP4. It is obviously noticed from Fig. 3(a–d), that the solute environment (pH) plays a vital role in its surface morphology during the preparation of CeO₂ nanoparticles. Fig. 3 displays that the samples CP1 and CP2 are composed of small crystallites and shows the irregular particles with soft agglomeration. When the environment of the solute is highly basic i.e., (pH > 10), the small nano particles of CeO₂ aggregate and gradually evolved into spherical assembly, in which a minimum energy is required to form the ceria particle. It may be due to the nucleation effect of nano particles. It is described that the pH of the medium used in co-precipitation method has an acute and significant impact in the final product. The inset of Fig. 3(d) exhibits the typical EDX spectrum, which reveals the several well defined bands of Ce and O in the as-synthesized CeO₂ nanoparticles.

6. TEM analysis

To further examine the morphology and size of the as-synthesized sample, it has been subjected to the transmission electron microscopic (TEM) investigation with the selected area electron diffraction analysis (SAED). The TEM overview of the optimized sample (CP4) is shown in Fig. 4(a). This clearly displays the uniform distribution of the particle along with its size and shape. The particle size has been measured using Measure IT software (Olympus soft imaging solution GMBH product) to ensure a reliable representation of the actual size distribution and the estimated particle size is about 27 nm. From Fig. 4 (b), it is clearly seen that the high crystallinity of the powder leads to its respective well-pronounced diffraction rings in the SAED pattern [18,19]. Fig. 4(b) can be assigned to the reflection (111), (400), (311), and (200) planes of cubic CeO₂. There are no additional rings in the SAED pattern due to any other crystalline impurities. These entire outcomes are in accordance with the XRD results. Therefore, it can be used as suitable filler in the fabrication of composite electrolytes in Lithium secondary

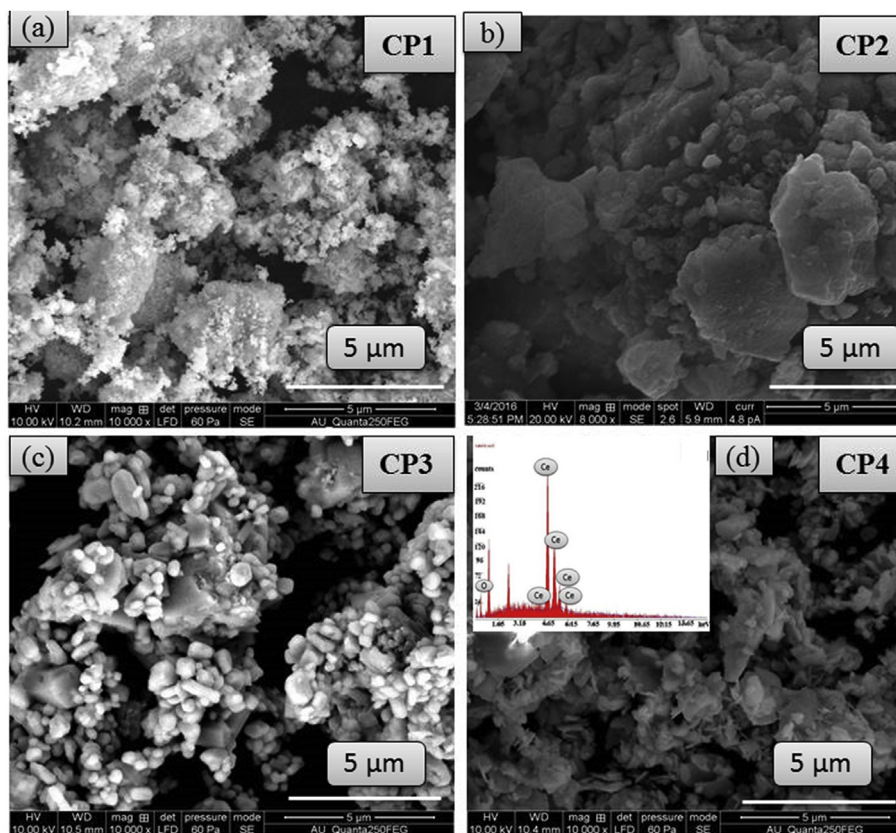


Fig. 3. SEM images of CeO_2 nano particles prepared by varying pH as a) 9(CP1), b)10(CP2), c) 11(CP3) and d) 12(CP4) (Inset: EDX spectra of CP4).

batteries.

7. XPS analysis

The chemical valence state of the prepared CeO_2 (CP4) has been examined by XPS analysis and the high resolution XPS spectra of wide, Ce 3d, O1s of CeO_2 are shown in Fig. 5(a–c). Fig. 5(a) shows the wide range scanning XPS spectrum and it reveals that the sample consists of Ce, O and C elements on the surface of the sample. Fig. 5(b) demonstrates the Ce 3d core level peak of ceria. The symmetric peaks of $\text{Ce}^{4+} 3d_{3/2}$ and $\text{Ce}^{4+} 3d_{5/2}$ have been observed at binding energies 874.42 and 880.86 eV respectively. The spin-orbit split energy is about 6.44 eV for the sample. These values are in good agreement with Ce^{4+} ion in the sample [20,21]. The binding energy of oxygen O1s is superposed around 530.24 eV with two more peaks in higher and lower sides,

which is shown in Fig. 5(c). The high binding energy is recognized to chemisorbed oxygen that is known to be the oxidation activity. The lower binding energy is analogous to the lattice oxygen in CeO_2 [12]. All perceived binding energy values are in agreement with the literature, which reveals the chemical stability of the sample.

8. PL analysis

The photoluminescence spectroscopic analysis has been performed with an excitation wavelength of 270 nm for all the samples (CP1–CP4) and the spectra are given in Fig. 6. It is noticed from the typical fluorescence spectrum of all samples (CP1–CP4) that a UV band has been occurred around 363 nm (3.4 eV). The peaks at 434 and 523 nm corresponds to energies 2.86 and 2.37 eV respectively are evidently lower than the deduced band gap. This is likely to be related with band

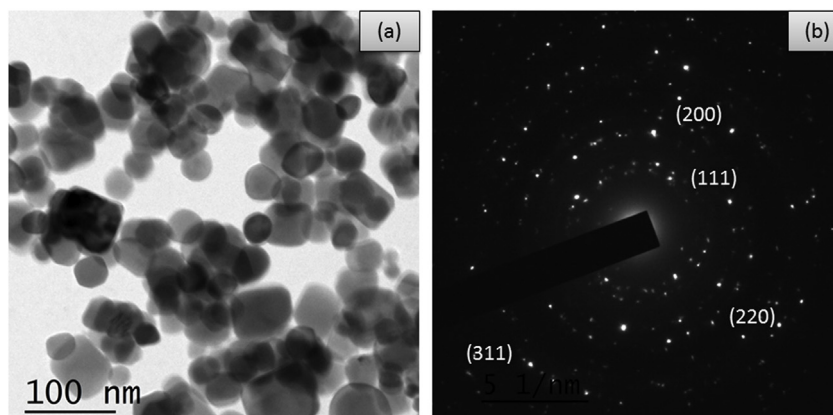


Fig. 4. a) TEM image b) SAED pattern of CP4.

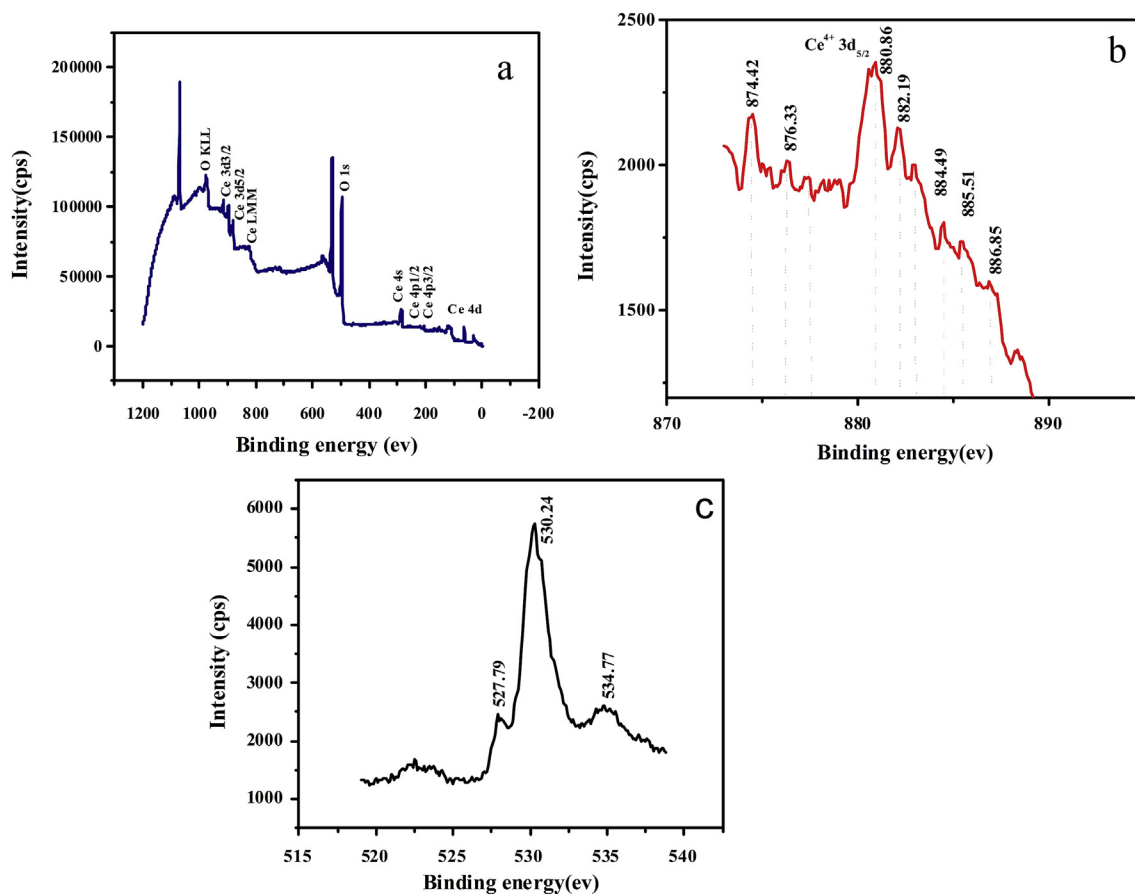


Fig. 5. XPS spectra of (a) wide b) Zr c) O1s of CP4.

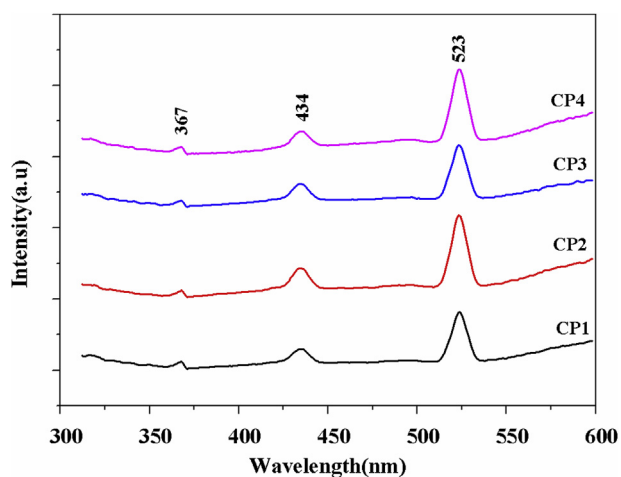


Fig. 6. Photoluminescence spectra of CeO₂ nano particles prepared by varying pH as 9(CP1), 10(CP2), 11(CP3) and 12 (CP4).

to band emission which is probably involving the localized or free excitons. It reveals the mid-gap trap states such as oxygen vacancies or defect states.

9. Conclusion

The CeO₂ nano particles have been synthesized using co-precipitation method by varying pH values such as 9, 10, 11 and 12 (CP1-CP4). The cubic structure with crystallite size between 33 and 19 nm of CeO₂ has been ascertained using XRD. The functional group vibrations have been confirmed through FT-IR analysis. The aggregated spherical nano

particles are evolved when pH approaches 12. The spherical morphology with particle size 27 nm has also been confirmed through TEM analysis. The chemical stability has been affirmed using XPS analysis. The band to band transition has been observed at 3.57 eV from photoluminescence study, which is related to the mid band transition. From the above analyses, the optimized sample is believed to serve as suitable filler in the Lithium polymer electrolyte in the Li-secondary battery fabrication.

Acknowledgements

One of the authors M. Sivakumar gratefully acknowledges University Grants Commission (UGC), New Delhi, India for the financial support for this work under physical sciences- major research project (F.No. 41-839/2012(SR)) scheme.

Appendix A. Supplementary data

Supplementary data to this article can be found online at <https://doi.org/10.1016/j.vacuum.2018.12.002>.

References

- [1] C. Sun, L. Hong, Z.X. Wang, L. Chen, X. Huang, O₂ Gas sensor using supported hydrophobic room-temperature ionic liquid membrane-coated electrode, *Chem. Lett.* 33 (2004) 6–7.
- [2] S. Phokh, S. Pinitsoontor, P. Chirawatkul, Y. Poo-arporn, S. Maensiri, Synthesis, characterization and magnetic properties of monodisperse CeO₂ nanospheres prepared by PVP-assisted hydrothermal method, *Nanoscale Res. Lett.* 7 (2012) 1–13.
- [3] H. Zhang, C. Wu, W. Wang, J. Bu, F. Zhou, B. Zhang, Q. Zhang, Effect of ceria on redox-catalytic property in mild condition: a solvent-free route for imine synthesis at low temperature, *Appl. Catal. B Environ.* 227 (2018) 209–217.
- [4] E. Sasmaz, C. Wang, M.J. Lance, J. Lauterbach, In situ spectroscopic investigation of

- a Pd local structure over Pd/CeO₂ and Pd/MnOx–CeO₂ during CO oxidation, *Mater. Chem.* 5 (2017) 12998–13008.
- [5] M. Hasanpoor, M. Aliofkhaezrai, M. Hosseinali, Electrophoretic deposition of ZnO–CeO₂ mixed oxide nanoparticles, *J. Am. Ceram. Soc.* 100 (2017) 901–910.
- [6] M.P. Kalamuei, S. Alizadeh, M.M. Kamazani, M.S. Niasari, Synthesis and characterization of CeO₂ nanoparticles via hydrothermal route, *J. Ind. Eng. Chem.* 21 (2015) 1301–1305.
- [7] K. Polychronopoulou, A.F. Zedan, M.S. Katsiotis, M.A. Baker, A.A. Alkhoori, S.Y. Alqaradawi, S.J. Hinder, S. Alhassan, Rapid microwave assisted sol-gel synthesis of CeO₂ and Ce_xSm_{1-x}O₂ nanoparticle catalysts for CO oxidation, *J. Mol. Catal. Chem.* 428 (2017) 41–55.
- [8] H. Liu, H. Liu, X. Han, Core-shell CeO₂ micro/nanospheres prepared by microwave-assisted solvothermal process as high-stability anodes for Li-ion batteries, *J. Solid State Electrochem.* 21 (2017) 291–295.
- [9] M. Sivakumar, R. Muruganatham, R. Subadevi, Synthesis of surface modified LiFePO₄ cathode material via polyol technique for high rate Lithium secondary battery, *Appl. Surf. Sci.* 337 (2015) 234–240.
- [10] K.S. Ranjith, P. Saravanan, S.H. Chen, C.L. Dong, C.L. Chen, S.Y. Chen, K. Asokan, R.T. Rajendra Kumar, Enhanced room-temperature ferromagnetism on Co-doped CeO₂ nanoparticles: mechanism and electronic and optical properties, *J. Phys. Chem. C* 118 (2014) 27039–27047.
- [11] J. Zdravkovic, B. Simovic, A. Golubovic, D. Poleti, I. Veljkovic, M. Scepanovic, G. Brankovic, Comparative study of CeO₂ nanopowders obtained by the hydrothermal method from various precursors, *Ceram. Int.* 41 (2015) 1970–1979.
- [12] M. Guangyu, W. Qinglian, H. Yongmin, Facile fabrication of CeO₂ hollow microspheres with yeast as bio-templates, *J. Rare Earths* 33 (2015) 1329–1334.
- [13] S. Lakhwani, M.N. Rahaman, Adsorption of polyvinylpyrrolidone (PVP) and its effect on the consolidation of suspensions of nanocrystalline CeO₂ particles, *J. Mater. Sci.* 34 (1999) 3909–3912.
- [14] E.K. Goharshadi, S. Samiee, P. Nancarrow, Fabrication of cerium oxide nanoparticles: characterization and optical properties, *J. Colloid Interface Sci.* 356 (2011) 473–480.
- [15] H.I. Chen, H.Y. Chang, Synthesis of nanocrystalline cerium oxide particles by the precipitation method, *Ceram. Int.* 31 (2005) 795–802.
- [16] S.W. Bian, I.A. Mudunkotuwa, T. Rupasinghe, V.H. Grassian, Aggregation and dissolution of 4 nm ZnO nanoparticles in aqueous environments: influence of pH, ionic strength, size, and adsorption of humic acid, *Langmuir* 27 (2011) 6059–6068.
- [17] V. Ramasamy, G. Vijayalakshmi, Synthesis and characterization of ceria quantum dots using effective surfactants, *Mater. Sci. Semicond. Process.* 42 (2016) 334–343.
- [18] D. Zhang, X. Du, L. Shi, R. Gao, Shape-controlled synthesis and catalytic application of ceria nanomaterials, *Dalton Trans.* 41 (2012) 14455–14475.
- [19] Y. Sasikumar, A. MadhanKumar, Z.M. Gasem, E.E. Ebenso, Hybrid nanocomposite from aniline and CeO₂ nanoparticles: surface protective performance on mild steel in acidic environment, *Appl. Surf. Sci.* 330 (2015) 207–215.
- [20] N. Wang, S. Li, Y. Zong, Q. Yao, Sintering inhibition of flame-made Pd/CeO₂ nanocatalyst for low-temperature methane combustion, *J. Aerosol Sci.* 105 (2017) 64–72.
- [21] N.S. Ferreira, R.S. Angélica, V.B. Marques, C.C.O. deLima, M.S. Silv, Cassava-starch-assisted sol-gel synthesis of CeO₂ nanoparticles, *Mater. Lett.* 165 (2016) 139–142.

Facile Synthesis and Characterization of ZrO₂ Nanoparticles via Modified Co-Precipitation Method

M. Ramachandran^{1,2}, R. Subadevi², Wei-Ren Liu^{3,*}, and M. Sivakumar^{2,*}

¹Department of Physics, Arumugam Pillai Seethai Ammal College, Tiruppattur 630210, Tamil Nadu, India

²Energy Materials Lab, School of Physics, Alagappa University, Karaikudi 630004, Tamil Nadu, India

³Department of Chemical Engineering, Chung-Yuan Christian University, Chung-Li, Taiwan, 32023, ROC

The crystalline Zirconium oxide (ZrO₂) nano particles were synthesized using optimized content of Zirconium nitrate (Zr(NO₃)₂ · 3H₂O) with varying KOH concentration (0.5, 1 and 1.5 M) by co-precipitation method. The thermal history of the precursor was carefully analyzed through Thermogravimetric (TG/DTA) measurement. The as prepared samples were characterized to ensure structural, functional, morphological, compositional, chemical composition and band gap by X-ray diffractometer (XRD), Fourier transform infrared spectroscopy (FTIR), Laser Raman, scanning electron microscopy (SEM), High resolution Transverse Electron Microscopy (HR-TEM), X-ray photo electron spectroscopy (XPS), EDX, Photo luminescence spectroscopy (PL). The monoclinic structure with space group P21/c has been confirmed from XRD (JCPDS 89-9066). The Zr–O stretching vibration and Zr–O₂–Zr bending vibrations were confirmed through FTIR analysis. The well dispersed particles with spherical morphology were confirmed through SEM and TEM analysis. The oxidation states of Zr, O and C were confirmed through XPS analysis. The oxygen vacancies and band gap of the particles were investigated through PL analysis.

Keywords: ZrO₂, Co-Precipitation Method, Luminescence.

1. INTRODUCTION

Nano materials are considered as intermediate between classical molecular scale and micron sized entities. The synthesis of nano materials with structural stability are great importance with unique physical and chemical properties in comparison with those of their bulk counterparts, and their properties based on quantum size effect and high surface area.^{1–3} Recently, many studies performed on the oxide material such as TiO₂, Al₂O₃, ZnO and ZrO₂ etc., among these, Zirconia is very fascinating material in current technology. It has been renowned as a high-eminent in energy storage due to its thermal, chemical stability and outstanding mechanical properties such as high strength and crack robustness, high melting point, low thermal conductivity, high coefficient of thermal expansion, wide band gap (5.0–5.5 eV), high resistance to rust and high fracture toughness. ZrO₂ is always a very significant ceramic material due to its extensive range of application as structural

materials, solid-state electrolytes, thermal barrier coatings, electro-optical materials, gas-sensing, corrosion-resistant, automobile parts, metal components and catalysts etc.,⁴ Stabilized Zirconia is used in oxygen sensors and fuel cell membranes, because it had the competence to allow oxygen ions to move freely through the crystal structure at high temperature. The amorphous nature of the polymer electrolyte was enhanced when the addition of ZrO₂, because it had high dielectric constant.⁵

There are three polymorphic modifications of Zirconia: monoclinic (*m*), tetragonal (*t*) and cubic (*f*).^{6,7} Various method of synthesis of ZrO₂ nano crystalline have been established and inspected including sol–gel,⁸ combustion,⁹ Microwave assisted,¹⁰ hydrothermal¹¹ and co-precipitation method¹² etc., co-precipitation methods have been a widely practiced for production of homogenous, high-purity and crystalline oxide powders at low cost and simplicity of the method allows the mass production.¹³ Furthermore, the ceramic particles with preferred shape and size can be produced if solvent pH, solute concentration, reaction temperature, reaction time, seed material and the type of solvent

*Authors to whom correspondence should be addressed.

conditions are optimized.¹⁴ Drazin et al.,¹⁵ were reported monoclinic ZrO₂ phase was prepared via modified reverse-strike co-precipitation synthesis route at calcination temperature 1100 °C for 12 h using organic additive. Huazhou et al.,¹⁶ reported monoclinic ZrO₂ phase with average grain size of 110 nm using surfactant by two-step sintering by hydrothermal corrosion method.

However, Zirconia metal oxide with pure monoclinic phase attained is still difficult. Of particular interest of this issue, motivation towards facile synthesis and characterize the pure monoclinic ZrO₂ nanoparticles using aqueous solution in the absence of surfactant with controlled morphology and crystalline nature in the present study using modified co-precipitation method.

2. MATERIAL AND METHOD

Zirconium nitrate hexahydrate [Zr(NO₃)₂ · 6H₂O], Potassium hydroxide [KOH] and double distilled deionized water were purchased from Alfa Aesar with analytical grade. All the chemicals were used without further purification. In a typical reaction, 0.2 M of Zirconium nitrate (Zr(NO₃)₂ · 6H₂O) was dissolved in three beakers using deionized water under stirring at 500 rpm at room temperature. Potassium hydroxide (KOH) with 0.5, 1.0 and 1.5 M (B1, B2 and B3) was slowly added in the respective three beakers until pH > 10 were attained; the products were filtered and repeatedly washed with deionized water and acetone simultaneously. The Zirconia precursor was dried in vacuum oven for 4 h followed by milling it for 30 minutes. Then, the sample was calcined at 900 °C for 4 h in the muffle furnace. Finally, ZrO₂ nanoparticles were obtained.

The samples B1, B2 and B3 obtained by a co-precipitation method were characterized by high resolution electron microscopy (HRTEM, FEI Techno F30 ST equipped with a field emission gun at 300 KV). The morphology of the B1, B2 and B3 samples was analyzed by scanning electron microscopy (SEM, Hitachi S-4700 Type II) operated at an accelerating voltage of 25 KV. The phase and crystalline size of the three samples were estimated through X-ray Diffraction measurements (XPRT-PRO with CuK α radiation). FTIR study was made using Thermo Nicolet 380 Instrument Corporation and KBr in the 4000–400 cm⁻¹ region. TG/DTA was measured on thermal analyzer (SHI-MADZU DTG-60AH). The operating temperature was increased from 30 to 1000 °C at heat rate of 10 °C min⁻¹ in nitrogen atmosphere. The presence of a monoclinic structure was confirmed through Micro Raman spectroscopy (STR-500 Laser Raman spectrometer, SEKI, Japan), chemical valence state of the elements was analyzed by X-ray photon electron spectroscopy (XPS, PHI model 5802). Optical properties of the products were carried out by photo luminescence (PL, Fluoromax-4 spectra fluorometer with Xe lamp excitation light source).

3. RESULTS AND DISCUSSION

TG/DTA analysis was carried out to study the transformation process of the precursors throughout calcination process. Figure 1(a) showed the profile of weight loss of precursor as function of temperature as measured in TGA. The precursor showed gradual weight loss between 30 and 200 °C, followed by feeble weight loss between 200 and 700 °C; Also, a rapid weight loss has been occurred in the range 700–800 °C. The uppermost rate was attributed to the loss of moisture. The second weight loss was attributed to exclusion of potassium nitrate from the mixture. The DTA curve also exhibited that broad endothermic curve around 400 °C, which is in accordance with TGA curve. The third weight loss was attributed to transform the precursor hydroxide in to Zirconium oxide particles. There was an exothermic peak at 820 °C in the DTA curve correlated to the transition in TGA data. The total weight loss (23%) observed from TGA study is well in agreement with that of theoretical weight loss;¹⁷ also, these results were good agreement with the previous literatures.^{17–20}

The phase purity and crystalline nature of the as-synthesized ZrO₂ samples were analyzed by X-ray Diffraction (XRD). Figure 1(b) depicted that XRD pattern

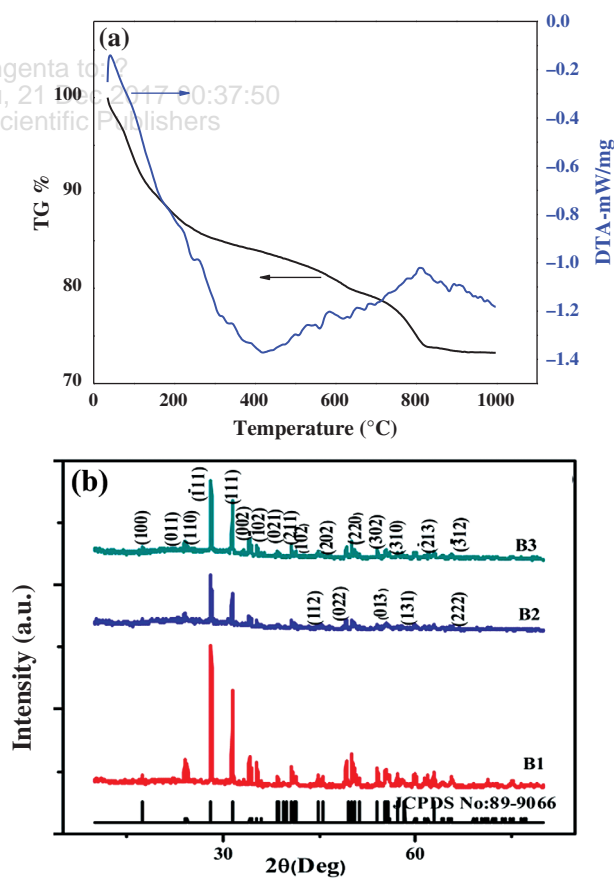


Figure 1. (a) TG/DTA profile for the precursor; (b) XRD pattern of ZrO₂ prepared using 0.5 (B1), 1.0 (B2) and 1.5 (B3) M of KOH as precipitating agent.

of the as prepared sample using solutions of varying KOH concentration. All the diffraction peaks have been indexed to the monoclinic ZrO₂ (JCPDS: 89-9066). The peak at ($\bar{1}11$) orientation have high intensity than the other peaks, which was attributed to the high crystalline nature the particular orientation of the samples. The average crystallite size was estimated as 58.6, 49.7, 60.3 nm for the samples B1, B2 and B3 respectively using Debye-Scherrer formula²¹ and the values are comparable with the previous studies.^{22–25}

Further, the fundamental vibrational group analysis of nanoparticles was studied by the FTIR and is shown in Figure 2(a). The strong bands at 1635, 1382 and 757 cm⁻¹ are attributed to the stretching vibration of O–H, absorption of non-bridging OH groups and the characteristic of *m*-ZrO₂ respectively. These peaks are shifted to

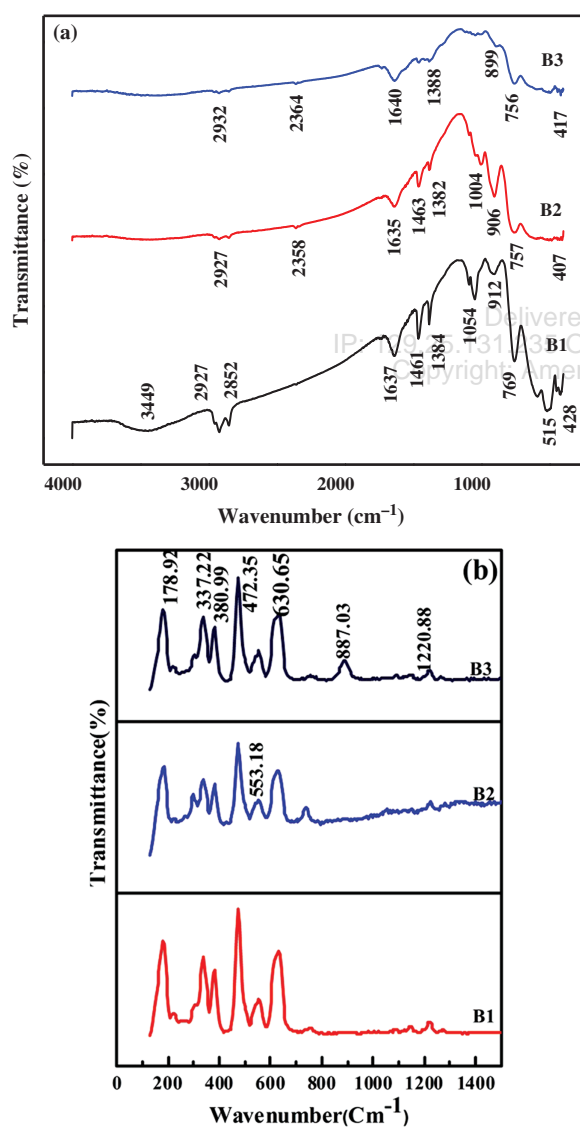


Figure 2. (a) FTIR spectrum, (b) Laser Raman spectra of ZrO₂ prepared using 0.5 (B1), 1.0 (B2) and 1.5 (B3) M of KOH as precipitating agent.

(1637, 1635, 1640 cm⁻¹), (1384, 1382, 1388 cm⁻¹) and (769, 757, 756 cm⁻¹) in the complexes. The peaks particularly at 757 and 407 cm⁻¹ ascribed to Zr–O₂–Zr asymmetric and Zr–O stretching modes, respectively, which are the characteristic bonds of monoclinic phase of ZrO₂. The FTIR studies were in good agreement with the XRD pattern of the ZrO₂ phase.^{26–28}

The Raman spectra of prepared samples were given away in Figure 2(b). The active peaks were observed at

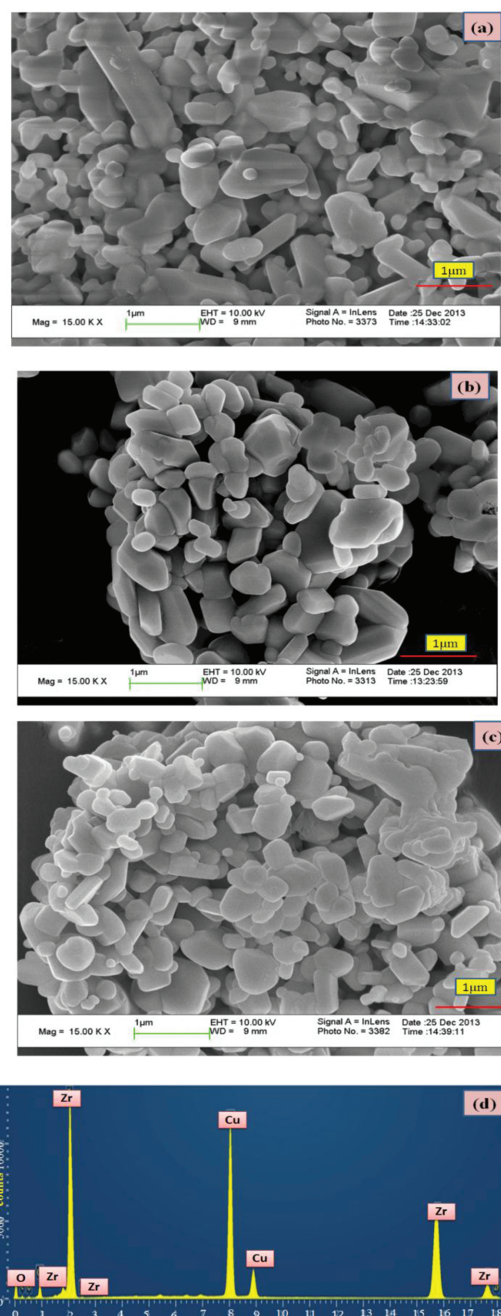


Figure 3. SEM images (a–c) of ZrO₂ prepared using 0.5 (B1), 1.0 (B2) and 1.5 (B3) M of KOH as precipitating agent and EDX image (d) of 0.2 M Zr(NO₃)₂ · 6H₂O and 1 M of KOH.

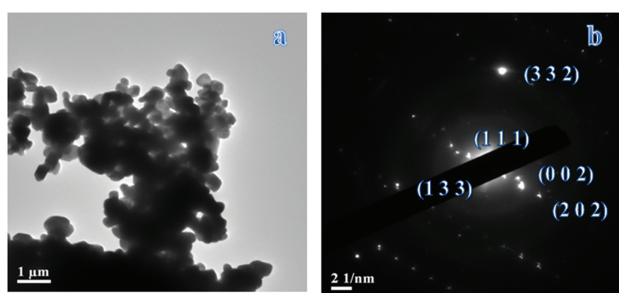


Figure 4. (a) TEM image and (b) SAED pattern of ZrO₂ prepared using 1.0 (B2) M of KOH as precipitating agent.

179, 337, 381, 472, 554 and 631 cm⁻¹ in Raman spectra, which belong to the monoclinic phase of zirconium. The peaks at 337 and 631 cm⁻¹ are assigned to A_g mode. The peaks at 381 and 608 cm⁻¹ could be corresponding to the B_g mode. The remaining peak at 179 cm⁻¹ could be identified as the A_g + B_g mode of monoclinic ZrO₂ phase. Based on the present results, we could identify the Raman active optical phonons through co-precipitation method. Raman active optical phonons were substantiated with other findings using precipitation method,²⁹ phase transition method,³⁰ sol-gel method³¹ and hydrothermal method.³²

Figures 3(a)–(d) display the SEM micrographs and EDX spectrum of ZrO₂ samples prepared using co-precipitation

route with the magnification of 15 K. Two kinds of particle morphologies such as primary particles with spherical shape (size approximately 340 nm) and secondary particles with rod like morphology (0.38 μm × 0.24 μm) were observed (Fig. 3(a)). In Figure 3(b), spherical like shape (size approximately 184 nm) and in Figure 3(c), the two kinds of particle morphologies viz., small spherical shape morphologies (size approximately 192 nm) and secondary particles hexagonal rod like morphology (size approximately 0.21 × 0.42 μm) were observed (using IT-measure software). It can be concluded that the catalyst has played a pivotal role in the surface morphology of the powder. Further, the EDX spectrum of ZrO₂ powder for 1 M of KOH is showed in Figure 3(d). The result clearly exhibits the presence of Zr and O₂. The Cu species indicate that Cu plate was used while EDX analysis was performed.

Figures 4(a)–(b) explained TEM images and SAED pattern for the sample B2. Figure 4(a) can be perceived that ZrO₂ particles were almost agglomerated with a natural sensation. In the case of nanoparticles, agglomeration happens very easily, because the surface forces such as Van-der-walls forces, capillary forces and electrostatic forces can overwhelmed only against gravitational and inertial forces for particular in size assortment.³³ The average diameter of the particles was estimated around 190 nm. The spherical particles distribution might be mainly fabricated

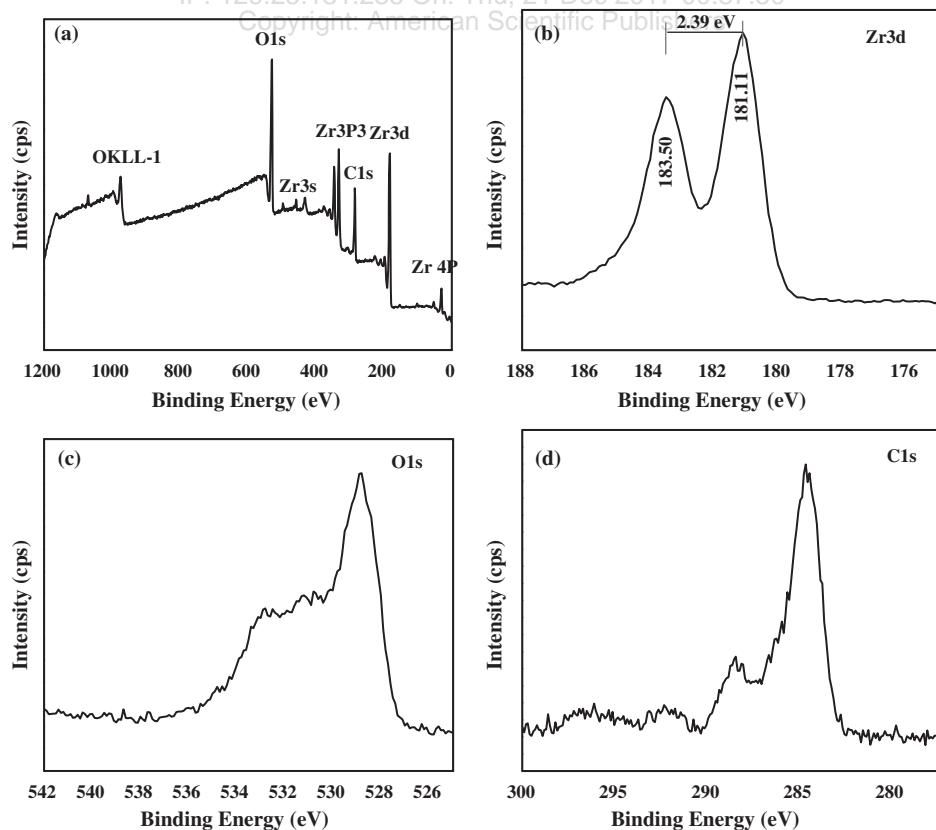


Figure 5. XPS spectra of (a) core, (b) Zr, (c) O1s and (d) C1s of ZrO₂ prepared using 1.0 (B2) M of KOH as precipitating agent.

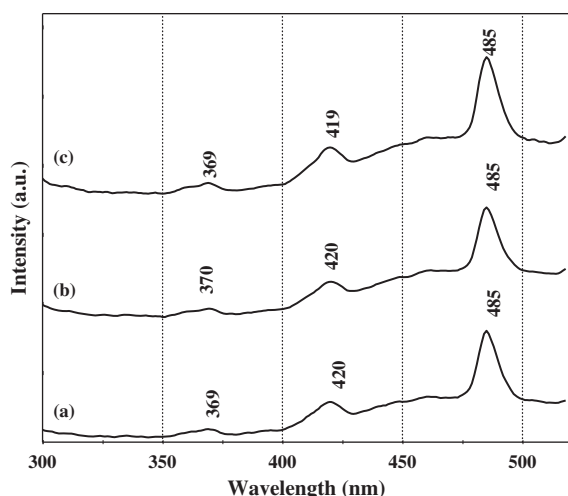


Figure 6. Photo luminescence spectra (a–c) of ZrO₂ prepared using 0.5 (B1), 1.0 (B2) and 1.5 (B3) M of KOH as precipitating agent.

by an Oswald ripening mechanism, i.e., the dissolving of fine particles and the depositing of components on larger particles. The size and shape of the ZrO₂ nanoparticles observed from TEM images were found to coincide with the previous literature.³⁴ From Figure 4(b), it is revealed that the orientation along (332), (111), (002) and (202) directions are in accordance with the *d*-spacing values 3.457, 2.8860, 2.6261 and 1.6958 Å in the XRD pattern.

The chemical valence state of the zirconia nanoparticle was investigated by XPS analysis. The high resolution XPS spectra of wide, Zr 3*d*, O1*s* and C1*s* core levels of ZrO₂ were exemplified in Figures 5(a)–(d). Figure 5(a) shows the wide range scanning XPS spectrum and it can be seen that the sample consists of Zr, O and C elements on the surface of the sample. The doublet of binding energy at 180.9 and satellite peak at 183.2 eV of Zr 3*d* spectra (Fig. 5(b)) correspond to Zr 3*d*_{5/2} and Zr 3*d*_{3/2} with spin orbit splitting of 2.3 eV. The binding energy of O1*s* and C1*s* peak in Zirconia is located at 528.23 eV and 284.64 eV respectively. The peak positions and their relative intensities were in line with earlier literatures.^{35–39}

The photoluminescence spectra Figures 6(a)–(c) has observed a representative fluorescence spectrum with an excitation wavelength of 270 nm, whereas a high intense broad fluorescence band was also seen around 369 nm with corresponding energy of 3.36 eV is called the near band edge emission. This is likely to be associated with band-to-band emission possibly involving localized or free excitations.^{40–42} The weak peaks at 416 and 485 nm respectively with corresponding energies of 2.96 and 2.56 eV, are obviously lower than the deduced band gap, which can be attributed to the presence of oxygen vacancies.

4. CONCLUSION

The ZrO₂ nano particles were successfully synthesized via the co-precipitation method using three different KOH

(precipitating agent) compositions viz., 0.5, 1 and 1.5 M. The monoclinic structure with Fm-3*m* space group was confirmed through (JCPDS: 89-9066) using XRD analysis. Further, the presence of Zr, O species was inveterate via FT-IR, RAMAN, EDX and XPS analyses. The morphology of ZrO₂ nano particles was highly dependent on the concentration of the precipitation agent. The well dispersed spherical morphology with particle size of 193 nm in TEM analysis was observed. Also, it has a band gap of 3.36 eV, which was lower than bulk. Based on these analyses, one can accomplish that this material can eventually be used as filler for Lithium polymer battery electrolyte fabrication.

Acknowledgment: One of the authors M. Sivakumar gratefully acknowledges University Grants Commission (UGC), New Delhi, India for the financial support to carry out this work under physical sciences UGC-MRP F. No. 41-839/2012. This research is also partially supported by the Ministry of Science and Technology under contract numbers: MOST 104-2628-E-033-002-MY3 and 105-2622-E-033-003-CC2.

References and Notes

1. K. Ariga and J. Li, *Adv. Mater.* 29, 987 (2016).
2. H. Abe, J. Lin, and K. Ariga, *Mater. Mater. Today.* 19, 2 (2016).
3. K. Ariga, Q. Ji, W. Nakanishi, J. P. Hill, and M. Aono, *Mater. Horiz.* 2, 406 (2015).
4. R. Jain, D. C. Tiwari, and S. Shrivastava, *J. Electrochem. Soc.* 161, B39 (2014).
5. S. W. Nam, J. H. Yoo, S. Nam, D.-H. Ko, C.-W. Yang, and J.-H. Ku, *J. Electrochem. Soc.* 150, G849 (2003).
6. M. N. Tahir, L. Gorgishvili, J. Li, T. Gorelik, U. Kolb, L. Nesadala, and W. Tremel, *Solid State Sci.* 9, 1105 (2007).
7. F. Zhang, P. J. Chupas, S. L. A. Lui, J. C. Hanson, W. A. Caliebe, P. L. Lee, and S. W. Chan, *Chem. Mater.* 19, 3118 (2007).
8. M. Alianti, B. Baps, N. Blangenois, J. Nand, P. Grange, and B. Delmon, *Chem. Mater.* 15, 395 (2003).
9. G. R. Rao and H. R. Sahu, *J. Chem. Sci.* 113, 651 (2001).
10. R. Drivedi, A. Maurya, A. Verma, R. Prasad, and K. S. Bartwal, *J. Alloys Compd.* 24, 6848 (2011).
11. G. Xu, Y. W. Zhang, C. S. Liao, and C. H. Yan, *Solid State Ionics* 166, 391 (2004).
12. Z. Tang, J. Zhang, Z. Cheng, and Z. Zhang, *Mater. Chem. Phys.* 77, 314 (2002).
13. M. Razaei, S. M. Alavi, S. Sahebald, and F. Y. Zi, *J. Porous Mater.* 15, 171 (2008).
14. J. Li, C. Peng, Z. Li, Z. Wu, and S. Li, *RSC Adv.* 6, 61393 (2016).
15. J. W. Drazin and R. H. R. Castro, *J. Am. Ceram. Soc.* 99, 1778 (2016).
16. H. Zhou, S. X. Pu, J. M. Huo, W. B. Cao, B. Wang, and J. G. Li, *Ceram. Int.* 42, 15005 (2016).
17. N. Zink, F. Emmerling, T. Haser, M. Panthofer, M. N. Tahir, Utekolb, and W. Tremel, *Dalton Trans.* 42, 432 (2013).
18. J. Joo, T. Yu, Y. W. Kim, H. M. Park, F. Wu, J. Z. Zhang, and T. Hyeon, *J. Am. Chem. Soc.* 125, 6553 (2003).
19. O. Vagylkiv and Y. Sakka, *J. Am. Ceram. Soc.* 84, 2489 (2001).
20. C. Suci, L. Gagea, A. C. Hoffmann, and M. Mocean, *Chem. Eng. Sci.* 61, 7831 (2006).
21. R. Muruganatham, M. Sivakumar, R. Subadevi, and N. L. Wu, *J. Mater. Sci. Mater. Electron.* 26, 2095 (2015).

22. F. J. Pereira, M. T. Diez, and A. J. Aller, *Mater. Chem. Phys.* 152, 135 (2015).
23. Q. Wang, C. Li, M. Guo, C. Hu, and Y. Xie, *J. Mater. Chem. A* 2, 1346 (2014).
24. G. C. C. Costa and R. Muccillo, *Solid State Ionics* 179, 1219 (2008).
25. D. S. S. Padovini, D. S. L. Pontes, C. J. Dalmaschio, F. M. Pontes, and E. Longo, *RSC Adv.* 4, 38484 (2014).
26. Z. Shu, X. Jiao, and D. Chen, *Cryst. Eng. Comm.* 15, 4288 (2013).
27. J. Li, C. Peng, Z. Li, Z. Wu, and S. Li, *RSC Adv.* 6, 61393 (2016).
28. X. Yang, N. Zhao, Q. Zhou, C. Cai, X. Zhang, and J. Xu, *J. Mater. Chem. C* 1, 3359 (2013).
29. R. A. Koeppe and A. Baiker, *App. Catal. A* 84, 77 (1992).
30. M. Yashima, H. Arashi, M. Kakihana, and M. Yoshimura, *J. Am. Ceram. Soc.* 77, 1067 (1994).
31. J. M. Miller and L. J. Lakshmi, *J. Phys. Chem. B* 102, 6465 (1998).
32. J. M. E. Matos, F. M. A. Junior, L. S. Cavalcante, V. Santos, S. H. Leal, L. S. S. Junior, M. R. M. C. Santos, and E. Longo, *Mat. Chem. Phys.* 117, 455 (2009).
33. S. Bajpai, S. Singh, and V. Srivastava, *RSC Adv.* 5, 28163 (2015).
34. D. Fang, K. Huang, Z. Luo, Y. Wang, S. Liu, and Q. Zhang, *J. Mater. Chem.* 21, 4989 (2011).
35. S.-M. Chang and R. Doong, *Thin Solid Films* 489, 17 (2005).
36. X. Qiu, Y. Zhao, and C. Burda, *Adv. Mater.* 19, 3995 (2007).
37. J. R. Scheffe, A. Frances, D. M. King, X. Liang, B. A. B. Andrews, Cavanagh, S. M. George, and A. W. Weimer, *Thin Solid Films* 571, 1874 (2009).
38. S. N. Basahel, M. Mokhtar, E. H. Alsharaeh, T. T. Ali, H. A. Mahmoud, and K. Narasimharao, *Nanosci. Nanotechnol. Lett.* 8, 448 (2016).
39. Y. Shen, J. W. Du, X. Zhang, X. Huang, Y. Song, H. Wu, Y. H. Lin, M. Li, and C.-W. Nan, *Mater. Express* 6, 277 (2016).
40. U. Baig and M. A. Gondal, *Nanosci. Nanotechnol. Lett.* 8, 998 (2016).
41. A. Afzal, C. D. Franco, E. Mesto, N. Ditaranto, N. Cioffi, F. Scordari, G. Scamarcio, and L. Torsi, *Mater. Express* 5, 171 (2015).
42. D.-T. Vu, Y.-H. Han, F. Chen, D. Q. Jin, J. M. Schoenung, and D.-Y. Lee, *Sci. Adv. Mater.* 8, 312 (2016).

Received: 18 October 2016. Accepted: 17 November 2016.

Delivered by Ingenta to :
IP: 129.25.131.235 On: Thu, 21 Dec 2017 00:37:50
Copyright: American Scientific Publishers

ICMCT-2014 [10th – 12th March 2014]
International Conference on Materials and Characterization Techniques

Structural, morphology and ionic conductivity studies on composite P(S-MMA)-ZrO₂ Polymer electrolyte for Lithium Polymer battery

M.Ramachandran¹, R.Subadevi², Fu-Ming Wang³, Wei-Ren Liu⁴, M.Sivakumar^{2,*}

¹ Department of Physics, Arumugam Pillai Seethai Ammal College,
Tiruppattur 630 211 India

² Department of Physics, Alagappa University, Karaikudi-630 003. India.

³ Graduate Institute of Engineering and Technology, National Taiwan University of
Science and Technology, Taipei-106, Taiwan, ROC.

⁴ Department of Chemical Engineering, Chung Yuan Christian University, Chung Li,
Taiwan, ROC.

*Corres. author: susiva73@yahoo.co.in

Abstract: In the present study, the composite material ZrO₂ has been prepared using NH₃ and Na₂CO₃ as precipitation agents, via co-precipitation technique. The as prepared ZrO₂ has been characterized using XRD, FE-SEM, FTIR analyses. The ZrO₂ composites were used as filler in the parent polymer electrolytes based on P(S-MMA)-LiClO₄ by solution casting techniques. Electrical, structural and functional analyses of P(S-MMA) based polymer electrolytes comprising ZrO₂ were studied and the results are reported. The incorporation of ZrO₂ filler greatly enhanced the ionic conductivity and other electrochemical properties of P(S-MMA) based polymer electrolytes.

Key words- P(S-MMA); ZrO₂; LiClO₄.

Introduction and Experimental

The rapid development of new technologies such as cell phone, notebook PC, and electric vehicle (EV) has promoted research aimed at improving battery performance with special effort devoted to Lithium batteries [1]. Numerous methods have been reported for improving characteristics of polymer electrolytes such as cross-linking, incorporation of organic solvents and fillers, etc., An attempt has been made to study the effect of addition of ZrO₂ in PS-MMA based SPEs for various compositions using conventional solution casting technique. Towards attaining good properties of filler, ZrO₂ was prepared laboriously by co-precipitation method using NH₃ and Na₂CO₃ as precipitating agents. Based on the properties of as-prepared optimized filler, the various compositions of composite polymer electrolytes were prepared.

The ZrO₂ fillers were synthesized by co-precipitation method using 0.2M Zr (NO₃)₂.3H₂O and Na₂CO₃ or NH₃ as precipitation agent [2]. The prepared composites of different weight ratio were added into the optimized P(S-MMA)-LiClO₄ as dopant salt by solution casting technique.

Results and discussion

In order to determine the thermal property of the ZrO₂precursors, the calcinations temperatures were fixed as 700 and 900 °C for NH₃ and Na₂CO₃ as a Precipitation agent respectively. Fig 3.1.A shows the TG curves of the precursors of ZrO₂ whose precipitation agents are NH₃ and Na₂CO₃. X-ray diffraction pattern and IR Spectra of the as prepared ZrO₂ filler using NH₃ and Na₂CO₃ as precipitation agents are represented in Fig.3.1 (B & C).

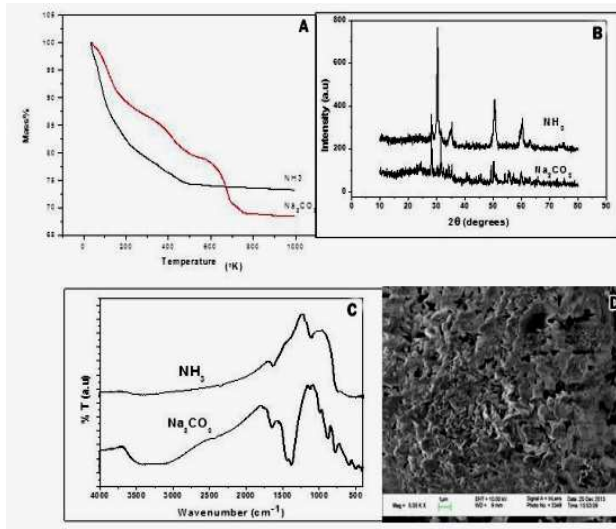


Fig.3.1 (A)TG curves (B) XRD patterns and (C) FT-IR spectra of ZrO₂ precursors when NH₃ and Na₂CO₃ are used as precipitation agents. D) SEM image of ZrO₂ Precursors when Na₂CO₃ as precipitation agent.

From the XRD pattern it is confirmed that the as-prepared samples are ZrO₂ with the monoclinic structure which is in agreement with the JCPDS 781807. However, all the peaks are in very good agreement with the standard for the sample prepared while using Na₂CO₃ as precipitation agent than the other one. Using the Scherer's relation the crystalline domain size was determined as 110 nm. The IR spectra of ZrO₂ crystalline samples show various stretching frequencies around 740 and 500 cm⁻¹[3], which are attributed to Zr-O₂-Zr asymmetric Zr-O stretching vibrations. These peaks are shifted to 780 and 499 cm⁻¹ respectively confirms the formation of ZrO₂ in Na₂CO₃ based ZrO₂ samples. Fig. 3.1 D showed that the SEM image of Na₂CO₃ based ZrO₂ particles; most of the particles are found to have hexagonal structure with needle shape. The particle size is estimated as 294nm for Na₂CO₃ based ZrO₂ and has uniform morphology. It reveals that ZrO₂ filler aiding in the formation of amorphous phase into the parent polymer matrix. The XRD pattern, (Fig.3.2 (a)) shows few intense peaks like 2θ=28.3, 31.6° which shows the monoclinic structure of ZrO₂ filler. [JCPDS:78-1807]. Also two intense peaks at 2θ=13.1 and 22.9° which reveal the hexagonal structure for LiClO₄ [JCPDS: 30-0751]; these intensity are comparatively low while incorporating ZrO₂ in the parent polymer electrolyte. Actually, the intensity of bare electrolytes is reduced while incorporating the ceramic fillers as contradict one. This may be caused the complete dissociation of inorganic salt (which is acting as a dissociating agent) in to the polymer matrix which leads to the amorphous nature. The OH stretching vibration of PS-PMMA around 3500cm⁻¹ is shifted in between 3533-3650 cm⁻¹ in the complexes (Fig.3.2). The vibration peaks at 2990 and 2940cm⁻¹ are ascribed to the asymmetric and C-H stretching of the absorption peak of PS-MMA. The characteristic vibration peak appearing at 940cm⁻¹ is assigned to per chlorate anion that is shifted to 960 cm⁻¹ in the complexes. The characteristic peaks of Zr-O stretching and Zr-O₂-Zr asymmetric modes are appeared at 500 and 740 cm⁻¹. The addition of new peaks, shifting of peaks and absence of peaks in the complexes ensures the complexation had taken place between PS-MMA and LiClO₄ and ZrO₂ filler composites polymer electrolytes. In the present work, ZrO₂ concentration has been varied as (3, 6, 9 and 12)wt% on the bare P(S-MMA)-LiClO₄ electrolyte. The parent electrolyte exhibits the conductivity of 6.8×10⁻⁷Scm⁻¹ at 303 K. While incorporating the ZrO₂ filler, conductivity enhances two orders of magnitude at 303 K. The temperature dependent ionic conductivity plots are shown in Fig 3.3 in the temperature range 303-353K. The conductivity of the electrolyte increases with the increase of temperature. Also it is clear that the conductivity increases upon the addition of ceramic filler up to 9 wt%; further addition of ZrO₂ makes the conductivity dips down. The same trend was obtained for our previous studies on PVdF-PEMA based composite gel polymer electrolyte and for PEO based composite polymer electrolyte [4]. For all complexes, the conductivity increases with increase of temperature and this can be rationalized by free volume model. The curvature of the plots indicates that ionic conductivity seems to obey

Arrhenius relation, which describes that ion transport in polymer electrolytes is dependent on polymer segmental motion. The activation energy of the system varies within the range 0.14 to 0.37 eV. It reveals that highly conducting sample possesses lesser activation energy.

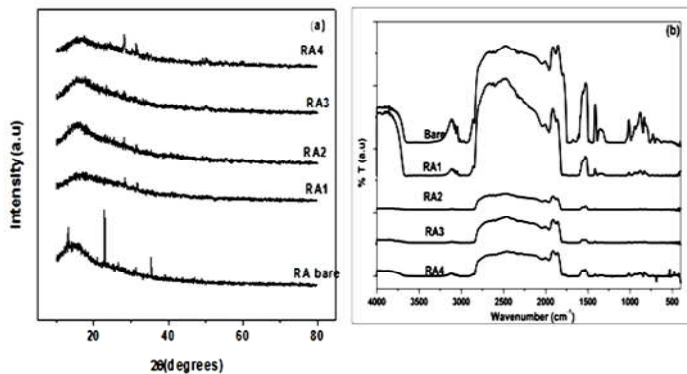


Fig.3.2 (a) XRD patterns and (b) IR spectra of bare PS-MMA-LiClO₄ and 3 (RA1), 6 (RA2), 9 (RA3) and 12 wt% (RA4) of ZrO₂ based polymer electrolytes.

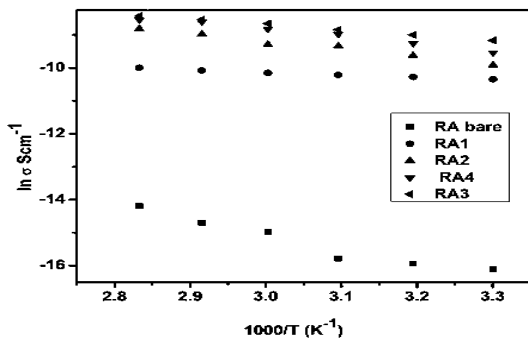


Fig.3.3 Temperature dependent ionic conductivity plots of P(S-MMA) (80)-LiClO₄ (20) + ZrO₂ (bare, 3, 6, 9, 12) wt% based electrolytes in the temperature range 303-353K.

Conclusion

The ZrO₂ filler were synthesized by co-precipitation method using Na₂CO₃ and NH₃ as precipitation agents. The as-prepared samples were ZrO₂ with the monoclinic structure which is in agreement with the JCPDS 781807. The 3, 6, 9 and 12 wt% of ZrO₂ was dispersed in to P(S-MMA) (80)-LiClO₄(20) polymer matrix by solution casting method. P(S-MMA) (80)-LiClO₄ (20)-9wt% ZrO₂ exhibits maximum ionic conductivity 2.2 × 10⁻⁴ Scm⁻¹ at 303K. The ionic conductivity of composite polymer electrolytes increases in two orders of magnitude on the bare polymer electrolyte. The activation energy varies between .14 to .37 eV.

Acknowledgements

One of the authors, M.Sivakumar gratefully acknowledged UGC-MRP F.No.41-839/2012 under physical sciences for the financial support to carry out this work.

References

1. Jingyu Xi, Xinping Qiu and Liquan chen, PVDF-PEO blends based microporous polymer electrolyte: Effect of PEO on pore configuration and ionic conductivity, *J. Power Sources.*, 2006,157,501-506.
2. Rezaei M, Alavi S.M, Sahebdehfar S and Feng yan Zi, Effect of process parameters on the synthesis of mesoporous nanocrystalline zirconia with triblock copolymer as template, *J.Porous Mater.* 2008, 15, 171-179.
3. Ranjan Sahu H, Ranga and Rao G, Characterization of combustion synthesized Zirconia powder by uv-vis IR and other techniques, *Bull.Mater.Sci.*, 2000, 23, 339-354.
4. Rajendran. S, Sivakumar M and Subadevi R, Effect of Plasticizers in Poly (Vinyl alcohol)-based Hybrid Solid Polymer electrolytes, *J. Appl. Polym. Sci.*, 2003, 90,2794-2800.